MEASUREMENTS ON THE ABSOLUTE INTENSITY OF INFRA-RED ABSORPTION

by

Thomas F. Hunter

Thesis presented for the degree of
Doctor of Philosophy.

University of Edinburgh May, 1963

CONTENTS

1 INTRODUCTION

1.1 General Introduction

The study of the absorption of infra-red radiation by gases, liquids and solids has to date been mainly concentrated on the measurement of the frequency at which a particular stretching or bending mode of vibration within a molecule oscillates. This has given rise to infra-red spectroscopy being used as an analytical tool, certain absorption frequencies being characteristic of particular groups in a molecule. In addition to this, the technique, when it also included a study of the corresponding rotational absorption, has produced a very detailed account of molecular properties and constants especially in the case of gases when intermolecular forces are of little importance. These properties include internuclear distances, bond force constants and moments of inertia, and much work has been carried out in the elucidation of these for a wide variety of molecules.

However, until recently, relatively little work had been done on the intensity of absorption i.e. a measure of the actual amount of energy absorbed during a vibrational or rotational transition, and on the related properties of molecular transition moments, bond dipole moments, change of dipole with

internuclear separation and dependence of dipole moment functions on the electron wave-functions. Interest has been more directly stimulated in intensity measurements because of the relationship with infra-red emissivities, calculation of which leads to information on radiant-heat transfer. Emissivity computations for heated air during re-entry of missiles to the atmosphere, and calculations on the effect of radiation on the burning of solid and liquid propellants are two modern expressions of this interest. (1)

A detailed knowledge of strength, shape and width of rotational lines and vibrational bands has also become increasingly important in recent years in subjects such as chemical kinetics, meteorology and astrophysics. Among the many applications are the use of intensities to study population distributions in gases and therefore the temperature if the system is in equilibrium, deviations from equilibrium in a similar system, concentrations of a particular constituent during a reaction, determination of excitation effects behind a shock front, abundances in terrestrial, planetary and stellar atmospheres and the problems of radiant energy transfer between the layers of such atmospheres.

The resulting greater number of measurements has given rise to many advances on the theoretical front. (2) Considerable progress has been made in

deducing the dependence of the molecular dipole moment on the internal nuclear co-ordinates, although a clear understanding of these functions in terms of the electron wave-functions has not yet been attained. Because of the difficulties of allowing correctly for molecular interactions, the interpretation of intensities in terms of transition moments and dipole functions has been confined to gas-phase measurements.

The following thesis is restricted to a dis-:cussion of intensity and line-width measurements on gases.

1.2 Infra-red Intensities and Dipole Moments

In the harmonic oscillator approximation to a normal mode of vibration in a molecule, the value of the dipole moment change with normal co-ordinate change at the equilibrium position governs the intensity of the particular fundamental band in the infra-red spectrum. Before indicating the proof of this in terms of the transition moment it is advan-:tageous to define the measurable intensity of a transition, and also to briefly elucidate the selection rules determining the probability of absorption.

1.2.1 Integrated Absorption Intensity

For monochromatic radiation of frequency ν the fundamental law of absorption by gaseous molecules is

$$I = I(o) \exp\left[-k(\nu)\, X\right]$$

where I and I(o) are the transmitted and incident light intensities,

$k(\nu)$ is the absorption coefficient of the gas,

and X is the reduced pathlength which equals p l, where p is the pressure in atmospheres and l is the optical path in cm.

i.e. $$k(\nu) = \frac{1}{X} \ln \frac{I(o)}{I}$$

Since band absorption takes place over a def-:inite range of frequencies it is possible to define

a quantity, the integrated absorption or intensity A as

$$A = \int_{band} k(\nu)d\nu = \frac{1}{X} \int_{band} \ln \frac{Io}{I} d\nu$$

1.2.2 Selection Rules

Although in a polyatomic molecule, which will be treated here, the vibrations of the nuclei are seemingly disorderly, they represent the sum of displacements due to the fundamental modes of vibration. Without involving inessential complications, each of these modes can be treated as an harmonic oscillator which has access to many states. A transition can occur with calculable probability between two adjacent states, m and n. (95) It follows from basic quantum mechanical considerations that this probability

$$|c|^2 = \frac{4\pi^2}{h^2} \mathcal{E}_x^{o\,2} \left\{ \int m^* \; e \; x \; n \; dx \right\}^2 t \qquad (1$$

with $\int m^* \; e \; x \; n \; dx$ = the transition moment, M (2

and $\mathcal{E}_x^o$ derived from $\mathcal{E}_x = 2\,\mathcal{E}_x^o \cos 2\pi\nu t$

where $\mathcal{E}_x$ is the component of the electric field of the radiation along the x coordinate of the oscillator; t is the time; ν is the frequency of the oscillator; and e is the electronic charge.

In a molecule consisting of a group of charges

representing the nuclei and the electrons, e x is effectively replaced by the dipole moment μ. For a polyatomic molecule the dipole and transition moments are vectors with components μ_x and M_x, μ_y and M_y, etc., and x is replaced by the volume element dV.

$$\text{Thus } M_x = \int m^* \mu_x \, n \, dV \qquad (3$$

$$\text{Assuming that } \mu_x = \mu_x^o + \sum_i \left(\frac{\delta \mu_x}{\delta Q_i}\right)_o Q_i \qquad (4$$

where μ_x^o is the dipole moment when the nuclei are in their equilibrium positions; and Q_i is the normal co-ordinate of the i^{th} normal mode,

to a first approximation.

$$M_x = \mu_x^o \int m^* \, n \, dV + \sum_i \left(\frac{\delta \mu_x}{\delta Q_i}\right)_o \int m^* \, Q_i \, n \, dV \qquad (5$$

If m (or n) is supposed to have strictly the form of a product of harmonic oscillator wave-functions the first term in (5 gives

$$\mu_x^o \left\{ \int m_1(Q_1)^* \, n_1(Q_1) dQ_1 \ldots\ldots \int m_i(Q_i)^* \, n_i(Q_i) dQ_i \ldots \right\} \qquad (6$$

which vanishes unless $m_1 = n_1 \ldots\ldots m_i = n_i \ldots$, and so has the value zero for any change of the vibrational quantum numbers i.e. in absorption of radiation.

Each term in the summation in (5 splits into a product:

$$\left(\frac{\delta \mu_x}{\delta Q_i}\right)_o \int m^* \, Q_i \, n \, dV$$

is equal to $\left(\frac{\delta \mu_x}{\delta Q_i}\right)_o \left\{ \int m_1(Q_1)^* Q_1 n_1(Q_1)\, dQ_1 x \ldots\ldots \right.$

$\left. \ldots\ldots \int m_i(Q_i)^* Q_i n_i(Q_i)\, dQ_i \ldots\ldots \right\}$ (7

If (7 is not to vanish then $m_1 = n_1$, $m_2 = n_2$, etc. except for the i^{th} normal vibration where $m_i = n_i \pm 1$.

Therefore, for polyatomic molecules, the harmonic oscillator selection rule restricts transitions occurring with absorption (or emission) of radiation to those in which one vibrational quantum number changes by one unit only. The frequencies absorbed are then the fundamental frequencies of the normal modes. It must be remembered, however, that the harmonic oscillator selection rule depends on the form of expression (7; hence it is subject to the assumption that m and n are strictly products of harmonic oscillator wave-functions, and that the dipole moment at any instant is given by expressions of the type (4. Transitions will appear in violation of the selection rule should either of these assumptions fail.

As well as the above selection rule the symmetry properties of the molecule must also be considered, and, when symmetry requires a dipole moment derivative to vanish, the corresponding fundamental band is for-:bidden in the infra-red spectrum. From group theory it is found that should the integrals representing

M_x, M_y and M_z simultaneously vanish the transition is a forbidden one. The integral $m^* \mu_x n$, since the ground state wave-function is totally symmetrical, will be identically zero unless m and μ_x have the same symmetry species. The components of the dipole moment are given by the expressions

$$\mu_x = \sum_{i=1}^{N} e_i x_i \quad , \text{ etc.}$$

in which x_i, y_i and z_i are the co-ordinates, and it is fairly readily shown that μ_x has the same symmetry species as x_i.

The symmetry selection rule therefore allows transitions in absorption from the ground state to any excited vibrational state whose wave-function has the same symmetry species as at least one of the axes x, y or z.

Whether a transition is allowed, with the absorption of infra-red radiation, is thus dependent to a first approximation on the above two selection rules.

1.2.3 Dipole Moment Change

From eq^n (1 it follows that the probability of transition is proportional to the square of the transition moment; this assumes that the intensity of the radiation and the time are not changing. It is this probability which is directly related to the absorption intensity of a band, and theory gives the

overall proportionality constant as $\frac{8\pi^3 n_o \nu_i}{3ch}$

where n_o is the number of molecules per c.c. at NTP,

and ν_i is the absorption frequency.

Thus

$$A_i = \frac{8\pi^3 n_o \nu_i}{3ch} \left[M_x(i)^2 + M_y(i)^2 + M_z(i)^2 \right] \quad (8$$

with

$$M_x(i) = \left(\frac{\delta\mu_x}{\delta Q_i}\right)_o \int m(Q_i)^* \, Q_i \, n(Q_i) \, dQ_i \quad (9$$

A_i is the integrated intensity as defined in 1.2.1 applied to the i^{th} fundamental, and m and n are for the zeroth and first states.

Substituting in (9 the well-known expressions for a strictly harmonic oscillator, viz.

$$n(Q_i) = \left(\frac{1}{a_i \pi}\right)^{\frac{1}{4}} \exp\left[\frac{-\frac{1}{2}Q_i^2}{a_i}\right]$$

and

$$m(Q_i) = \left(\frac{4}{a_i^3 \pi}\right)^{\frac{1}{4}} Q_i \exp\left[\frac{-\frac{1}{2}Q_i^2}{a_i}\right]$$

$$\text{where } a_i = \frac{h}{4\pi^2 \nu_i}$$

it follows that

$$\int m(Q_i)^* \, Q_i \, n(Q_i) \, dQ_i = \left(\frac{2}{a_i^2 \pi}\right)^{\frac{1}{2}} \int Q_i^2 \exp\left[\frac{-Q_i^2}{a_i}\right] dQ_i \quad (10$$

and performing the integration yields

$$M_x(i) = \left(\frac{\delta\mu_x}{\delta Q_i}\right)_o \left(\frac{h}{8\pi^2 \nu_i}\right)^{\frac{1}{2}}$$

and similarly for $M_y(i)$ and $M_z(i)$.

Thus

$$A_i = \frac{\pi n_o}{3c}\left[\left(\frac{\delta\mu_x}{\delta Q_i}\right)_o^2 + \left(\frac{\delta\mu_y}{\delta Q_i}\right)_o^2 + \left(\frac{\delta\mu_z}{\delta Q_i}\right)_o^2\right] \quad (11$$

which is the desired expression connecting the experimentally observable intensity of the i^{th} fundamental band with the components of the dipole moment change.

Results for the integrated intensities of diatomic molecules have made possible the deduction in some detail of dipole-moment functions around the equilibrium configuration. Because theory only yields the square of the dipole moment derivative with respect to internuclear distance much work has been done on finding the sign of this quantity (3). Work by Herman and Wallis (4) on vibrational-rotational interactions would seem to offer in some cases an immediate correlation of sign between the equilibrium dipole and its derivative.

In the case of band intensities in polyatomic molecules measurements on the fundamentals give dipole moment derivatives with respect to the normal co-ordinates. Difficulty is encountered in giving a correct interpretation of the form of the normal co-ordinates due to lack of knowledge of the anharmonicities and of the constants contained in the force field calculations. One method (2) of surmounting these difficulties has been by studying a variety of isotopic species, although advances have

also been made in the use of microwave data to supply extra information on the necessary constants (5). An extension of the Herman-Wallis theory to polyatomic molecules would be of considerable value. (6)

In polyatomic molecules results are very often interpreted in terms of the bond-moment hypothesis (7) in which independent dipoles are assigned to the various bonds in the molecule. Correlation between similar vibrations in different molecules has not been too good, although much work has been done on assessing the effect of lone-pair electrons, rehybridisation and incomplete orbital-following (7) (8). Calculations of molecular charge dis-:tributions and therefore of dipole moment derivatives have been attempted (9) (10) (11) (12) but have been beset with difficulties.

Although the interpretation of intensities in terms of bond moments seems theoretically dubious because of the necessary distribution of electrons throughout the whole molecule, it has been suggested that empirical relationships between bond moments and group electronegativities exist. (13) (14)

1.3 Theories of the Energy Absorbed by a Vibrational Band

The theoretical relationships involved in a gas absorbing infra-red radiation are described in some detail since the work described later is related both to the intensity of absorption of a band and to the general shape of the rotational lines making up the band. The following theory therefore contains, not only a discussion of the energy absorbed over a wide range of reduced pathlengths, but also the various approaches to finding the change of rotational line-width with pressure.

The process of absorption can be discussed from two rather different standpoints, the titles 'spectroscopic absorption' and 'energy transfer' being thought the best to fit the two overlapping categories.

1.3.1 Spectroscopic Absorption

A vibrational band in a molecule consists of many rotational sub-levels of absorption. Depending on the symmetry species of the ground and excited states the band is made up of a P and an R branch, with their well-separated rotational lines, or also contains a central Q branch, where at reasonable pressures the rotational lines completely overlap although at very low pressures considerable separation

occurs. The intensity of the Q branch with respect to that of the P and R branches depends on the particular symmetry of the molecular transition, and the various possibilities need not be discussed here. (15)

In discussing the energy absorbed by a vibrational band it is much simpler to take the case where no Q branch is present, and therefore initially this is done here.

The intensity distribution of the rotational lines in a band branch is essentially determined by the population of the lower levels, and the individual intensity is given by a formula of the type: (taking, for example, the case of a symmetrical top molecule)

$$S_{J,K} = C \frac{(J+1)^2-K^2}{(J+1)(2J+1)} g_{J,K} \exp\left(-F(J,K).\frac{hc}{kT}\right) \qquad (12$$

where J and K are the two quantum numbers involved in the transition for a symmetrical top,

C is a factor depending on the permanent dipole of the molecule,

$g_{J,K}$ is the statistical weight of the lower state and depends on the type of symmetry, and

$F(J,K) = BJ(J+1) + (A-B)K^2$ for a symmetrical top molecule,

with B and A the two rotational constants corresponding to the two moments of inertia.

The individual lines are broadened by several factors; the three most important symmetrical effects

being natural broadening (N), collision broadening (C) and Doppler broadening (D). Following Penner (1), the half-intensity line-widths b for each of those pro-:cesses are derived readily as follows.

$$b(N) = \frac{1}{4\pi}(\gamma_u + \gamma_1) \qquad (13$$

where b(N) is the line-width due to natural broadening;

and γ_u and γ_1 are the reciprocal lifetimes of the upper and lower states.

$$b(C) = \frac{1}{4\pi}(2Z_u + 2Z_1) \qquad (14$$

where b(C) is the line-width due to collision broadening;

and Z_u and Z_1 are the number of collisions per unit time for the two states.

$$b(D) = \left(\frac{2kT\ln 2}{mc^2}\right)^{\frac{1}{2}} \nu_{ul} \qquad (15$$

where b(D) is the line-width due to Doppler broadening;

ν_{ul} is the frequency difference between the two states,

and the other symbols have their usual meaning.

b(N) is invariably very small, b(D), for a typical ν_{ul} of 2000 cm^{-1}, is around $2\times10^{-3} cm^{-1}$ at room temperature and b(c) at N.T.P. is approximately $0{\cdot}1 cm^{-1}$. Therefore except at high temperatures or low pressures, when b(C) is small, b(C) can be taken as the overall line-width. Using this fact, the shape of each line is represented by the relationship,

$$k(\nu) = \frac{Sb}{\pi} \frac{1}{(\nu-\nu_o)^2+ b^2} = \frac{k(o)b^2}{(\nu-\nu_o)^2+ b^2} \qquad (16$$

where S is the line intensity,

and k(o) is the absorption coefficient at the centre of the line which has a frequency ν_o.

As would be expected, this simple shape is very inadequate when Doppler broadening is of importance, and it has also been shown to give a poor representa-:tion of the true shape at large distances from the line centre. (16) In the wings of the line, the shape appears to be governed by the specific inter-:molecular forces operative during collision, forces which in the case of highly polar molecules can affect the value of the line-width. (17)

Much use of this relationship, however, has been made and many useful results obtained.

Several approaches to the problem of the varia-:tion of the energy absorbed, by a vibrational trans-:ition, with the reduced pathlength exist, and, having established the above simple model of a band as a series of lines, these are now enumerated.

1.3.1.1 Simple, Semi-Quantitative Model

The great advantage of this simple treatment lies in the fact that it gives a ready physical picture of the amount of energy absorbed by a band or single line.

It is found that the validity of the Lambert Law of absorption is held to a good approximation pro-:vided that:-

1) $k(\nu)$ does not vary greatly over the band

2) very small pathlengths are being used.

The line spectrum of a gas with a value of b at one atmosphere of around 0.1 cm^{-1} and a spacing between lines of approximately 3 cm^{-1} obviously does not fulfil these conditions, although for very small pathlengths most of the contribution to the absorbed energy comes from the intense part of the lines, i.e. that part with large values for $k(\nu)$, and it is seen that in this region the energy absorbed is initially proportional to the pathlength. However, as the pathlength increases the exponential term arising from this intense absorption rapidly becomes negligible, and the variation of energy absorbed with pathlength comes from parts of the spectrum where $k(\nu)$ is much smaller, i.e. the overlapping wings ofthe lines in the band.

This qualitative approach can be extended in a more quantitative manner for a single line by using equation (16 and noting that

$$E = I(o) \int_{line} \left[1-\exp\left(-k(\nu)\, X\right)\right] d\nu \qquad (17$$

where E is the energy absorbed,

and the other symbols are as normal.

It is not easy to evaluate this expression using

equation (16 unless the discussion is limited to regions of the line some distance from ν_o.

Thus, provided that $b \ll |\nu - \nu_o|$

$$k(\nu) = \frac{k(o)b^2}{(\nu-\nu_o)^2}$$

and $$E = I(o) \int_{line} \left[1 - \exp\left(-\frac{k(o)b^2X}{(\nu-\nu_o)^2}\right)\right] d\nu \qquad (18$$

On changing to a variable y given by $(\nu-\nu_o) = \frac{1}{y}$, and considering the limits of integration as $\pm\infty$,

$$\frac{dE}{dX} = I(o)k(o)b^2 \int_{-\infty}^{\infty} \exp\left(-k(o)Xb^2y^2\right)dy$$

and

$$\frac{dE}{dX} = \frac{I(o)\ \pi^{\frac{1}{2}}\ k(o)^{\frac{1}{2}}b}{X^{\frac{1}{2}}} \qquad (19$$

Since E(o) = 0, then

$$\underline{E(X) = 2I(o)\ b\ (\pi\, k(o)X)^{\frac{1}{2}}} \qquad (20$$

or $\underline{E(X) = 2I(o)\ (SbX)^{\frac{1}{2}}}$ from equation (16.

Thus it follows that, as the reduced pathlength increases, the relationship between the energy absorbed and the reduced pathlength changes from a linear one, in which the line shape is of no consequence as regards the dependence, to one involving the square root. (18) In the case of study on a pure gas, when the pressure alone is changed, the dependence at higher pressures is linear because to a first approximation b is proportional to the total pressure of gas present.

This treatment can be extended to the overlapping wings of a large number of lines comprising

a band.

1.3.1.2 Theory of Elsasser

This analysis (19), similar in many respects to 1.3.1.1, disregards all broadening processes except collision broadening, and makes the assumption that all lines in a band consisting of P and R branches are equally intense and equally spaced, each obeying the normal dispersion principle. Although extensions of this approach to the case of real vibration-rotation bands have been proposed (20) and more sophisticated analyses are discussed later (1.3.1.3 and 1.3.1.4), it has been pointed out and verified experimentally that the results of this idealised distribution give essentially correct relationships between energy absorbed, pressure and pathlength. The following treatment is based on the remarks of Penner (1).

Consider a vibration-rotation band with equally spaced and equally intense lines whose centres are located at the wave-numbers nd where d is the distance apart of the lines and n is an integer, positive, negative or zero.

From equation (16,

$$k(\omega) = \sum_{n=-\infty}^{+\infty} \frac{S}{\pi} \frac{b}{(\omega-nd)^2+b^2} \qquad (21$$

where ω is the wave-number.

This is a periodic function and can therefore be expressed trigonometrically. By doing this and sub-:stituting in the expression

$$T_R = \frac{1}{d} \int_{-\frac{d}{2}}^{\frac{d}{2}} \exp(-k(\omega)X)d\omega \qquad (22$$

where T_R is the total fractional transmissivity of the spectral region,

Elsasser has shown the result to be

$$T_R = \sinh\beta \int_{\frac{SX}{d\sinh\beta}}^{\infty} \left[\exp(-y\cosh\beta)\right] J_o(iy)dy \qquad (23$$

where $J_o(iy)$ is the Bessel function of degree zero,

$$y = \frac{S}{d}\,\frac{X}{\sinh\beta},$$

$$\text{and } \beta = \frac{2\pi b}{d}$$

The limits of integration bave been taken in such a way that:

$$T_R = 0 \text{ for } y = X = \infty$$

$$\text{and } T_R = 1 \text{ for } y = X = 0$$

Various interesting limiting forms can be derived from this for special cases, the most important being given now.

1.3.1.2.1

When $\beta \ll 1$, $\cosh\beta = 1$ and $\sinh\beta = \beta$; if also $X \ll 1$ then $\frac{SX}{d\beta}$ is small compared with unity and (23 reduces to

$$T_R = \beta \int_{\frac{SX}{d\beta}}^{\infty} \left[\exp(-y)\right] J_o(iy)\, dy$$

For $2\pi b \ll d$, this is shown to be

$$T_R = 1 - \frac{SX}{d}\left[\exp\left(-\frac{SX}{2\pi b}\right)\right]\left[J_o\left(i\frac{SX}{2\pi b}\right) - iJ_1\left(i\frac{SX}{2\pi b}\right)\right]$$

and is usually expressed in terms of the radiation function f(x) of Ladenburg and Reiche (21), where

$$x = \frac{SX}{2\pi b},$$

by $$\underline{T_R = 1 - \frac{2\pi b}{d} f(x)} \qquad (24$$

f(x) is defined as $x\left[\exp(-x)\right]\left[J_o(ix) - iJ_1(ix)\right]$ and is tabulated in several references (1) (22).

Since $T_R = 1 - \frac{E}{I(o)\Delta\omega c}$

where $\Delta\omega$ is the bandwidth in wavenumbers,

$$E = I(o)\,\Delta\omega\,\frac{2\pi b}{d}\,f(x)$$

or $$\underline{E = I(o)\ m.\ 2\pi b\ f(x)} \qquad (25$$

where m is the number of lines in the absorption band.

Two useful asymptotic forms follow (21):-

$$E = I(o)\ m.\ 2\pi b\ x$$

i.e. $$E = I(o)\ m\ S\ X \qquad (26$$

for small values of x.

and $$E = 2I(o)\ m\ (S\ b\ X)^{\frac{1}{2}} \qquad (27$$

for larger values of x.

This is the same result as obtained in 1.3.1.1, and again there are the two different cases, one for the pure gas in which b varies with pressure, and one

for a gas made up to a constant total pressure with a non-absorbing constituent when b is constant.

In the latter case x varies directly with pressure and therefore at low pressures x is small. At larger values of x the relationship is

$$E = I\ (o)\ m2\ (S\ \delta\ p_T\ p\ l)^{\frac{1}{2}} \qquad (28$$

where δ is the line width of the absorbing gas per atmosphere of non-absorbing gas in collision with the absorbing molecules, the total pressure being p_T

All other factors being constant it follows that E is proportional to $p^{\frac{1}{2}}$.

In the case of the pure gas, x is constant in the region where collision broadening is completely dominant over the other broadening processes, and this extends to very low pressures at room temperature. It follows that f(x) is also constant and that E is therefore proportional to pressure. Except for the low pressure influence of Doppler broadening this treatment would predict a linear region extending to almost zero pressure. This conclusion will be exam-:ined in more detail when experimental results are available.

1.3.1.2.2.

When $b \ll d$, but X is considerably bigger than in 1.3.1.2.1., the range of integration in equation (23 is effectively restricted to large values of y.

Since $\lim_{y\to\infty} J_o(iy) = \exp(y)\,\frac{1}{(2\pi y)^{\frac{1}{2}}}$

and $\sinh\beta = \beta$, and $\cosh\beta - 1 = \frac{\beta^2}{2}$ for small β,

then $T_R = \beta\int_{\frac{SX}{d\beta}}^{\infty}\left[\exp(-\frac{y\beta^2}{2})\right]\frac{dy}{(2\pi y)^{\frac{1}{2}}}$

Now the error integral is defined as

$$\Phi(y) = \frac{2}{\pi^{\frac{1}{2}}}\int_o^y \exp(-t^2)\,dt \quad ; \Phi(\infty) = 1,$$

therefore

$$T_R = 1 - \Phi\left(\frac{SX\beta}{2d}\right)^{\frac{1}{2}}$$

It follows that

$$E = I(o)\,\Delta\omega\;\Phi\left[\frac{(\pi SbX)^{\frac{1}{2}}}{d}\right] \qquad (29$$

for large values of X

It is seen from the above that the simple, partially qualitative treatment of a single line, carried out in 1.3.1.1, led to essentially the same relationships.

The importance of these considerations is the prediction of the variation of the energy absorbed with the reduced pathlength, and the fact that from this variation at low reduced pathlengths a very good approximation of the intensity of absorption can be obtained.

$$\text{i.e.} \quad A = \frac{\lim_{X\to o} E}{I(o)X} \qquad (30$$

where $A = m\,S$

As an analysis of average line-shapes and line-

widths, however, this treatment suffers from the fact that no account is taken of the varying intensities of the lines in the band, and it is this variation with which the next two sections deal.

1.3.1.3 Theory of Matheson

One of the first attempts to elucidate the dependence of the energy absorbed on the reduced pathlength was that of Matheson in 1932 (23) when he used the old quantum theory to assess the varying intensities of the lines. In essence this is as accurate as the modern quantal treatment, and lends itself to more rapid use with most molecules which do not contain a Q branch. His theory is detailed here with several small modifications.

Referring to one line, say, the j^{th} line, in one branch of an absorption band,

$$k(\nu)_j = \frac{k(o)_j \; b^2}{b^2 + (\nu - \nu_j)^2}$$

and $$E_j = I(o) \int \left[1 - \exp\left(-k(\nu)_j X\right)\right] d\nu$$

assuming I(o) constant over the frequency range of the line.

Thus $$E_j = I(o) \sum_{n=1}^{\infty} \frac{(-1)^{n-1}}{n!} X^n \int k(\nu)_j^{\,n} d\nu \qquad (31$$

Assuming that all lines have the same line-width, and that the relative intensities of the lines in a band branch are given by

$$k(o)_j = c \; j \exp\left(-\sigma j^2\right) \qquad (32$$

where $\sigma = \frac{h^2}{8\pi^2 IkT}$ with I as the moment of inertia in the simplest case of a molecule with only one moment of inertia.

it follows that $\sum_{j=1}^{\infty} k(o)_j = K$, referring to one branch of the band.

Replacing the summation by an integral from 0 to ∞ over dj,

$$K = \frac{c}{2\sigma}$$

and $k(o)_j = 2K\sigma j \exp(-\sigma j^2)$ (33

Now $E = \sum_{j=1}^{\infty} E_j$

and therefore $\frac{E}{I(o)} = \sum_{n=1}^{\infty} \frac{(-1)^{n-1}}{n!} X^n \int k(\nu)_j^{\,n} \, d\nu$

where $\int k(\nu)_j^{\,n} \, d\nu = k(o)_j^{\,n} \int_{-\infty}^{\infty} \frac{b^{2n}}{(b^2+t^2)^n} \, dt$

with $t = \nu - \nu_j$

The evaluation of the right-hand side of this equation by standard forms leads to

$$\frac{E}{I(o)} = \sum_{n=1}^{\infty} \pi b \frac{(-1)^{n-1}}{n!} \frac{(2n-3)(2n-5)\text{-----}1}{2^{n-1}(n-1)!} \sum_{j=1}^{\infty} X^n k(o)_j^{\,n} \qquad (34$$

Substituting equation (33 in (34, and replacing the summation over j by an integration gives

$$\frac{E}{I(o)} = \sum_{n=1}^{\infty} \pi b \frac{(-1)^{n-1}}{n!} \frac{(2n-3)(2n-5)\text{-----}1}{2^{n-1}(n-1)!} (2XK\sigma)^n \int_0^{\infty} j^n \exp(-\sigma n j^2) \, dj$$

Using standard forms for n odd and for n even

$$\int_0^\infty j^n \exp(-\sigma n j^2)\,dj = \frac{(\frac{n-1}{2})!}{2(\sigma n)^{\frac{n+1}{2}}} \quad \text{for } n \text{ odd}$$

$$= \frac{(n-1)(n-3)\text{----}1\ \pi^{\frac{1}{2}}}{(2\sigma n)^{\frac{n}{2}}\ 2(\sigma n)^{\frac{1}{2}}} \quad \text{for } n \text{ even.}$$

Thus

$$\frac{E}{I(o)} = \sum_{n=1}^{\infty} g_n X^n \qquad (35$$

where $g_n = \pi b \frac{(-1)^{n-1}}{n!} \frac{(2n-3)(2n-5)\text{----}1}{2^{n-1}(n-1)!} (2K\sigma)^n \frac{(\frac{n-1}{2})!}{2(\sigma n)^{\frac{n+1}{2}}}$ for n odd

and $g_n = \pi b \frac{(-1)^{n-1}}{n!} \frac{(2n-3)(2n-5)\text{----}1}{2^{n-1}(n-1)!} (2K\sigma)^n \frac{(n-1)(n-3)\text{---}1\ \pi^{\frac{1}{2}}}{(2\sigma n)^{\frac{n}{2}}\ 2(\sigma n)^{\frac{1}{2}}}$

for n even.

Matheson then introduced the model of a beam of radiation producing heat along its length in an absorption cell. If the total length of the beam is 2a and the heat produced for any length q is con-:sidered, it is found (see original paper) that the volume change, to a first approximation, produced in the gas is

$$\Delta v = \frac{\epsilon(q)\ (2aq - q^2)}{6\rho T} \qquad (36$$

where $\epsilon(q)$ is the strength of the heat source at a point a distance q along the beam,

ρ is the thermal conductivity,

and T is the temperature,

and $\epsilon(q) = \frac{\delta E(q)}{\delta q}$ where E(q) is the energy ab-:sorbed in the length q.

Now $E(q) = I(o) \sum_{n=1}^{\infty} g_n \left(\frac{qX}{2a}\right)^n$ (37

where X is replaced by $\frac{qX}{2a}$,

and therefore $\frac{\delta E(q)}{\delta q} = I(o) \sum_{n=1}^{\infty} g_n \left(\frac{X}{2a}\right)^n nq^{n-1}$ (38

Substituting equation (38 in (36 and integrating over all values of q from 0 to 2a yields

$$\Delta V = I(o) \sum_{n=1}^{\infty} g_n X^n \frac{2na^2}{\rho T} \frac{1}{(n+1)(n+2)} \quad (39$$

and gives the final equations as:

$$\Delta V = \frac{I(o)\pi ba^2}{6\rho T\sigma^{\frac{1}{2}}} \sum_{n=1}^{\infty} U^n \frac{3\left(\frac{n-1}{2}\right)!\,(2n-3)(2n-5)\text{-----}1}{2^{n-2}\, n\, \frac{n-1}{2}!\,(n-1)!\,(n+2)!} \quad (40$$

for n odd

$$= \frac{I(o)\pi ba^2}{6\rho T\sigma^{\frac{1}{2}}} \sum_{n=1}^{\infty} h_n U^n$$

and $$\Delta V = \frac{I(o)\pi ba^2}{6\rho T\sigma^{\frac{1}{2}}} \sum_{n=1} U^n \frac{3\pi^{\frac{1}{2}}(2n-3)(2n-5)\text{----}1\ (n-1)(n-3)\text{---}1}{(n+2)!\,(n-1)!\,n^{\frac{n-1}{2}}\,2^{\frac{3n-4}{2}}}$$

for n even. (41

where $U = 2KX(\sigma)^{\frac{1}{2}}$

When Matheson developed the above theory he was interested in finding the change in volume produced in a system which explains his choice of calculation. It is retained in this form for similar reasons although his heat conduction theory is approximate and, as will be shown later, the assumption that all absorbed energy is converted to heat energy is only valid under certain conditions.

The procedure which is followed to obtain values for the intensity of absorption and the average line-width in the band is to plot the logarithm of $\sum_{n=1}^{n=f} h_n U^{n-1}$ against the logarithm of U for various values of U and for an appropriately chosen value for f. This curve is fitted to an experimental one of the logarithm of absorbed energy divided by reduced pathlength against the logarithm of the reduced pathlength. Although equations (40 and (41 as derived above are different from those in Matheson's original paper, the logarithm plot takes exactly the same form for both results.

From the low pathlength asymptote the value of the intensity follows from

$$A = \lim_{x \to o} \frac{E}{I(o)X}$$

The curve-fitting allows the ratio of U:X to be found, and since $U=2KX(\sigma)^{\frac{1}{2}}$ and $A=2\pi bK$, a good approximation of the average line-width is obtained.

The advantage of the above relationships, which are similar to those of Ladenburg and Reiche (section 1.3.1.2), lies in the fact that, without the com-:plexities of section 1.3.1.4, account is taken of the varying intensities of the lines in a band branch.

1.3.1.4. Theory of Penner.

This treatment, similar in purpose to 1.3.1.2 and 1.3.1.3, takes account fully of the variation of the line intensities in the band. The method used is only indicated here and a full treatment is to be found in references (24,(25) and (26)

In terms of wavenumbers and for the transitions as indicated,

$$k(\omega) = \frac{b}{\pi} \sum_j \frac{S^{o\rightarrow 1}_{j\rightarrow j-1}}{(\omega-\omega^{o\rightarrow 1}_{j\rightarrow j-1})^2 + b^2} + \frac{S^{o\rightarrow 1}_{j-1\rightarrow j}}{(\omega-\omega^{o\rightarrow 1}_{j-1\rightarrow j})^2 + b^2} \qquad (42$$

where

$$S^{o\rightarrow 1}_{j\rightarrow j-1} = A \frac{\omega^{o\rightarrow 1}_{j\rightarrow j-1}}{\omega^*} j \frac{\left[\exp.\left(-\frac{E(o,j)}{kT}\right)\right]}{Q(T)}$$

and similarly for the $j-1\rightarrow j$ transition.

A is the intensity of the band,

ω^* is the wavenumber corresponding to the forbidden transition $j=o\rightarrow j=o$ and $n=o\rightarrow n=1$,

$E(n,j)$ represents the energy of the n^{th} vibrational and j^{th} rotational level, and

$Q(T)$ is the complete internal partition function at temperature T.

The case considered is for non-overlapping lines, when for each line

$$A_R \Delta\omega = 2\pi b \sum_j x_j \exp(-x_j) \left[J_o(ix_j) - iJ_1(ix_j)\right] \quad (43$$

where A_R is the total fractional absorptivity;

$\Delta\omega$ is the bandwidth,

and $x_j = \frac{S^{o\rightarrow 1}_{j\rightarrow j-1} X}{2\pi b}$ or $\frac{S^{o\rightarrow 1}_{j-1\rightarrow j} X}{2\pi b}$ depending on the transition.

By introducing a value for A, known from experi-:ment, the intensities of the isolated lines are cal-:culated (1), and thus the quantity $A_R \Delta\omega$ found. To ascertain the value of the line-width, various estimates of it are introduced into equation (43, until a fit with the experimental data is obtained. This gives a very good lower limit for the average value of the line-width (only a lower limit because the effect of overlapping is ignored).

1.3.1.5. <u>The Effect of Doppler Broadening</u>

The positions enumerated in 1.3.1.2, 1.3.1.3 and 1.3.1.4 deal only with lines which are broadened by molecular collisions, and, as has been stated, the Doppler effect acquires significance at high tempera-:tures and low pressures.

An approach involving both dispersion and Doppler broadening is detailed by Penner(1). Although there are many theoretical complexities, the relationships are graphed in a readily available form by Van der Held

(1)(27). In these theoretical graphs the energy ab-:sorbed is plotted as a function of reduced pathlength for different values of the ratio $b_c : b_D$ where these symbols have their previous meaning.

A statement of the results of Plass and Fivel is very useful (16)(28). This can best be done by giving two equations in which the absorption coefficient is the result of both collision and Doppler broadening, and is applicable for $(\nu-\nu_o) \gg b$.

$$k(\nu) = \frac{Sb_c}{\pi(\nu-\nu_0)^2}\left[1 + (\frac{3}{2a^2} -1)(\frac{b_c}{\nu-\nu_o})^2 + \{\frac{15}{4a^4} - \frac{5}{a^2}+1\}\{\frac{bc}{\nu-\nu_o}\}^4 + \text{----}\right.$$

where $a = (\ln 2)^{\frac{1}{2}} \frac{bc}{b_D}$ and the other symbols have their usual meaning.

$$\frac{E(\text{total})}{E(\text{collision})} = 1 + \frac{3}{16}a^{-2}x^{-1} + \frac{45}{512}a^{-4}x^{-2} - \frac{3}{32}a^{-2}x^{-2} + \text{----} \qquad (44$$

where $x = \frac{SX}{2\pi b}$

1.3.1.6 Splitting of lines

In the foregoing discussion it has been assumed that P and R branches are composed of single lines with a definite shape. Although this is true at reasonable pressures when a broadening of very fine structure takes place, at lower pressures each line is split into several components. This is due to the Coriolis interaction with neighbouring absorption bands. Perturbations are especially high for combin-

:ation and overtone bands, but in, for example, the case of methane this splitting is readily observed for the ν_4 band due to its proximity to the ν_2 band. In an extremely accurate measurement on the ν_3 band of CH_4(29) using a grating spectrometer of resolution 0.02 to 0.03 cm^{-1} in the required region, it was found that each line was split into four or five sub-levels and pointed out that an extension of present theory was necessitated to take into account second and third order effects.

This means, of course, that although line-width is a useful and valid concept for lines which are broadened sufficiently it does not give in any way full details of the band structure.

1.3.1.7 Q branch

Many fundamental bands of diatomic and polyatomic molecules possess Q branches, and because of the extensive overlapping of the lines in this branch a separate treatment of the energy absorbed is usually required.

The extent of the overlapping is seen by giving the example of a spherical top molecule. The series of lines in the P and R branches is given by

$$\nu = \nu_0 + (B^1 + B^{11} - 2B^1\zeta)m + (B^1 - B^{11})m^2$$

where ν_0 is the zero line frequency,

m = J+1 for the R branch, and m = -J for the P branch,

ζ is the Coriolis coupling factor,

and B^{1} and B^{11} are the rotational constants for the ground and excited states.

This is to be compared with the Q branch series

$$\nu=\nu_{o}+ (B^{1}-B^{11})J + (B^{1}-B^{11}) J^{2}$$

Since values of $(B^{1}-B^{11})$ are usually of the order $0.001cm^{-1}$ (in some cases they are much higher) it is obvious that low pressures are needed before even partial splitting of the Q branch occurs.

Continuing with the example of a spherical top molecule, the importance of considering the Q branch is seen from the fact that, approximately, the intensity of each branch is the same. (15) For a symmetric top the relative intensities are very dependent on the ratio of the two moments of inertia. It is obvious from this that any band containing a Q branch demands a separate treatment to give a correct relationship between energy absorbed and reduced pathlength. Various methods have been attempted and some of these are very briefly indicated here.

1.3.1.7.1.

From section 1.3.1.2 it can be assumed that the Q branch is made up of a number of lines each contri-:buting in a similar way to the individual lines in the P and R branches. Equation (27 is then used in a

straightforward manner with a value for m which in-:cludes the number of lines in the Q branch. This treatment obviously leads to rather big errors, although it may be meaningful, in the case of spherical top molecules, when the relative intensi-:ties of the branches are very similar, and espec-:ially in those cases of study on a band of a pure gas with a large value for $B^{1}-B^{11}$.

1.3.1.7.2

The analysis of 1.3.1.4 can be extended by replacing equation (42 by

$$S^{o\rightarrow 1}_{j\rightarrow j-1}=A\,\frac{\omega^{o\rightarrow 1}_{j\rightarrow j-1}}{\omega^{*}}\,\frac{(j-D)(j+D)}{j}\left[\exp\frac{(-E(o,j)}{kT}\right]\quad Q(T)^{-1}$$

where D is the quantum number measuring the component of electronic angular momentum about the internuclear axis for the simplest case of a diatomic molecule and which equals zero for a molecule without a Q branch. (24). A good fit with experimental data can be ob-:tained by allowing an empirical constant to correct for the close spacing, or overlapping, of the lines in the Q branch.

1.3.1.7.3

One approach to this problem (22) is to derive an expression for the absorption coefficient over the Q branch, and by numerical integration of the

resultant area, for varying values of the reduced pathlength, find the curve of energy absorbed against pathlength. This is then additive to the absorption of the P and R branches. The whole procedure is repeated for different values of the band intensity and the line-width until a fit with the experimental data is obtained.

This procedure has also been discussed (30) in relation to low pressure measurements when both collision and Doppler broadening contribute to the Q branch shape.

This section, 1.3.1, on the spectroscopic approach to absorption is far from being fully descriptive of the many complexities in this subject, and is designed merely to indicate the possible evaluation of intensity from low reduced pathlength measurements and to assess the possibilities of estimating the change of collisional line-width with pressure. The various theories on evaluating average values for the line-widths have been necessitated by the scarcity of measurements on individual lines. Where these have been measured (16)(31)(32) much more detail was obtained in terms of the variation of the line-width in a band branch, although experimental difficulties (see section 1.4) resulted in the individual line-widths being very approximate.

1.3.2 Energy Transfer involved in Absorption and Resulting Processes.

The model which is used here is that of an infra-red active gas gaining internal energy by the absorption of radiation quanta and losing this energy by several de-activating processes.

The Einstein coefficient for induced absorption, say of a vibrational quantum, B_{ol}, is defined in such a way that the probability of a transition from the lower state o with energy E(o) to the state 1 with energy E(1) in unit time in a radiation field of spectral density $\rho(\nu)_{ol}$ at the frequency ν_{ol} is $B_{ol}\ (\nu)_{ol}$.

For a black-body radiating system at the temperature T,

$$\rho(\nu)_{ol} = \frac{8\pi h\nu_{ol}^{3}}{c^{3}} \quad \frac{1}{\left[\exp\left(\frac{h\nu_{ol}}{kT}\right)-1\right]}$$

where the symbols have their usual meaning.

B_{lo} is the coefficient for induced emission and

$$g_o B_{ol} = g_l B_{lo} \qquad (45$$

where g_o and g_l are statistical weights and are usually effectively equal.

A_{lo} is the coefficient for spontaneous emission and

$$A_{lo} = \frac{8\pi h\nu_{ol}^{3}}{c^{3}} B_{lo} \qquad (46$$

It therefore follows that in equilibrium and in the absence of any other transfer process

$$N_o B_{ol} \rho(\nu)_{ol} = N_1 (A_{1o} + B_{1o} \rho(\nu)_{ol})$$

where N_o and N_1 are the number of molecules in the lower and upper state respectively.

Except for close energy levels, $N_o \gg N_1$, and the number of transitions from state o to state 1 in unit time can be written

$$N(tr) = N B_{ol} \rho(\nu)_{ol} \qquad (47$$

where N is the number of molecules per cubic centimetre.

In the practical case of a pathlength of gas absorbing over a range of frequencies the number of transitions as defined above varies along the path-:length, as has been discussed in terms of energy absorbed in the previous sections. The overall number of quanta absorbed (or the number of trans-:itions involved) is given for $\frac{E}{V.h\nu_{ol}}$ per unit volume and time.

Here E is the energy absorbed for the whole absorption cell which has a volume V.

The relationship between the Einstein coeffic-:ients and the band intensity of absorption (1) is given by

$$A^1 = N_o B_{ol} (1 - \frac{N_1}{N_o} \frac{g_o}{g_1}) \frac{h\nu_{ol}}{C}$$

which for $g_o = g_1$ and $N_o \gg N_1$ reduces to

$$A^1 = N B_{ol} \frac{h\nu_{ol}}{C} \qquad (48$$

where A^1 is a pressure dependent intensity in units $cm^{-1}sec^{-1}$

In an absorption cell under constant illumination after a short time a steady state is set up with three processes involved; the absorption of radiation, the deactivation of this internal energy and the loss of this deactivated energy as heat to the walls of the cell. The following equilibrium then obtains:

E(absorbed) = E(deactivated) = E (lost to walls)

The position of E(absorbed) has been examined, and it is now valuable to discuss the various methods of de-activation, viz. molecule-molecule collisions involving vibrational-translational energy transfer, molecule-wall collisions with loss of excitation energy, spontaneous emission and induced emission.

1.3.2.1 Molecule-molecule Collisions.

The total number of collisions of this type which involve an excited molecule

is $N_e ZV$

where N_e is the number of excited molecules per c.c.,

Z is the number of collisions made by each molecule per second,

and V is the volume of the cell.

If p_{1o} is the probability of vibrational-translational energy transfer per collision then the total amount of energy lost is

$$N_e Z V p_{1o} h\nu_{1o} \quad \text{per second} \qquad (49$$

p_{1o} is related to the relaxation time of the process (33), and this relationship for the simple case of one excited mode is

$$p_{1o} = \frac{1}{Z\tau\left[1-\exp(-\frac{h\nu}{kT})\right]}$$

where τ is the relaxation time for the particular mode of vibration con-
:sidered.

Calculation of Z can be most easily based on the kinetic theory expression for a gas of rigid spheres

$$Z = 4 N\sigma^2 \left(\frac{\pi kT}{m}\right)^{\frac{1}{2}}$$

where m is the mass of the molecule, and σ is the collision diameter.

1.3.2.2 Molecule-wall collisions

The total number of collisions between excited molecules in the gas phase and the walls of the cell is

$$\frac{1}{4} N_e \bar{c} A$$

where $\bar{c}$ is the average velocity of the gas molecules, and A is the inside sur-
:face area of the cell,

and therefore the energy deactivated in this process is

$$\frac{1}{4} N_e \bar{c} A p_{10}(wc) h\nu_{10} \qquad (50$$

where p_{10} (wc) is the probability per collision of transfer of energy to the walls.

At this stage it is helpful to estimate the ratio of processes 1.3.2.1 and 1.3.2.2 by making calculations based on the orders of magnitude of the various quantities.

$\bar{c} = 6 \times 10^4$ cm sec^{-1} ; $Z = 10^{10}$ sec^{-1} ;

$\frac{A}{V} = \frac{1}{2}$, this ratio is low since only the surface area in direct contact with the excited molecules in the beam of radiation need be included;

$\frac{p_{10}(wc)}{p_{10}}$ can be estimated by considering three main factors:

a) During one theoretical collision with the wall an effective number of collisions occur due to the roughness of the surface. This factor can be deduced from a knowledge of the appropriate accommodation coefficient and is usually of the order of 5.

b) A difference exists in mass between the gas and wall molecules.

c) The relative velocity of a molecule-molecule collision is higher than that of a wall-molecule collision.

From these $\frac{p_{10}(wc)}{p_{10}}$ can be estimated as being not greater than 10.

An order of magnitude calculation therefore results in the ratio of equation (50 to equation (49 being approximately 10^{-5} at one atmosphere pressure and 10^{-3} at one hundredth of an atmosphere. This result indicates that, for the model chosen, wall collisions play a negligible part in deactivating ex-:cited molecules except at extremely low total pressures.

1.3.2.3 Spontaneous Emission

From equations (46 and (48 a value for A_{10} can be derived dependent on the intensity and frequency of the absorbing transition, but independent of the number of molecules present per unit volume.

The deactivation of vibrational energy per second in this case is

$$N_e A_{10} V h\nu_{10} \qquad (51$$

However, in the steady state, since this re-emitted energy has the same emission spectrum as the absorption spectrum of the gas, a considerable re-absorption is to be expected.

Thus the deactivation of vibrational energy per

second for steady state conditions changes to

$$N_e A_{10} V h\nu_{10}(1-g) \qquad (52$$

where g is the fraction of re-emitted energy which is re-absorbed.

This fraction depends on the gas and on the effective reduced pathlength of re-absorption and will be discussed at some length in a later section.

1.3.2.4 Induced Emission

The radiation field can induce a loss of quanta in excited molecules, the probability of this occuring being given by $B_{10}\rho(\nu)_{01}$ sec^{-1}.

From equations (45 and (46,

$$A_{10} = \rho(\nu)_{01} B_{10} \left[\exp\left(\frac{h\nu_{01}}{kT}\right)-1\right] \qquad (53$$

assuming black-body properties, and therefore, for energy levels separated by more than $1000cm^{-1}$, induced emission as a process of losing energy is negligible compared to spontaneous emission.

Having considered the four processes involved in deactivation it is now possible to set up equa-:tions for the overall equilibrium between the energy absorbed and the energy deactivated. Processes 1.3.2.2 and 1.3.2.4 are ignored.

When no external radiation beam is involved and the gas is in thermal equilibrium,

$$NZp_{01} + y = N_e^{1}(Zp_{10}+(1-g)A_{10}) \qquad (54$$

considering unit volume and time.

Here, NZp_{01} is the number of transitions produced by thermal excitations;

$$p_{01}=p_{10}\exp\left(-\frac{h\nu}{kT}\right) ;$$

and y is the number of transitions produced by the surrounding radiation field of walls, etc.

When a continuous source of external radiation is illuminating the gas, and a steady state has been attained,

$$NZp_{01}+y+\frac{E}{V.h\nu_{01}} = N_e(Zp_{10}+(1-g)A_{10}) \qquad (55$$

where E is the energy absorbed from the external source.

Therefore the change in the system due to the absorption is,

$$\frac{E}{V.h\nu_{01}} = \Delta N_e\left[Zp_{10}+(1-g)A_{10}\right]$$

where ΔN_e is the change in the number of molecules in state 1

The ratio of Zp_{10} : $(1-g)A_{10}$ depends on the pressure of the system, since Z is directly proportional to the number of molecules in unit volume, and on the particular values of p_{10} and A_{10}. This

is discussed in full later when it is allied to measurements of the energy absorbed which only record the translational energy produced.

The above analysis only deals with transitions between states 0 and 1 and would be complicated if the conditions of experiment allowed transitions 1 to 2 to take place. However, with a normal value for the volume density of radiation and thus, for $N_0 \gg N_1$, transitions to the first overtone occur only to a negligible extent.

1.4 Measurement of Intensities.

As was pointed out in equation (30, extra-:polation of the energy absorbed to zero optical pathlength presents a method of measuring the inten-:sity of an absorption band which is always theoreti-:cally applicable. This also applies to the extra-:polation of the corresponding emission. For this type of measurement, involving very small values of the reduced pathlength, the infra red spectrometer which is the only instrument so far used to any ex-:tent has serious limitations. These can be summarised as follows.

a) The finite resolving power of the spectrometer

The equation which is used for straightforward spectrometer measurements is

$$A = \frac{1}{X}\int_{band} \ln\frac{I(o)}{I}\, d\nu$$

The best prism spectrometers have a slit-width of around 1 to 2cm^{-1} and, considering the line-width to be 0.1$cm^{-1}atm^{-1}$, it follows that by simply inte-:grating over the band graphically the actual value obtained is

$$B = \frac{1}{X}\int_{band} \ln\frac{T(o)}{T}\, d\nu$$

where T(o) and T are values measured by the instrument averaging the true mono-:chromatic values I(o) and I over the slit-width.

Although this problem has been much discussed (34)(35)(36), and attempts made to calculate the spectrometer slit-function and therefore the error involved (1)(37), an instrument of infinite resolu-:tion is needed to give perfect results.

When a spectrometer employing a grating is used resolution as high as 0.03 cm^{-1} has been attained, but even here (16) the true line shape, especially near the line centre, is considerably modified. At pressures below an atmosphere, when splitting of the Q branch and even if the individual P and R lines occurs, then the approximation involved in averaging I(o) and I over the slit-width is of even more importance.

b) Losses due to Lack of Sensitivity

The pattern of vibration-rotation bands with their many overlapping wings means that in a graphical integration it is assumed that the instru-:ment can measure the very small differences between I(o) and I in the absorbing region outside the in-:tense lines. In these wings the weak signals pro-:duced are not easily distinguished from those associated with random noise. Since the frequency range in which intense absorption takes place is very small compared to the total band-width, even for pressures of one atmosphere, a correction factor

for wing-absorption is both necessary and difficult to ascertain. To assess this correction assumptions must be made about the line shape and as has previously been stated, the shape in the wings is more often governed by specific intermolecular forces than by the simple dispersion relationship.

To cope with these difficulties methods have been devised using a spectrometer to minimise the effect of averaging and the loss in the wings.

1.4.1 Pressure Broadening

This technique (34)(38)(39)(40)(41), by which the majority of infra-red intensities have been measured, is based upon the use of high pressures of a non-absorbing, foreign gas to broaden the rotational lines of the absorbing molecules. At sufficiently high pressures the absorption coefficient becomes a slowly varying function of the wave-number, and therefore graphical integration over the band is much more justified. By doing this for several partial pressures of the absorbing gas and extrapolating to zero optical pathlength a further improvement in the approximation is obtained.

The method has also been used with self-broadening (42) when very high pressures of the absorbing gas are used in a cell of small optical pathlength. The actual pathlength is varied and a similar extrapolation to above is applied.

However, with pressure-broadening several possible errors exist:-

a) Although the assumption of a constant absorp-:tion coefficient over the slit-width is well justified for pressures in excess of twenty atmospheres and for reasonable resolution, many measurements have been recorded for pressures below this value and are therefore of dubious value.

b) Considerable absorption occurs in the wings of a band which increases the higher the pressure of inert gas used. It therefore follows that correction factors, of a necess-:arily approximate nature, need be applied because of losses due to instrumental lack of sensitivity.

c) It is assumed by many authors that high pressure has no effect on the value of the intensity. For polar molecules this has been shown to be untrue (43)(44)(45) and a considerable percentage effect is observed at pressures above fifty atmospheres. Pressure induced absorption has also been observed for normally inactive gases such as nitrogen and hydrogen (45) which are often used for broadening purposes.

d) Many operational difficulties arise from working at high pressures, all of which are

probable sources of error. As well as cell construction problems, these include incomplete mixing in the lines leading to the cell and the selective, pressure-induced adsorption of polar molecules on the walls. Both of these lead to erroneous values for the amount of absorbing gas in the path of the radiation beam.

Having mentioned possible sources of error in the pressure-broadening technique it is of interest to give a table listing the results on the fundamentals of nitrous oxide. The pressure-broadening method was used in each case.

Table I

Band (cm^{-1})	Intensity ($cm^{-1}sec^{-1} \times 10^{10}$ at NTP) with references above.			
	(46)	(47)	(48)	(49)
1285	1150	734	-	653
589	120	62.5	-	60.5
2224	5600	4950	4850	2990

1.4.2 Curves of Growth

From measurements with the spectrometer of the integrated absorptivity, defined as

$$\int_{\omega_1}^{\omega_2} A_\omega \, d\omega = \int_{\omega_1}^{\omega_2} \left[1 - \exp\left(-k(\omega)X\right)\right] \, d\omega$$

in terms of

wavenumbers, a value for the intensity can be found for sufficiently low pathlengths of absorption. Although with a spectrometer this region is not attainable for previously stated reasons, the method consists in predicting from theoretical considerations the form of the low reduced pathlength extrapolation from higher pathlength measurements. From this extra-:polation the limiting gradient gives the intensity of absorption. The general principles of the method, which has been used both for bands (22) and for in-:dividual lines (16), were enumerated in section 1.3.1.2.

However, although this procedure is potentially powerful, it is limited by the need to know the structure of a band in great detail. This is parti-:cularly so when a band with a Q branch (22) is being studied, and the difficulties encountered are reflec-:ted in the small number of results obtained by this technique.

1.4.3 Other Methods

Nearly all intensity work has been done by the above two methods but there remain a few measurements carried out without the use of a spectrometer.

1.4.3.1 Infra-red Dispersion Studies

The theory of dispersion in the infra-red region

reveals that the dependence of the square of the index of refraction on the wavelength is partially governed by the intensity of absorption of the vib-:rational modes of the molecule. Instruments involv-:ing a monochromator and a refractometer linked to-:gether have been used to study this dependence and thus to derive a value for the intensity. This method is beset by many difficulties of theoretical interpretation, whilst the apparatus required is ex-:tremely elaborate. In spite of this Rollefson and other workers (50)(51)(52) have obtained results for a few molecules in general agreement with the values of pressure-broadening measurements.

1.4.3.2 Direct Measurement of the Energy Absorbed or Energy Emitted

The attraction of any method which offers a direct measurement of the absorbed energy lies in the fact that, with incident radiation which is filtered to a fairly narrow band-width, the absorbing band of the gas in question is allowed to act as its own mono-:chromator. The total energy absorbed in the filtered region can therefore be measured without any of the difficulties encountered with a spectrometer. Although the principles of pressure-broadening and curves of growth could still be used, the much more straightforward procedure of measuring at very low

values of the reduced pathlength and extrapolating to zero pathlength, a technique with no theoretical difficulties, is very attractive. This means that the sensitivity of the measuring device must be high. An evaluation of the incident energy with similar accuracy is also demanded.

All this is also true about measuring the energy emitted by a gas and, before discussing two methods applied to the direct measurement of absorbed energy, it is interesting to look at a rather novel procedure for determining the coefficient of spontaneous emission and therefore finding a value for the intensity.

1.4.3.2.1 Gerlovin's Method (53)

A signal due to the spontaneous emission of the 4.3μ band of carbon dioxide, the gas being contained in a small cell, was measured using an appropriate filter and a cooled lead telluride photoconductor. The size of this signal for very low partial pressures of carbon dioxide in nitrogen or oxygen was given by

$$M_1 = RA_{10}h\nu_{01}N_1 l F_1 F_2$$

where R is a proportionality constant determined by the apparatus,

N_1 is the number of excited molecules,

l is the cell length,

F_1 is the area of the cell window,

and F_2 is the effective surface area of the receiver.

On placing a black body, which had the same radiating surface area as the cell window, at the same distance from the receiver a signal M_2 was ob-
:tained.

$$M_2 = R\sigma T^4 \propto F_1 F_2$$

where σ is the Stefan-Boltzmann constant and T the temperature;

and $$\propto = \frac{\int_0^\infty f_1(\nu) f_2(\nu) f_3(\nu) d\nu}{\int_0^\infty f_1(\nu) d\nu}$$

Here $f_1(\nu)$ is the spectral intensity dis-
:tribution of the black-body radiation,

$f_2(\nu)$ is the spectral sensitivity of the receiver,

and $f_3(\nu)$ is the transmittance of the filter used.

From M_1 and M_2 it follows that

$$A_{10} = \frac{M_1 \sigma T^4 \propto}{M_2 h \nu_{01} N_1 l}$$

Since for the particular band considered the probability of collisional excitation is much greater than the probability of spontaneous emission, the relationship

$N_1 = N \exp\left(-\frac{h\nu_{01}}{kT}\right)$ can be used

where N is the number of mole-
:cules per unit volume.

Thus $$A_{10} = \frac{M_1 \sigma T^4 \alpha}{M_2 l h \nu_{01}} N \exp\left(-\frac{h\nu_{01}}{kT}\right)$$

With both the gas cell and the black-body at room temperature, the receiver cooled to the tempera-:ture of liquid air, the cell dimensions so arranged that effectively no radiation fell on the receiver from the walls and an accurate system of amplification in use a result was obtained for A_{10} of approximately 350 sec^{-1}. This result is about 20% lower than that expected from measurements of the intensity.

The difficulty in dealing with stray radiation would seem to be a limiting factor in the accuracy of such measurements.

1.4.3.2.2 Method of Veingerov and Slobadskaya (54)

The principle used was the measurement of the absorbed energy at a value of the reduced pathlength such that

$$A = \lim_{x \to o} \frac{E}{I(o)X}$$

The technique for measuring this energy was the optic-acoustic effect. If an absorption cell is built in two parts separated by the diaphragm of a microphone, a pressure rise will occur on one side when the gas in this part absorbs infra-red radiation from an external source. This is dependent on the transfer of energy from the excited vibrational mode

of the molecule to the translational energy of the gas by collision, and it was assumed that this was a full account of all energy transfer in the system. If the incident radiation beam is chopped at a certain frequency a sound wave is set up in the gas and an EMF developed in the microphone. This EMF is directly proportional to the energy absorbed.

The radiation was initially passed through a slit sufficiently wide, 2C, to ensure that the whole absorption band was included and thus

$$aV_1 = E_1 = I(o)XA$$

where a is a coefficient of proportionality, and V_1 is the EMF produced.

A second measurement was taken with a narrower width of the monochromator slit, 2D, and with the concentration of the gas claimed to be such as to effect complete absorption. Thus

$$aV_2 = E_2 = I(o)\int_{\nu_o-D}^{\nu_o+D} d\nu = I(o)2D$$

Therefore $A = \frac{2D}{X} \frac{V_1}{V_2}$

It was suggested that an alternative method of excluding the incident energy from the final equation was by making use of a stronger absorption band in the gas, when the assumption that all the energy was absorbed would be more realistic.

The method was tried out on the 2.7μ band of carbon dioxide. With a partial pressure of 1.2% carbon dioxide in the cell, the result obtained was 5×10^{12} $cm^{-1} sec^{-1} atm^{-1}$. This is larger by a factor of four than the usually accepted result, and the reasons for error can be summarised as follows

a) Instrumental factors such as the lack of linearity in the diaphragm response were not considered.

b) The assumption was made that, with a partial pressure of 1.2% carbon dioxide, the linear region of absorption was reached. This should have been validated by taking at least two measurements with different partial pressures.

c) By far the biggest source of error was in the measurement of the incident energy. With a pressure of only one atmosphere of carbon dioxide not nearly all the incident energy over the slit, 2D, would be absorbed. This would lead to a very high result for the intensity as, indeed, was obtained.

1.4.3.2.3 Matheson's Method (23)

The basis of this method is once more the direct measurement of absorbed energy, with small partial pressures of carbon monoxide being used in

an atmosphere of purified air. The pressure of carbon monoxide was varied over a considerable range in an effort to attain the appropriate region of absorption. Radiation in the frequency range required was obtained by using a monochromator, and the absorbed energy measured as a resultant change in volume in the system. The very small changes involved were measured by a micromanometer consisting of a low vapour pressure oil drop in a capillary tube. The relationship between absorbed energy and volume change, although approximately calculable, was calibrated by finding the volume change produced by heat energy from an electrically heated thin platinum wire contained in an exactly similar compensating cell.

The radiation energy per frequency unit incident on the gas was found by assuming an idealised distribution of energy over the slit-width of the monochromator, and was calculated from

$$I(o) = \frac{I(T)}{\Delta\nu(\max)}$$

where I(T) is the total radiation issuing through the monochromator, and $\Delta\nu(\max)$ is the frequency width of the widest slit used.

I(T) was ascertained using a calibrated thermopile, and $\Delta\nu(\max)$ measured both optically and mechanically. It was assumed that the monochromator possessed an ideal focus, that the incident slit was

uniformly illuminated and that the radiation from the source per unit frequency interval was constant.

As has been previously stated, Matheson deduced a theoretical curve equivalent to the plot of energy absorbed against reduced pathlength, and from a comparison of theory and experimental data derived values for both the intensity and the line-width. His value for the intensity of the carbon monoxide fundamental was 1.18×10^{13} $cm^{-1}sec^{-1}atm^{-1}$ which is approximately 50% higher than results obtained from other methods.

Several possible errors introduced in his procedure are as follows:

a) No allowance is made for the probability that some of the absorbed energy is re-emitted and does not go to translational energy. Although this is not very likely since an atmosphere of gas was always present, it is known that carbon monoxide-carbon monoxide and carbon monoxide-nitrogen collisions have a very low probability of vibrational-translational energy transfer (33), and the possibility of energy loss is present.

b) The method suffers from the disadvantage that the absorbed and incident energies are measured by different means. Many measured quantities enter multiplicatively into the

result, and thus errors of standardisation as well as measurement may exist.

c) The use of a very high optical pathlength (10 cm.) made it difficult to reach the required region of absorption.

d) The volume change was limited by the thermal conductivity of the gas since a steady state was not set up. The exact time for which absorption occurred was therefore an impor-:tant quantity in any comparative measure-:ments.

e) The electrical energy produced by the wire was only measured by taking values of the current so that variations in voltage with time were not considered.

f) The procedure employed to determine I(o) was limited and approximate in nature as indicated above.

g) Almost certainly the most significant error arose from the use of the micromanometer. Capillary forces acting on the oil drop were reported as being of the order of a thousand times the gas forces to be measured. Hysteresis and small unsteady drifts due to chemical activity and adsorption were also present. Although a large number of readings were taken in order to minimise the

error in the measured volume change, this method of determining the absorbed energy is obviously too crude to give accurate results.

1.5 Line-Width Measurements

Spectrometer measurements have been used, as detailed in section 1.3, to find the average line-width in a particular absorbing band. The variation of the total fractional absorptivity with reduced pathlength is the required relationship, and the various theories give means of finding the line-width from measurements at fairly high pathlengths. (55) (56)(57)(58)(59)

A method employing the principles of the curves of growth has also been used, when both the intensity and the line-width have been treated as variable parameters. (22) Their values are adjusted until a fit with experimental data is obtained.

As has been indicated, the more interesting study of the shape and line-widths of individual lines has been attempted. (16)(32)

1.6 The General Features of the Present Method

The object of the present work is to use and extend the method of Matheson by employing a more sensitive measuring device for the absorbed energy, by looking quantitatively at the various factors which influence such a measurement, and by devising a more accurate determination of the incident energy. When a gas, in a cell of constant volume, absorbs infra-red radiation the resultant increase in temperature gives a pressure rise in the system. When a steady state exists between the energy absorbed and the heat lost to the container, there is a direct relationship between the pressure rise and the amount of radiation energy absorbed. By having two chambers, one of which is illuminated by radiation, initially at the same pressure and separated by a thin metallised diaphragm, the pressure rise which takes place in one can be measured using the change in capacity induced between a fixed plate and the diaphragm. Although this system could be calibrated to give an energy determination from the capacity change, it was decided to simulate the effect on each occasion by incorporating in the absorption cell a thin electrically-heated wire supplying heat energy to the gas. This allows for variations of the diaphragm response and changes in the ambient temperature over a period of time.

The gas on absorbing radiation reaches a steady state with a small, average temperature rise. It is this small rise in temperature which is effectively simulated by the energy from the heated platinum wire. Since the geometry of the cell remains the same in the two cases, from the Fourier law of heat conduction it is seen that the energy lost to the walls must also be the same. Therefore for small temperature gradients between wire and wall, and con-:sidering the existence of a steady state in both cases, the energy supplied to the gas from the wire equals the energy absorbed from the radiation beam.

The incident energy determination is done in three ways:

a) Using the known properties of the source and the geometry of the optical system an esti-:mation is possible.

b) A direct measurement of the total energy issuing through the filters using a cali-:brated thermopile allows calculation of the incident energy per frequency unit.

c) A thin, blackened foil, which is removeable, is incorporated in the cell. All the radiation entering the cell through the filters can be absorbed by it and given out to the gas as translational energy. The resultant pressure rise is measured as for the absorbed energy above.

The reduced pathlength of absorbing gas is varied by changing its pressure, and measurements are made for both a pure gas and for this gas made up to constant total pressure with another. Any fall-off in the absorbed energy due to spontaneous emission becoming a competing process with vibrational-trans-:lational energy transfer is looked at quantitatively. Estimates of both the intensity and the line-width are made.

2. Experimental

The chronological development in understanding the many factors involved in measuring the absorbed energy, and of knowing the best conditions and de-:sign with which to deal with them dictates a cer-:tain order on this chapter. It will be divided into:-

'Experimental 1)' in which preliminary work is described leading up to the design of the first cell; the method of taking measure-:ments with this cell is described, as are procedures for obtaining the incident energy:

'Results 1)' where the results from work on this cell are analysed, and various factors affecting them discussed:

'Experimental 2)' in which the lessons learnt from the above measurements are used in the design of a second cell:

and 'Results 2)' where the final results obtained from this work are detailed.

2.1 Experimental 1)

2.1.1 Preliminary Work

Having decided to measure the pressure rise, due to the absorption of energy in a constant-volume cell, by making use of the change in capacity between a fixed plate and an easily moveable diaphragm, it

was necessary to ascertain if these measurements were quantitatively possible and if sufficient sens-:itivity could be obtained for the required accuracy. This was done in two ways.

2.1.1.1

There has been a considerable amount of study on this type of cell for infra-red gas analysers (60)(61), where the incident beam is modulated and not constant as in this case. From this work, as from methods of studying relaxation processes in gases using similar apparatus (62), it was obvious that great sensitivity was possible. However, the fact that reasonably high pressures of absorbing gas were used, and that the sensitivity was aided by selective amplification of certain frequencies of modulation, made it difficult to judge the appli-:cation of the technique to low energy work in the steady state.

From the literature it was possible to say (63)(64) that the extent of absorption in the gas, if large, would help the resultant signal, whilst a large dead space (i.e. the volume of gas in the cell through which radiation does not directly pass) would decrease the sensitivity of the measurements. These factors are fairly obvious and much more im-:portant are those involving the diaphragm:

Design of Preliminary Cell.

Figure 1

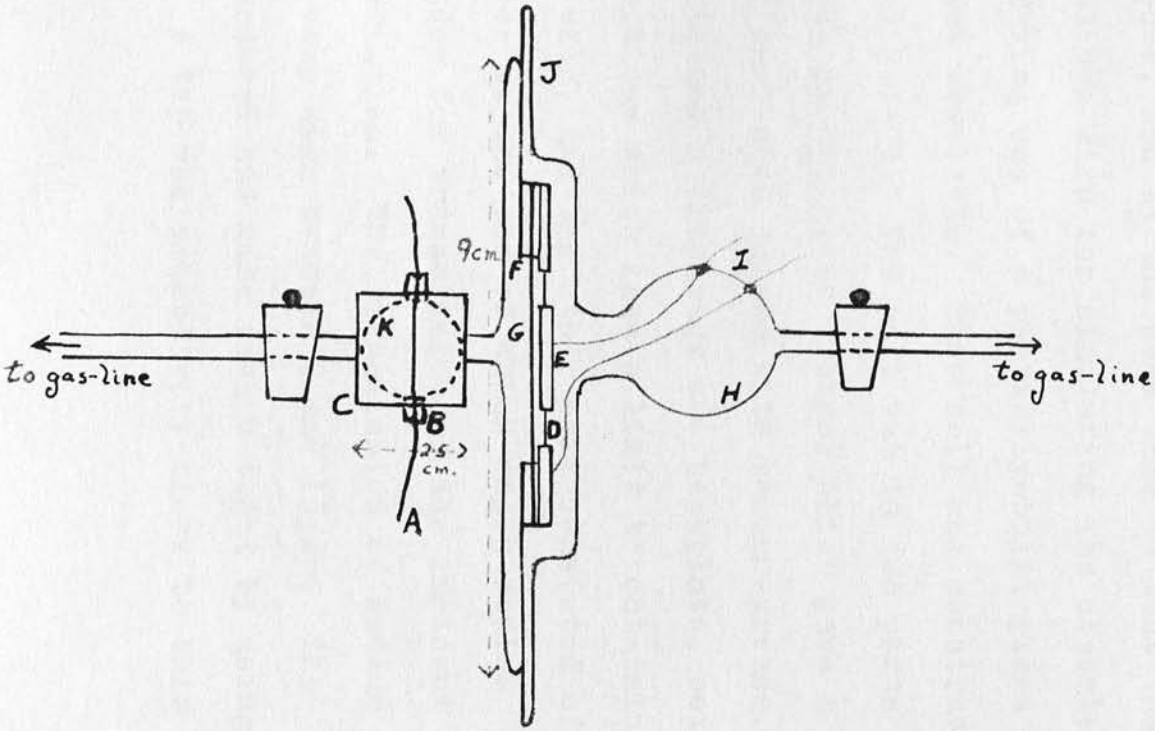

A. Platinum Wire
B. Glass Constrictions
C. NaCl Window
D. Plastic holders for backplate
E. Brass Backplate
F. Rings for holding diaphragm
G. Diaphragm
H. Constant-pressure chamber
I. Leads to Proximity Meter
J. Glass flanges
K. Cylindrical absorption cell.

its distance from the fixed plate is very critical since the capacity decreases with the inverse of the square of the distance;

the thinner and lighter it is the more readily will it move under pressure change;

and with regard to the sensitivity obtain-:ed, the tension on the diaphragm has been found (62) to be very critical.

2.1.1.2

It was decided to examine the magnitude of the signal produced, and at the same time to test the use of a platinum wire for simulating the absorbed energy, by making use of a partially-built glass cell which was available. This cell was constructed as shown in Figure I. The cell was in two parts both with wide ground-glass flanges which gave a vacuum-tight seal when joined with vacuum-grease. One part contained a diaphragm and backplate, both in fixed positions which gave a limit to obtaining high sensitivity, and the other part consisted of a glass cylinder on one end of which was a sodium chloride window for transmission of the incident infra-red radiation. The transmission of sodium chloride is very high between 2 and 15.4μ. The window was secured and made vacuum tight by using Picien wax. A tap was placed very close to this

Gas-line

Figure 2

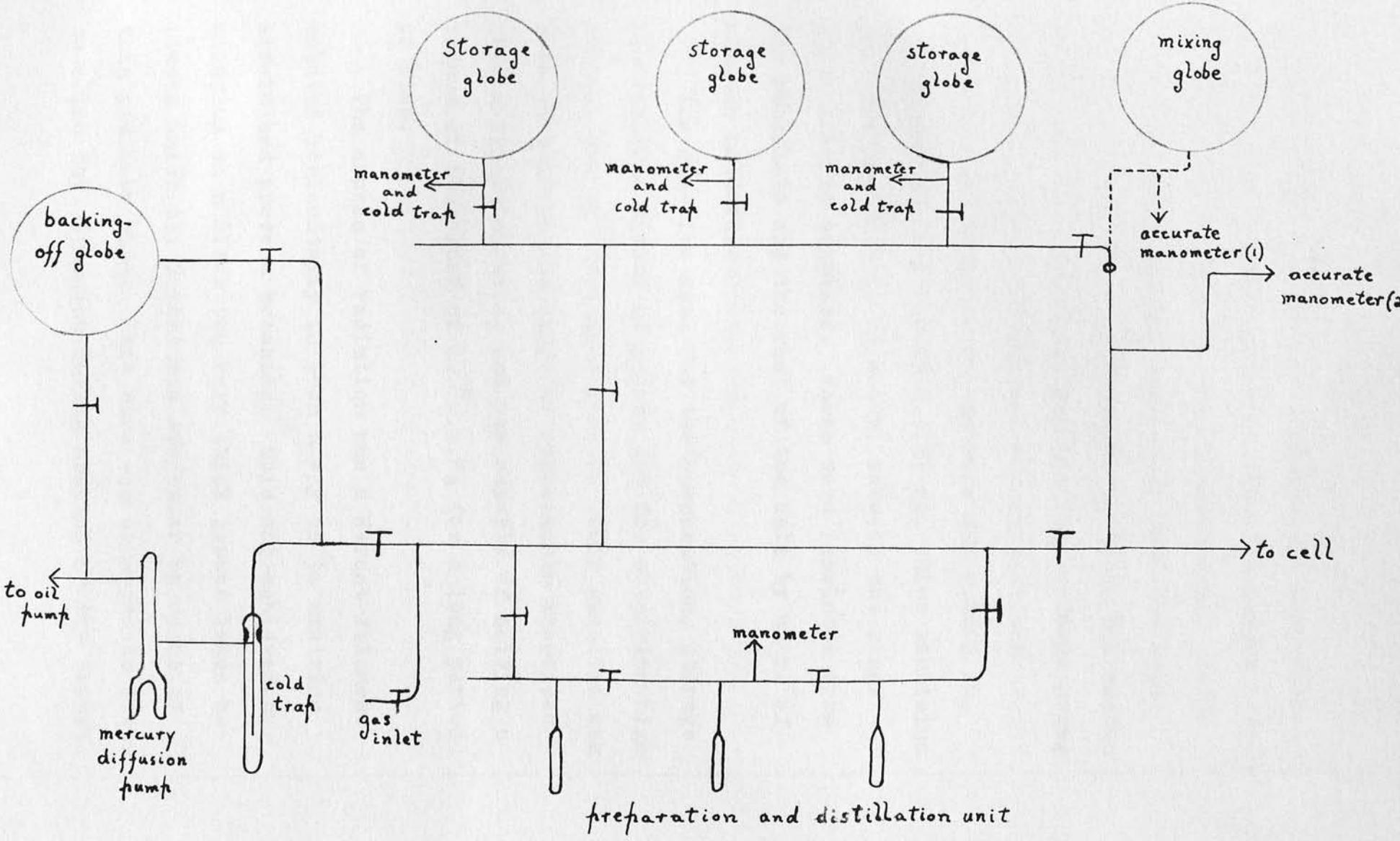

glass cylinder in order to minimise the dead-space and thus increase the pressure rise. A simple arrangement sufficed for the platinum wire: init-:ially it was stretched vertically down the cell through two opposite glass constrictions, the vacuum seal being made by Picien wax and the two ends going to suitable measuring devices for current and voltage. The diameter of the wire was 0.0202 cm. The diaphragm used was of 0.0025 cm. thick aluminium foil and was placed, as shown, between two rings which screwed together. These were insulated from the backplate and the rest of the cell by means of plastic holders.

The gas-line used for the preparation, storage and eventual mixing of gases, and for obtaining high vacuum, was as shown in Figure 2. This gas-line was used throughout the range of experiments described in the following work, and was capable of holding a vacuum of the order of 10^{-4}m.m.Hg for a long period of time.

The source of radiation was a Nernst filament mounted horizontally in such a way as to minimise strain and prevent breaking. This was achieved by mounting on a block two very thick copper leads be-:tween which the Nernst was suspended by means of thin platinum wire. This wire was arranged in loops to allow for expansion during heating of the Nernst.

The full circuit is as shown in Figure 5. Direct radiation from the source to the absorption cell was cut out by using an asbestos shield, and an incident beam was obtained by focussing the radiation with a nine-inch diameter, concave, circular mirror. The focussing was not ideal and a protective shield was placed in front of the cell to prevent unnecessary heating of the glass and metal. A mechanically operated opening in this shield allowed the radia-:tion entering the cell to be switched on and off as desired.

The range of incident radiation which was chosen, for all the measurements which were done, was 3 to 5μ. To achieve this two filters were used in conjunction, both supplied by Barr and Stroud Ltd., Glasgow. A specially prepared interference filter gave transmission over the band 3 to 5μ, filtering all other wavelengths except for some leaks below 2μ. A bloomed germanium filter was used to eliminate these leaks, and it also gave a 70% transmission from 3 to 5μ. Thus the desired band was isolated with an overall transmission of over 40% except at the extremes of the range, this change in transmission with wavelength being readily cal-:culated from data supplied by the manufacturers. The transmission is shown in Graph I for the inter-:ference filter.

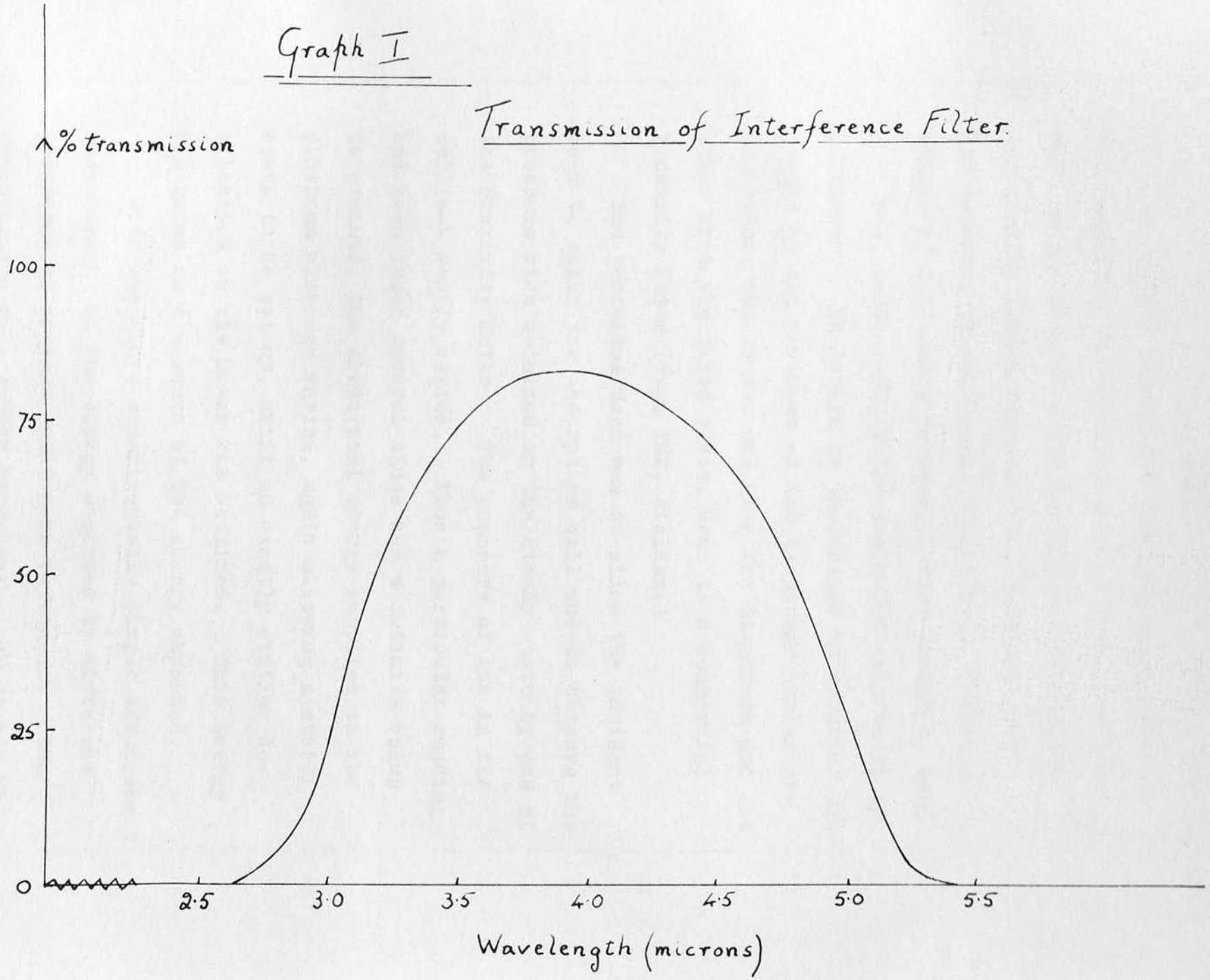
Graph I
Transmission of Interference Filter
% transmission
100
75
50
25
0
2·5
3·0
3·5
4·0
4·5
5·0
5·5
Wavelength (microns)

Two simple electrical devices were necessary. For measuring the energy supplied to the platinum wire an accurate milliammeter and millivoltmeter, supplied by Ernest Turner, Ltd., were employed (½% accuracy in full-scale deflection). Various ranges of full-scale deflection were possible, viz. 0-5, 0-10, 0-50, 0-100 and 0-500 millivolts or milliamps. To determine the change in capacity pro-:duced by the movement of the diaphragm during ab-:sorption, two leads, one from the diaphragm and the other from the fixed plate, went to a commercial Proximity Meter (Type PM2, Fielden.)

The technique used was to allow the incident beam to enter the absorption cell and to observe the pressure rise obtained in the steady state by use of the Proximity Meter. The pressure of gas in the cell was easily varied. When a particular reading had been taken several times and a definite value determined, the electrical energy supplied to the platinum wire was varied, again allowing a steady state to be set up, until an exactly similar de-:flection on the Meter was obtained. This energy was taken as a measure of the energy absorbed.

With the above experimentally simple arrangement measurements of the energy absorbed by different pressures of nitrous oxide were estimated. The measurements were rather inaccurate, but as the in-:tention was only to examine the possibility of

of obtaining a measurable signal the results were gratifying.

a) Easily distinguishable signals were ob-
:tained for pressures of nitrous oxide down to 4cmHg, and the measurements taken were obviously of the correct magnitude. Con-
:sidering the inability with this prelimin-
:ary cell to attain the optimum tension of the diaphragm, and also the optimum separa-
:tion of diaphragm and back-plate, the results were taken to mean that an improved cell design would lead to the desired sensitivity.

b) The question as to whether the position of the platinum wire was critical in simulating the amount of absorbed energy was also studied. This was accomplished by placing a straight wire initially, and then various shapes of the same wire, through the glass constrictions. It was found that the electrical energy needed to duplicate the signal produced by the radiation was con-
:stant to within the experimental error for four different positions and shapes of wire. This meant that, in the cases considered, the temperature gradient from the wire to the walls was low enough to ensure adequate simulation of the energy absorbed.

c) This preliminary work was invaluable in gaining experience of diaphragm difficulties, as well as indicating the possibilities of the method.

2.1.2 Design of the First Brass Cell

Using the knowledge gained in section 2.1.1 the first brass cell was built, and its design is shown in Figure 3 which also gives the dimensions. The details were as follows.

Many features in the design of this cell were similar to the preliminary glass one and, where possible, these will not be repeated. Brass of at least 0.63 cm thickness was used throughout in order to make the cell as stable as possible, and also to act as a heat sink for stray radiation and for atmos-:pheric temperature fluctuations. The whole struc-:ture was nearly surrounded with thick asbestos to prevent draughts and to ensure that outside inter-:ference with the electrical capacity was cut to a minimum.

Two concentric brass flanges on the two halves of the cell, as shown, were secured with four fixing screws, and vacuum sealed with an O-ring. Separa-:tions of these flanges allowed easy access to the internal components of the cell.

The connections to the gas-line were made by

Design of first brass Cell

Figure 3

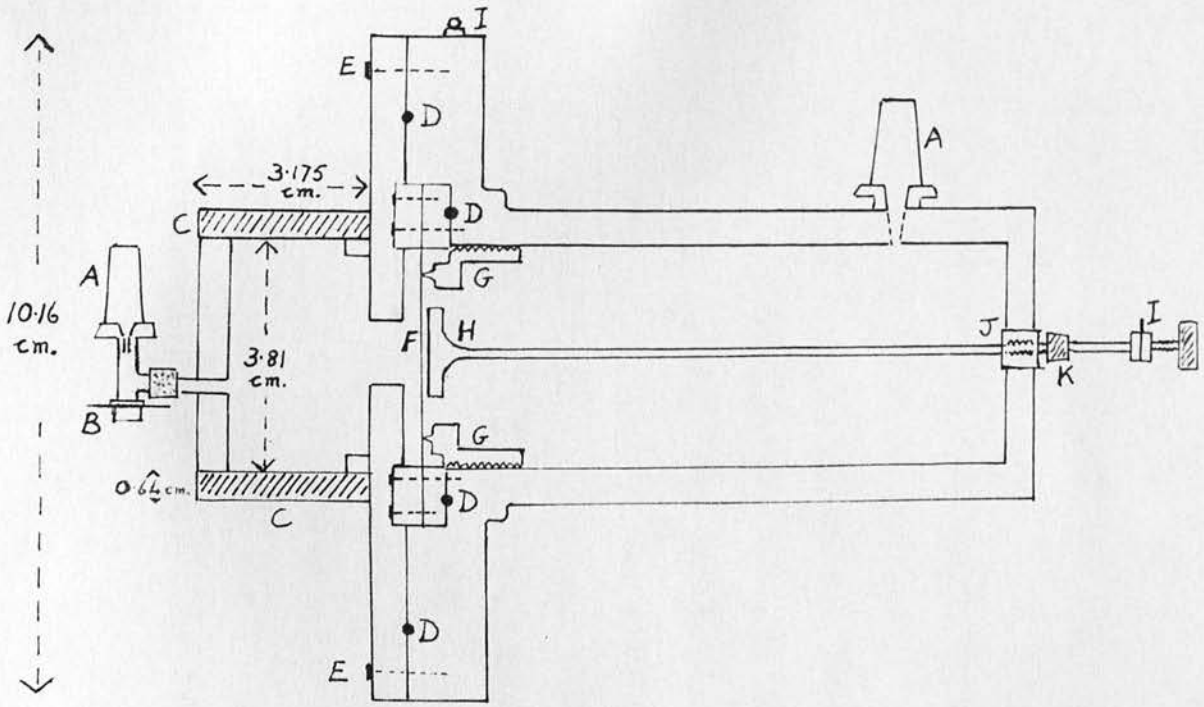

A. B 14 Cone
B. Needle-valve
C. NaCl window
D. O-ring
E. Screws
F. Diaphragm
G. Tensioning-ring
H. Backplate
I. Connections to Proximity Meter
J. Teflon plug
K. Bolt

L. Glass-metal seal
M. Blackened foil
N. Holder for foil with hinge
O. Platinum wire
P. Space through to diaphragm

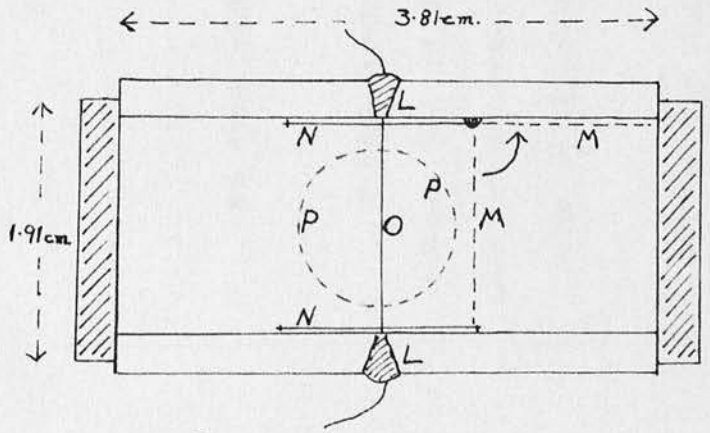

Cross-section of absorption part

two B14 metal cones, one in each part of the cell. In the absorption part, where dead-space was an im-:portant consideration, a needle-valve was incorpor-:ated (supplied by Edwards Ltd.)

Highly polished sodium chloride windows were placed at both ends of the cell in order to prevent transmitted radiation being absorbed by the brass. These were secured by means of the epoxy-resin Araldite.

The important internal components were as follows.

2.1.2.1 Diaphragm and Back-plate

The diaphragm was held between two rings which screwed together, and which were screwed in turn to the outside part of the cell. An adjustable tensioning-ring allowed the tension on the diaphragm to be altered and its optimum value to be found by trial and error. The diaphragm was of 'Melinex', a plastic metallised on one side, supplied by I.C.I. and approximately 0.001 cm. thick. The arrangement for securing it in position meant that it was very easily replaced if damaged. An O-ring was placed between the rings and the outside part of the cell to ensure that no leakage took place between the two parts, although a very slow leakage would not be critical since its time-constant would be much

longer than the rapid rise in pressure (the steady state was attained in 3 to 7 seconds) due to absorp-:tion of radiation.

It was necessary for the back-plate both to be adjustable, in order to get maximum sensitivity from being as near the diaphragm as possible, and to be insulated from the outside walls. The steel rod attached to the back-plate was placed within a brass tube and joined to it by means of a very fine screw which gave the necessary adjustability from outside the cell. The Teflon plug, through which the brass tube passed, acted as an insulator and also, by being screwed up tightly with a large nut, provided an adequate vacuum seal with the walls of the cell.

2.1.2.2 Platinum Wire

A straight platinum wire of length 1.27 cm. and diameter 0.0202cm. was used, being insulated from the brass at both ends by glass-metal seals. This insulation, although easily tested, showed a tend-:ency to be incomplete if any dust particles were allowed to form a 'track' across the glass surface connecting the wire and the brass of the cell.

2.1.2.3 Blackened Foil

To measure the energy incident on the gas a blackened foil was incorporated in the cell. A

measurement of the energy absorbed by the foil was equivalent to the total energy which filters and sodium chloride allowed to pass. It was thus assumed that with a perfectly black and sufficiently thin foil all radiation would be absorbed and given out again to any gas present in the cell as trans-:lational energy. This would thus show up as a pressure rise and be measured as in the case of the gas absorbing.

A thin (0.007 cm.), very flat piece of copper foil was coated lightly with varnish and, whilst this was still wet, a layer of carbon deposited from a smoky taper. The foil was attached to the cell by means of a small hinge and when in position absorbed all energy entering the cell. A narrow steel wire was built into the edges of the copper to enable the foil to be raised and lowered by a magnet acting through the brass from the outside. Thus, when measuring the energy absorbed by the gas under study, the foil could be swung effectively out of the beam.

2.1.3 The Optical and Electrical Apparatus

Although the optics used were essentially the same as for the preliminary work, they were made more stable and more adjustable by the use of an optical axis as shown in Figure 4. All components,

Optical System

Figure 4

A. Levelling screws
B. Optical axis
C. Adjustable bases
D. Mirror
E. Asbestos shield
F. Nernst filament
G. Stray-radiation shield
H. Aperture
I. Filters
J. Cell

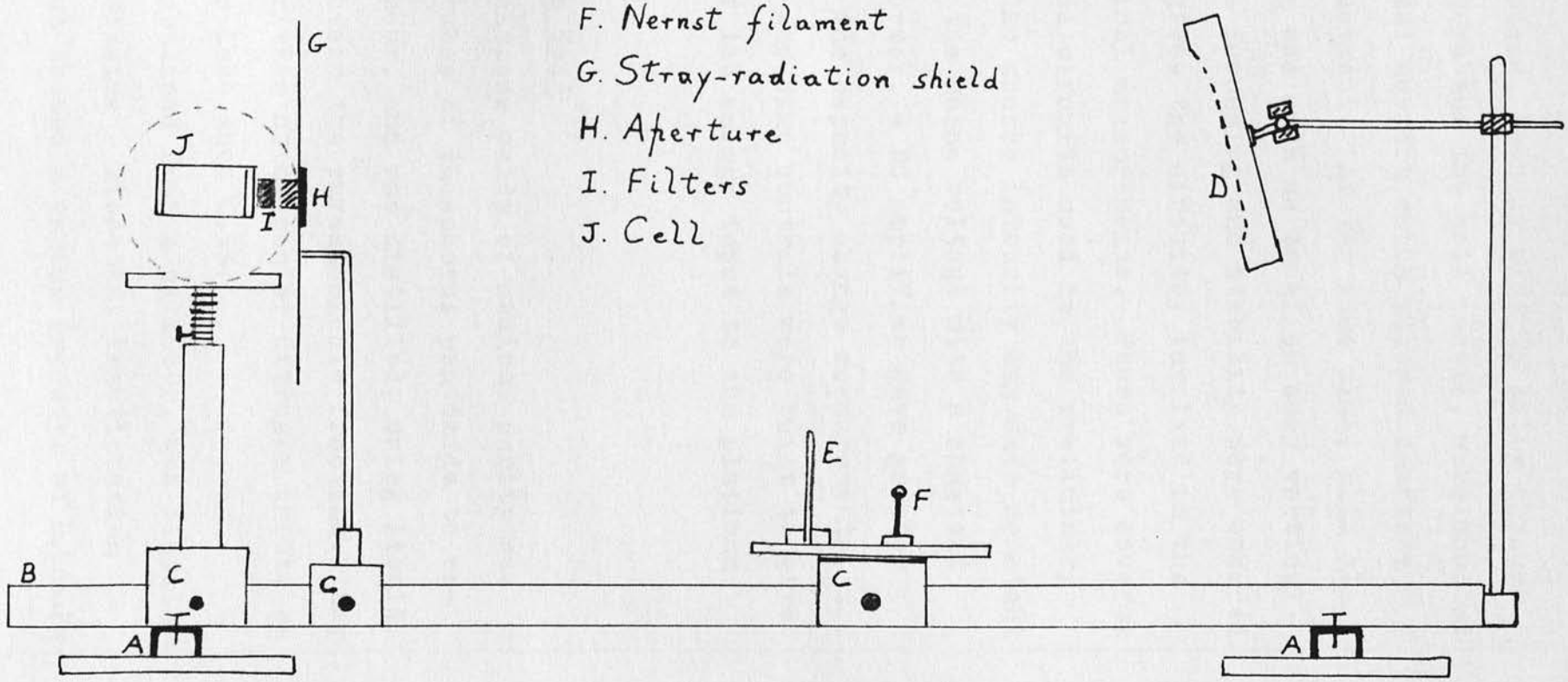

i.e. mirror, source, opening slit to allow through radiation, filters and the cell itself, were mounted on a single metal support which allowed complete horizontal adjustment. At the same time, with all parts, mounting was such as to allow easy vertical movement. Thus focussing and stability were ensured.

Figure 5 gives the circuitry involved in the various electrical measurements. There were several additions to the circuits used in the preliminary experiments. The source intensity was made constant by stabilising the mains voltage with a constant voltage transformer, a DC amplifier gave greater sensitivity to the capacity change measurements, and coarse, medium and fine controls were built to give full control of the energy input to the platinum wire.

2.1.4 Gases Used

Cylinder nitrous oxide of medical purity was drawn through tubes of phosphorus pentoxide to re-:move water vapour, and was distilled, using liquid nitrogen, to obtain the purest middle fraction. Any remaining impurities of oxygen or nitrogen should be present only to less than 0.5%.

Methane, obtained from a cylinder, was distilled in a modified Clusius - Riccobini fractionation column (65), and showed a vapour pressure of 8.5cm.Hg

Electrical Circuitry

Figure 5

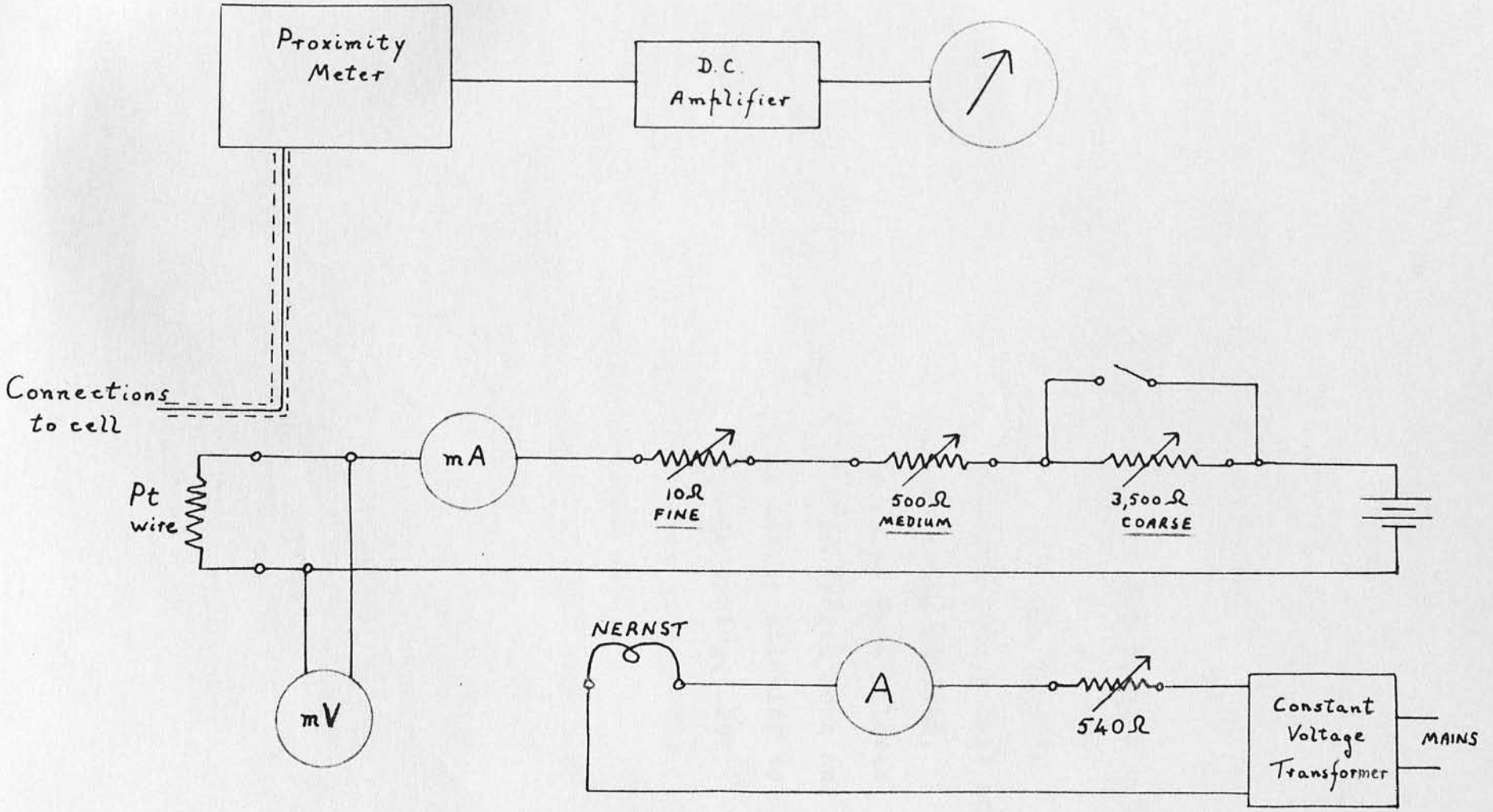

at -183.1°K and 0.93 cm.Hg at -196°K. The methane contained no more than 0.05% oxygen and nitrogen and 0.01% ethane and other hydrocarbons, the purity being ascertained by gas chromatography.

2.1.5 Typical Measurement of the Energy Absorbed

For measurements on pure gases, the gas was allowed to expand into the cell, with the taps to both parts of the cell open, straight from a bulb of purified gas. When mixtures were being studied, predetermined pressures of both gases were allowed into a mixing globe where they were frozen down and evaporated at least three times before allowing to stand for over one hour to complete mixing. For many mixtures a much longer time was given. The mixture was then expanded into the cell.

The pressures were measured using a wide bore (1cm. diameter) mercury manometer with two limbs very close together. At pressures above 4 cm.Hg the manometer was read with the eye, an accuracy greater than 1% being obtained. However, at lower pressures it was found necessary to use a travelling microscope when readings could be taken to 0.002 cm. with resultant high accuracy. The error which can be present due to different heights of the mercury meniscus in each limb was calculated as 0.002cm.Hg and was therefore negligible for all pressures used.

Since a small amount of fluctuation across the diaphragm tended to take place, a period of up to half-an-hour was allowed for equilibrium to be established before closing the needle-valve and the tap nearest the other part of the cell. Once more a period of time elapsed before perfect equilibrium was established.

With the blackened foil held by the magnet out of the way, the incident beam was allowed to enter the absorption cell until a steady state prevailed. The deflection registered by the Proximity Meter was noted. This was done several times and an exact value obtained before, with the radiation eliminated, this value was simulated by energy introduced from the platinum wire. Having ascertained this electri-:cal energy as closely as possible, the sensitivity of the Proximity Meter (or of the amplifying system if it were being used) was changed and the whole procedure repeated. This was done several times. Thus an accurate value for the energy absorbed was determined.

Having pumped out the cell, when this was necessary, a new sample of absorbing gas was intro-:duced and the measurement repeated.

2.1.6 Measurement of the Incident Energy

As has been indicated, the blackened foil

measures all the radiation energy incident on the gas, i.e. between 3 and 5μ. In order to calculate the incident energy per frequency unit (I(o)) appropriate to the absorption band under study, it is necessary to know the ratio

$$\frac{I(o)}{Q}$$

where Q is the energy entering the cell between 3 and 5μ in the absence of atmos-:pheric absorption between the source and the cell.

The temperature of the source was measured using a calibrated optical pyrometer and, using Planck's radiation law, the distribution of the intensities of the emitted frequencies was calcul-:ated. This distribution was corrected for the transmission characteristics of the filters. The ratio of the energy at the required frequency to the total energy between 3 and 5μ (Y) was calculated graphically, and it is readily seen that Y is equivalent to $\frac{I(o)}{Q}$.

The details of the atmospheric absorption were as follows. The two constituents of importance are carbon dioxide and water vapour with the following absorption bands in the region 3 to 5μ.

CO_2:- $2077cm^{-1}$ combination band,

$2285cm^{-1}$ the ν_3 fundamental of the carbon 13 isotope,

$2349cm^{-1}$ the ν_3 fundamental which is a very strong absorber.

H_2O:- $3151cm^{-1}$ overtone band.

The effect of these bands on the required ratio (their effect on the absorption bands of nitrous oxide and methane are discussed later) can be quite accurately calculated. In the case of carbon dioxide the energy absorbed by the $2077cm^{-1}$ and $2285cm^{-1}$ bands is approximately 1% of that absorbed by the $2349cm^{-1}$ band under the same conditions, and therefore their effect can be ignored. For the $2349cm^{-1}$ band the partial pressure of carbon dioxide in air is 3.3×10^{-4} and the measured distance between source and cell was 49cms, thus giving a reduced pathlength of 1.62×10^{-2}cm.atm. Considering that the carbon dioxide is pressure-broadened by an atmosphere of air this is effectively in the linear region of absorption. Therefore $\frac{E}{I(o)} = AX$, and the fraction of the energy absorbed by the carbon dioxide to the total energy between 3 and 5μ is given by

$$\frac{E}{I(3\rightarrow 5\mu)} = \frac{AX}{3\times10^{10}\times 1.33\times10^{3}} R ,$$

where R is the ratio of the intensity at 2349cm^{-1} to the average intensity between 2000 and 3,333cm^{-1} passing through the filters.

The result of this calculation was that the effect of carbon dioxide is to reduce the value of Q by 4%.

Thus the energy measured by the blackened foil is only 96% of Q.

It was found by calculating in a similar way, from a knowledge of the room temperature and the relative humidity, that the effect of the water over-:tone band on the measured value of Q was negligible (approx. 0.3%)

The desired quantity I(o) is thus most easily calculated from the relationship

$$I(o) = QY = 1.04Q(m)Y \qquad (57$$

where Q(m) is the energy measured by the absorption of the foil.

As has been indicated the value of the incident energy was found using two other techniques. One of those was entirely a calculation from the properties of the source and the optics, and is given in the next section as a valuable estimation of I(o). The

other method consisted of a measurement of the total energy incident on the gas between 3 and 5μ using a calibrated thermopile, followed by a calculation exactly as given above for the blackened foil method.

2.1.6.1 Thermopile Measurements

The thermopile was calibrated using actinometry. In a solution of 0.01M uranyl sulphate and 0.05M oxalic acid the quantum efficiency of the acid decomposition $(COOH)_2 = CO_2+CO+H_2O$ for blue light, say, from a mercury vapour lamp, is 0.6 (66).

The number of quanta per second falling on unit area of an absorption cell containing the above solu-:tion at a particular distance from a mercury vapour lamp is thus given by:

$$D = \frac{0.5(V_1-V_2)N \times 6.02 \times 10^{23}}{10^3 A(1 - \frac{G_2}{G_1})t.0.6}$$

where V_1 and V_2 are initial and final titrations of the same volume of oxalic acid with potassium permang-:anate of normality N,

A is the area of aperture allowing the light into the cell,

and t is the time of illumination in seconds.

The relationship follows since 1000ml.N$KMnO_4$ ≡ 0.5 mole oxalic acid.

$(1 - \frac{G_2}{G_1})$ is the absorption factor for the uranyl oxalate solution and is obtained, by means of a photo-electric cell - galvanometer system. The galvanometer deflection with the cell placed in the beam between the blue light source and the photocell is G_1 when the cell is filled with water and G_2 when the cell contains the uranyl oxalate solution.

In order to isolate light of the appropriate wavelength ($4360A^{o}$) a 2% solution of cuprammonium sulphate was used. The light was directed onto the cell by means of a highly polished cone which was also used with the thermopile.

The absorption factor, the wavelength of absor-:ption and the filter characteristics were all checked by doing an ultraviolet and visible spectrum on the uranyl oxalate and cuprammonium sulphate solutions.

Having calculated the number of incident quanta per unit time and area, the incident energy was $Dh\nu$. The thermopile was placed exactly in the position of the absorption cell and, using an accurate potentiometer-galvanometer system, the potential difference produced in it was measured.

The calibration measurements were done several times to ensure accuracy before the thermopile was used to measure the infra-red energy between 3 and 5μ incident upon the gas under study.

2.2 Results 1)

2.2.1 Tables of Results

The following tables of results were obtained with the described experimental arrangement. Because they showed peculiar features which were especially noticeable in the case of the blackened foil measurements on the incident energy, a number of gases were used in conjunction with the foil to attempt an elucidation of the factors causing error.

The following symbols are used:

P is the pressure of gas in cm.Hg,

E is the measured energy absorbed by the gas,

and Q(m) is the blackened foil measured incident energy from 3 to 5μ .

Table II N_2O alone.

P(cm.Hg)	E (ergs sec^{-1})	Q(m) (ergs sec^{-1})
74.0	2.27×10^5	1.84×10^5
14.74	1.72×10^5	2.12×10^5
7.37	1.28×10^5	2.20×10^5
3.69	1.07×10^5	2.16×10^5
1.83	0.92×10^5	2.80×10^5
0.92	-	3.06×10^5
0.37	0.64×10^5	4.40×10^5

Table III N_2O, made up to 1 atm. with dry air

P(cm.Hg)	Q(m) (ergs sec^{-1} x 10^5)
74.5	1.84
14.84	1.71
3.72	1.57
1.86	1.31
0.93	1.28

Table IV N_2O, made up to 1 atm. with H_2

P(cm.Hg)	Q(m) (ergs sec^{-1} x 10^5)
75.0	1.81
7.50	1.59
0.90	1.23

Table V Dry air

P(cm.Hg)	Q(m) (ergs sec^{-1} x 10^5)
75.0	1.32
37.0	1.38
14.80	1.60
7.40	1.68
3.70	1.74
1.85	2.21
0.93	2.42

Table VI H_2

P(cm.Hg)	Q(m) (ergs sec^{-1} x 10^5)
73.2	0.91
37.2	1.04
14.6	1.15
6.3	1.33
3.7	1.59
2.15	1.66
0.80	2.14

Table VII CH_4

P(cm.Hg)	E(ergs sec^{-1} x 10^5)	Q(m)(ergs sec^{-1} x 10^5)
74.9	1.09	1.20
38.5	0.75	1.39
18.6	0.52	1.54
6.8	0.45	1.70
2.0	0.48	1.93
0.95	0.43	2.25

Table VIII Dry air

P(cm.Hg)	E (ergs sec^{-1} x 10^4)
74.5	1.71
11.1	2.00
3.1	2.56

TABLE IX CH_4

P(cm.Hg)	E (ergs sec^{-1} x 10^4)
32.9	4.20
10.04	2.60
3.35	2.10
0.91	2.20

These measurements were taken with a much lower incident energy than the corresponding values in Table VII. The difference is discussed later.

TABLE X Argon

P(cm.Hg)	Q(m) (ergs sec^{-1} x 10^5)
75.5	1.02
14.3	1.50
4.3	1.98
2.1	2.13
1.0	2.35

The shape of this relationship was the point of interest, and the incident energy was different from all other results.

2.2.2 Factors Influencing these Results

It was obvious, on studying the values obtained for both the incident energy and the absorbed energy, that several experimental factors were having a com-:plicating effect on the results. These are now analysed, and in most cases treatment of the factor involves studying the effect on the platinum wire and on the blackened foil separately.

2.2.2.1 End-conduction of Heat

Considerable end-conduction of heat from the platinum wire to the lead-wires occurred due to the high thermal conductivity of the wire compared to that of the gas. This was more easily calculated than the conduction from the foil directly through the hinge to the walls of the cell, and therefore they are treated separately.

2.2.2.1.1 Platinum Wire Case

The problem of end-conduction has been studied extensively in the literature on the measurement of the thermal conductivity of gases using the 'hot-wire method.' Three main methods of dealing with it have been found.

a) Theory shows that for long wires there is a central portion in which the temperature is constant. Therefore if two cells are built, each containing a long wire of

different length, subtraction leaves a centre portion of the longer wire where end-conduction does not apply. (67)

b) Very fine potential leads are attached to the cell-wire leaving a central part over which the potential difference is measured. (68)

c) The use of a relatively short and thick wire allows the end-conduction to be calculated with adequate accuracy. In this case the temperature distribution along the wire is essentially parabolic and does not contain a central portion of constant temperature. (69)(70)(71)

Since with the absorption cell platinum wire it was necessary to calculate the effect of end-conduction, case c) above was considered in the first instance. The method involved can be summarised as follows.

If the centre of the wire is taken as origin, the temperature difference from room temperature at any point on it, at a distance a from the centre, is given by

$$t = c(l_w^2 - a^2)$$

where $2l_w$ is the total length of the wire, and c is a constant.

The temperature difference has a maximum value cl_w^2 at the centre and it is zero at both ends.

Therefore the mean temperature difference $\bar{t}$ is

$$\bar{t} = \frac{1}{2l_w}\int_{-l_w}^{+l_w} c(l_w^2 - a^2)da$$

$$= \frac{2cl_w^2}{3}$$

and the temperature gradient at any point on the wire is

$$\frac{dt}{da} = -2ca$$

At either end the gradient is therefore,

$$\left(\frac{dt}{da}\right)_{a=+l_w} = -\frac{3\bar{t}}{l_w}$$

Thus the rate at which heat is conducted from the wire at both ends,

$$-2\lambda A \left(\frac{dt}{da}\right)_{a=\pm l_w}, \quad \text{is}$$

$$\frac{6\lambda\pi b^2 t}{l_w} \qquad (58$$

where $A, = \pi b^2$, is the cross-sectional area of the wire, and λ is the thermal conductivity of the wire.

In order to evaluate $\bar{t}$, which is the only unknown quantity in equation (58, it was decided to determine the change in resistance of the wire with change in temperature.

However, on doing this it was found that rather a large error was present ($\pm$25%) due to the very small temperature, and therefore resistance, changes

involved. Therefore another method of finding either $\bar{t}$ or the end-conduction was necessitated.

Reference (67) in dealing with the theory of end-conduction shows the following relationship

$$t = \frac{U}{V} + C_1 \exp(V^{\frac{1}{2}}a) + C_2 \exp(-V^{\frac{1}{2}}a) \qquad (59$$

where t and a have their previous meanings,

C_1 and C_2 are constants determined from end conditions in the wire,

$$U = \frac{I^2 \rho_o}{J.\lambda A^2} \quad \text{and} \quad V = \frac{2\pi k}{\lambda A(\ln \frac{r_2}{r_1})} - \frac{I^2 \rho_o \alpha}{J\lambda A^2}$$

where I is the current in the wire in amperes,

ρ_o is the specific resistance of the material of the wire,

J is Joule's constant,

A is cross-sectional area of the wire,

λ and k are the thermal conductivities of the wire and the gas surrounding the wire respectively,

α is the coefficient of resistance of the wire,

and r_1 and r_2 are the radii of the wire and the outer cell.

Equation (59 was extended in the following way to meet the requirements of the absorption cell.

$$\frac{dt}{da} = C_1 V^{\frac{1}{2}} \exp(V^{\frac{1}{2}}a) - C_2 V^{\frac{1}{2}} \exp(-V^{\frac{1}{2}}a) \qquad (60$$

C_1 and C_2 were found using the condition that $t = 0$ at $a = 0$ and $2l_w$) i.e. at both ends of the wire (not using the centre of the wire as origin as was done for equation (58),

$$C_1 = - \frac{U}{V\left[1 + \exp(2V^{\frac{1}{2}}l_w)\right]}$$

$$\text{and } C_2 = - \frac{U \exp(2V^{\frac{1}{2}}l_w)}{V\left[1 + \exp(2V^{\frac{1}{2}}l_w)\right]}$$

On substituting in equation (60,

$$\left.\frac{dt}{da}\right|_{a=o} = - \frac{U}{V^{\frac{1}{2}}} \left[\frac{1 - \exp(2V^{\frac{1}{2}}l_w)}{1 + \exp(2V^{\frac{1}{2}}l_w)}\right]$$

and therefore the end-conduction of heat at both ends of the wire is

$$- 2\lambda A\left(\frac{dt}{da}\right)_{a=o} = - \frac{2U\lambda A}{V^{\frac{1}{2}}} \left[\frac{1 - \exp(2V^{\frac{1}{2}}l_w)}{1 + \exp(2V^{\frac{1}{2}}l_w)}\right] \qquad (61$$

Three procedures were thus available for the calculation of the end-conduction:- the use of equation (61; from equation (59 evaluating the temperature distribution and thus $-2\lambda A\left(\frac{dt}{da}\right)_{a=o}$; by finding the average temperature using (59 and then substituting in equation (58.

Sample results were taken and the three approaches

Graph II

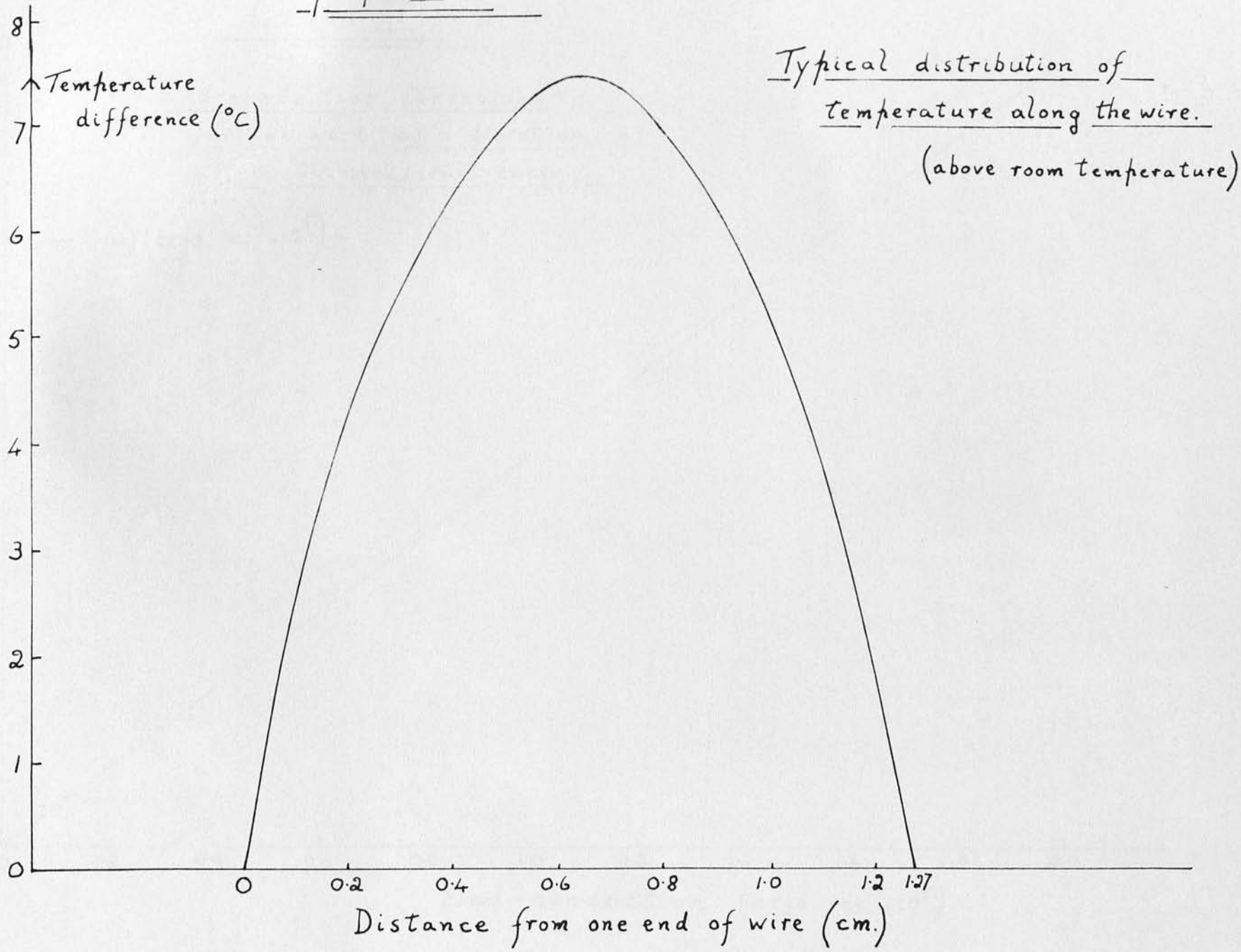
Typical distribution of temperature along the wire.
(above room temperature)
Temperature difference (°C)
8
7
6
5
4
3
2
1
0
0
0·2
0·4
0·6
0·8
1·0
1·2
1·27
Distance from one end of wire (cm.)

Graph III

End-conduction correction for the wire, as a function of the measured energy.

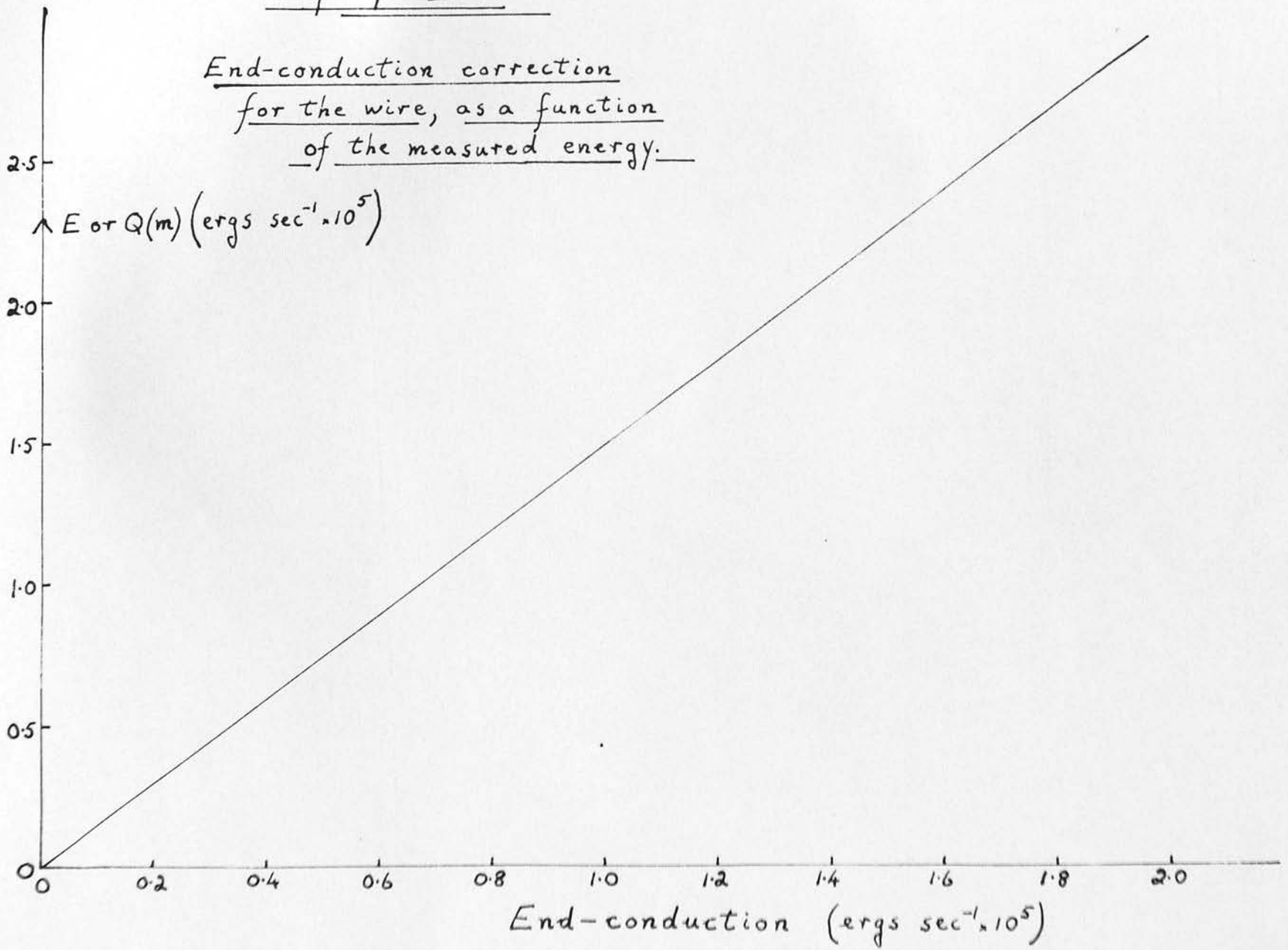

compared. For a current and a voltage of 577mA and 26.5mV respectively, the end-conduction was calcul-:ated to be 1.08×10^5 ergs sec^{-1}; the three approaches all gave this result to within 3%. The temperature distribution along the wire for this sample case was as shown in Graph II.

From equation (61 it is readily shown that for the conditions of study in the absorption cell the end-conduction is directly proportional to the measured current in the wire squared. This is so because the leading term in V, which does not involve I, is the dominant term. On the basis of this Graph III was plotted giving a ready measure of this loss of heat in each measurement.

2.2.2.1.2 Blackened Foil Case

The calculation of the temperature of the foil and especially of the amount of heat conduction from it gives results which are very inaccurate compared to the values obtained for the platinum wire. The purpose of this section therefore is not to calcul-:ate the exact heat loss but, in a semi-quantitative manner, to indicate its order of magnitude. Other methods of measuring the incident energy were, of course, available but a study of this factor, and other factors, for the blackened foil reveal sources of error in the design of the absorption cell.

Heat conduction from one surface to another at temperatures t_2 and t_1 with a gas of thermal conductivity k between them is

$$H = B\,k(t_2-t_1)$$

where B is a geometrical factor and is usually represented as $B = \frac{1}{\int_{r_1}^{r_2} \frac{dr}{A}}$ where r_1 and r_2 are distances measured from some origin, and A is the area of the conduction path.

For the foil, B was evaluated by approximation since it involves the geometrically difficult case of a heated wall surrounded by five other walls.

If the dimensions of the foil are a and b, its distance from the opposite wall is r and the total area of the five walls is y, then

$$B = (ab+y)\,\frac{y}{abr} \qquad (62$$

This approximation involves the model of two resultant parallel surfaces, one the foil and the other the total area of the walls, at a distance determined by the ratio of the areas of the two surfaces. They are now not enclosed at the ends and simple heat conduction theory can be applied. The fact that the foil conducts in two directions has been considered.

Thus

$$H = (ab+y)\left(\frac{y}{abr}\right) k(t_2-t_1) \qquad (63$$

In equation (63 H is the energy conducted by the gas, and is therefore that which is measured in the absorption cell in the absence of other extra-:neous effects; and (t_2-t_1) is the temperature in-:crease of the foil produced by the radiation.

Having estimated (t_2-t_1), the ensuing heat con-:duction from the foil to the supporting hinge is seen to be given by

$\lambda A \left(\frac{dt}{da}\right)_{a=o}$ as stated previously.

Using the same sample figures as in section 2.2.2.1.1,

$(t_2-t_1) = 0.4^{o}C$; $\lambda = 0.46 \times 10^{7}$ ergs $^{o}C^{-1} sec^{-1} cm^{-1}$;

and A and $\left(\frac{dt}{da}\right)_{a=o}$ can be approximated at

$0.012 cm^{2}$ and $6^{o}C cm^{-1}$ respectively.

The calculation then yields a value for the heat conduction from the foil of 3 to 4 x 10^{5} ergs sec^{-1}. This is to be compared with a measured H, the energy from the radiation actually measured as a pressure rise in the gas, of around 0.5 x 10^{5} ergs sec^{-1}.

It is obvious from the above order of magnitude calculations that most of the incident energy was lost by conduction directly through the hinge to the walls of the cell, and that only a fraction was trans-:ferred as translational energy to the gas. Thus

totally inadequate thermal insulation of the foil was employed making the results obtained in this way meaningless.

The overall results of this section 2.2.2.1 are to show the faults in the foil design, and also to indicate accurately that the simulation of the energy absorbed by the gas using the platinum wire gave a high result due to heat flowing from the heated wire to the lead-wires.

2.2.2.2 Radiation Effects

Since both the wire and the foil during measure-:ments were at a higher temperature than the sur-:roundings, it was necessary to assess the amount of energy lost from both due to radiation. This was done by assuming that both were black bodies (correction can easily be made for the emissivity of platinum) and applying the Stefan radiation law, viz.

$$E(r) = \sigma A(t_2^4 - t_1^4)$$

where $E(r)$ is the radiation energy emitted,

σ is the Stefan constant,

A is the surface area which is applicable,

and t_2 and t_1 are the temperatures of the heated wire or foil and the walls respectively.

The correction for this effect in the case of the wire, when simulating the energy absorbed by the gas, was found to be negligible (less than 1%) but for the foil measurements, which were of higher energy, both the foil and the wire required correc-:tion by a few per cent. This is not detailed because of the errors shown in section 2.2.2.1.

2.2.2.3 Convection

The problem of convection, like conduction, demanded different approaches for the wire and for the foil. However, the general treatment of this factor is given first.(72)(73)

The method of dimensional analysis yields four important quantities:

$$\text{Nusselt Number, Nu, } = \frac{Gl}{k\theta} ,$$

$$\text{Reynold's Number, Re, } = \frac{v\rho l}{\mu} ,$$

$$\text{Prandtl Number, Pr, } = \frac{c\mu}{k} ,$$

$$\text{Grashof Number, Gr, } = \frac{ag\theta l^3\rho^2}{\mu^2}$$

where G is the total heat transferred per unit area per unit time (i.e. both by conduction and con-:vection), and is related to h, the heat transfer coefficient, by $G=h\theta$ where θ is a characteristic temperature difference in the geometrical shape con-:sidered,

l is the characteristic linear dimension of the system,

k is the thermal conductivity,

v is the forced velocity of the gas,

ρ is the density,

μ is the viscosity,

c is the specific heat at constant pressure,

a is the coefficient of thermal expansion,

and g is the acceleration due to gravity.

Nu is a measure of the ratio of the total heat transferred to that transferred by conduction alone, i.e. G/Gk.

Since the problem of convection in the absorption cell is purely one of natural convection Re is eliminated, i.e. there is no forced velocity.

2.2.2.3.1 Convection in the case of the Wire

The geometry of the wire convection was approximated to that of two concentric cylinders with a large value of $\frac{d_o}{d_i}$, where d_o and d_i are the diameters of outer and inner cylinders respectively.

Much work (74) has been done relating the extent of convection for the above case to the product Gr.Pr. The form of the relationship is

$$Nu = C(Gr.Pr.)^n$$

where C is a constant dependent on the geometry of the system, and n takes values which are valid for certain ranges of the variable Gr.Pr. At low Gr.Pr, n tends to zero and convection dis-:appears.

When $\frac{d_o}{d_i}$ is very big it was found (74) that heat transfer tended to conduction only, and this has been examined in detail by Beckmann (75) who worked up to values of $\frac{d_o}{d_i}$ equal to a hundred. He took θ to be the full temperature difference between the two cylinders, and d_i as the characteristic linear dimension. His results are shown in Graph IV.

For the platinum wire, with $\frac{d_o}{d_i}$ equal to approx-:imately 100, the product Gr.Pr was calculated for the sample values of one atmosphere of methane and a temperature difference of $4^{o}C$ with the result ____ $Gr.Pr = 4.3 \times 10^{-3}$.

It is readily seen from Graph IV that even for these high sample values, convection is effectively absent.

Therefore for all measurements on the energy ab-:sorbed by the gas, as simulated by the wire, below a

Graph IV

Convection for the wire,
log Nu against log (Gr.Pr)

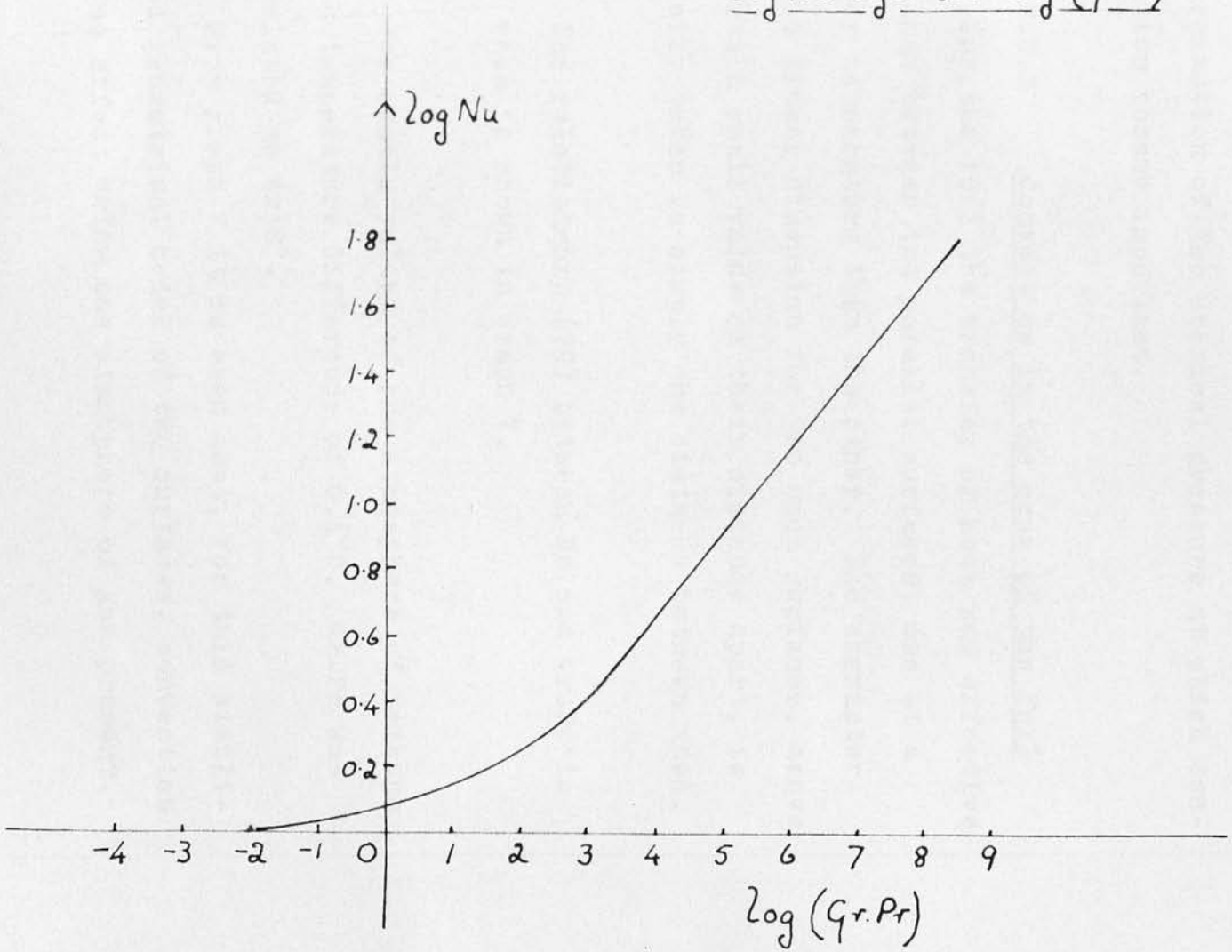

total pressure of one atmosphere convection was negligible, except for cases involving gases of high molecular weight. For these gases the effect of convection was sufficiently calculable to allow the determination of the critical pressure at which con-:vection became important.

2.2.2.3.2 Convection in the case of the Foil

For the foil the transfer of heat was effective-:ly that between two parallel surfaces, one at a higher temperature than the other. The character-:istic linear dimension for two such surfaces, above a certain small value of their distance apart, is normally taken as simply the distance between them.

The relationship (72) between Nu and Gr.Pr in this case is shown in Graph V.

For sample values of one atmosphere of methane and a temperature difference of $0.4^{o}C$. Gr.Pr was calculated as $4x10^{2}$.

From graph V it is seen that, for this simpli-:fied geometrical model of two surfaces, convection had no effect below one atmosphere of gas present.

Graph V

Convection for the foil,
Nu against log (Gr.Pr).

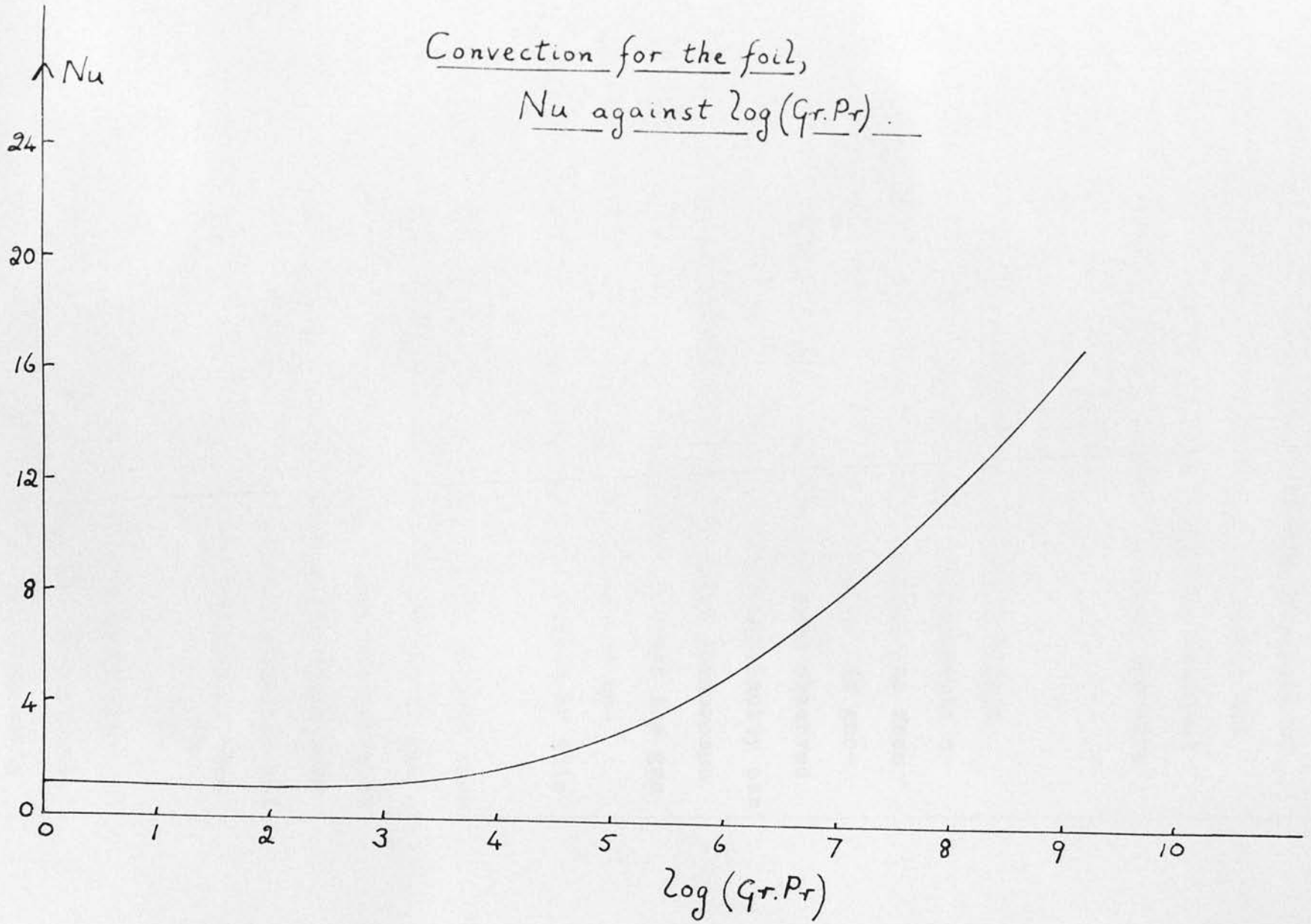

It would therefore seem from the analyses of convection carried out in sections 2.2.2.3.1 and 2.2.2.3.2 that conduction was always the dominant process in the transfer of heat from both the wire and the foil.

2.2.2.4 Surface Temperature Discontinuities

In both the wire and the foil measurements a small temperature gradient existed in the gas from the heated body to the walls of the cell. At gas-:solid interfaces of this type it has been observed that at low pressures a temperature discontinuity can exist. Early work (76)(77) related this phenomenon to the efficiency of energy transfer between the gas and the surface, using α, the accommodation co-:efficient, to express the fractional extent of this transfer.

If E_i denotes the energy brought up to unit area of surface per second by the incident stream of gas molecules, E_r that carried away by these molecules as they leave the surface, and E_w that which would have been removed from the surface if perfect exchange had been established between the gas and the solid, then

$$E_r - E_i = \alpha(E_w - E_i)$$

or $T_r - T_i = \alpha(T_w - T_i)$ where T represents the corresponding temperature.

In the presence of a temperature discontinuity both T_i and T_r are constant for a small distance g out

from the surface, due to the fact that equilibrium is not established with the incident molecules, the surface and the reflected molecules.

Depending on the pressure of the system two distinct processes are possible:

a) Free molecule heat conduction

When two surfaces are very near to one another, or alternatively when the gas between them is at an extremely low pressure, the number of collisions between gas molecules becomes small in comparison to the number of gas-surface collisions. Under these conditions heat conduction is dependent on the pressure. For this process to occur the mean free path, L, of the gas must be of the same size as the distance between the surfaces.

For measurements with the wire and the foil the necessarily low pressure was never used, and therefore free molecule heat conduction was never present.

b) Long mean free path processes

The normal Fourier law of heat conduction ($q = k \text{ grad } T$ where q, the heat crossing unit area in unit time, $=kE$ with k the thermal conductivity and E the field intensity) breaks down whenever the number of carriers of heat, their frequency of

collision or their mean free path vary with E. However, it also breaks down in systems with long mean free paths.

The fundamental difference between the two types of heat flow appropriate to long and short L's has been stressed by Jaffe (78) who obtained a solution of the Boltzmann integro-differential equation for the rate of change of the properties of a gaseous assembly by expansion of L in series. For L small compared to the linear dimens-:ions of the cell, the expression may be ex-:panded in ascending powers of L which thus constitutes a convergent series if L is small. The first term in this series gives Fourier's law and the succeeding terms correspond to departures from it due to variation in the number of carriers, etc.

For L large, however, this series of terms is no longer convergent. Jaffe showed that the Boltzmann equation can then be expanded in powers of L^{-1}. The first term of this series corresponds to process a) above, and the succeeding terms to the effect of gas collisions on the long mean free path process. In a more recent paper (79) he has shown that, in the immediate

vicinity of a temperature discontinuity, processes involving long mean free path conditions apply and not the Fourier law.

The above discussion suggests the existence of a temperature discontinuity in a normal temperature gradient, when a low pressure of gas is adjacent to a heated surface.

Two expressions have been derived to formulate quantitatively the extent of the discontinuity, g, from the heated surface, and the magnitude of the temperature difference involved.(80)

$$g = \frac{2-\alpha}{\alpha} \cdot \frac{4d}{\gamma+1} \cdot \frac{k}{\mu c_v} L \qquad (64$$

where k is the thermal conductivity,

μ is the viscosity,

c_v is the specific heat at constant volume.

γ is the ratio of the specific heats,

and d is a constant, $0.491 < d < 0.499$, determined from the relationship

$\mu = d\rho\bar{v}L$

where ρ is the density,

and $\bar{v}$ the average velocity of the gaseous molecules.

$$\delta = \frac{15}{2\pi} \frac{2-\alpha}{\alpha} L \frac{dT}{dn} \qquad (65$$

where δ is the magnitude of the temperature discontinuity,
and $\frac{dT}{dn}$ is the normal temperature gradient.

On examining the results in Tables II to X it is found that high values of the energy were obtained for low pressure measurements. This is particularly noticeable with the foil measurements when the energy absorbed should be independent of pressure. The reason for these high values is therefore that, as the total pressure in the system is reduced, both g and δ increase and therefore the average rise in tem-:perature in the gas is affected. A certain rise in temperature (measured as a pressure change) occurs with the absorption of radiation, but when simulating this with the heated wire more energy has to be supplied to give the same temperature increase be-:cause of the presence of the temperature discon-:tinuity.

This rise in the measured energy at low pressures has been explained by the above, but it is possible that another process was contributing to the change in energy with pressure, viz. the inefficient trans-:port of heat by the internal modes of the molecule during collision. Heat conduction (and therefore the apparent thermal conductivity) involves both the translational and the internal modes in a molecule.

Although translational and rotational energy are brought to an equilibrium distribution after a few collisions, for vibrational energy thousands of collisions are normally required. Thus, at low pressures, there might be too few collisions for ex-:cess vibrational energy to be released (81). This effect has been reported by several authors (82)(83) (84) for pressures below approximately 5 cm.Hg.

It was decided to determine the possibility of this effect competing with the long mean free path process. This was done by taking measurements on a monatomic gas, argon, where there are no vibrational degrees of freedom, and the results are given in Table X. It was found from these measurements that the percentage increase in the measured energy was almost precisely the same for monatomic and poly-:atomic molecules. This could mean either that the effect due to the inefficient transport of heat by the internal modes was absent for the gases consid-:ered, or that the effect is exactly the same for the absorbed energy (of gas or foil) and the simulation energy (of the wire).

Whichever reason is correct,the increase in the required energy at low pressures was due to the tem-:perature discontinuity at the gas-solid interface alone.

To allow for the presence of this factor in the foil measurements was unnecessary, but it was of value to estimate the effect for the measurement of the energy absorbed by the gas. There are several papers dealing with the effect in measurements of thermal conductivities of gases (85)(86)(87)(88)(68). However, their case is simplified by the fact that the energy input to the wire is kept constant for all pressures, whereas this is obviously not true when simulating the energy absorbed by the gas.

Perhaps the most accurate method of dealing with the problem is that of Dickens (87), and it is a procedure which enables an estimate of the percentage effect for the varying simulation energy to be cal-:culated.

The model used is that of a heated wire within a concentric cylinder when the energy conducted to the gas is

$$G_k = \frac{2\pi k l_w \theta}{\ln \frac{r_2}{r_1} + \frac{m}{r_1} + \frac{m^1}{r_2}} \qquad (66$$

where l_w is the length of the wire,

θ is the temperature difference between the wire and the walls,

r_1 and r_2 are the radii of wire and cylinder respectively,

and m and m^1 are determined as follows.

For the wire - gas surface,

$$\delta = \frac{15}{2\pi}\,\frac{2-\alpha}{\alpha}\,L\left(\frac{dT}{dn}\right)_{wire} = m\left(\frac{dT}{dn}\right)_{wire}$$

and for the wall - gas surface, $\delta^1 = m^1\left(\frac{dT}{dn}\right)_{wall}$ in a similar manner.

From equation (66, since m and m^1 are proportional to L which is inversely proportional to the pressure,

$$G_k = \frac{2\pi k l_w \theta}{\ln\frac{r_2}{r_1} + \frac{W}{p}}$$

where W is a constant of the apparatus, and p is the pressure of the gas.

$$\text{and } G_o = \frac{2\pi k l_w \theta}{\ln\frac{r_2}{r_1}}$$

where G_o is the energy conducted in the absence of the temperature dis-:continuity effect.

For the straightforward case of a constant energy input at all pressures, G_o is readily found as the reciprocal intercept in a plot of $1/G_k$ against $1/p$.

For the varying simulation energy in the ab-:sorption cell an adequate estimation is obtained from

$$G_k - G_o = 2\pi k l_w \theta\left[\frac{1}{\ln\frac{r_2}{r_1} + \frac{m}{r_1}} - \frac{1}{\ln\frac{r_2}{r_1}}\right]$$

$$= C\left[\frac{1}{\ln\frac{r_2}{r_1} + \frac{m}{r_1}} - \frac{1}{\ln\frac{r_2}{r_1}}\right] \qquad (67$$

where C can be regarded as a constant at each pressure, and the factor $\frac{m^1}{r_2}$ has been ignored because of the very low tempera-:ture gradient prevailing in the gas next to the walls.

m can be calculated by using experimental values of the accommodation coefficient and substi-:tuting in

$$m = \frac{15}{2\pi} \quad \frac{2-\alpha}{\alpha} \quad L.$$

α for both methane and nitrous oxide on a plati-:num surface was taken as 0.5 (68) and the result obtained for 1cm.Hg pressure was that G_k was 5% higher than G_o.

This value was checked in several ways by using the literature (89)(88) on thermal conductivity measurements, and was found to be in agreement with calculations based on several different approaches.

Graph VI was therefore plotted showing the per-:centage effect of the temperature discontinuity factor at different pressures of gas. This graph is applicable to results taken on the energy absorbed by the gas, although, because of the geometrical approx-:imations used, is only of an approximate nature.

2.2.2.4.1 <u>Blackened Foil</u>

Although, as has been indicated, no quantitative calculations were attempted for the case of the foil,

Graph VI

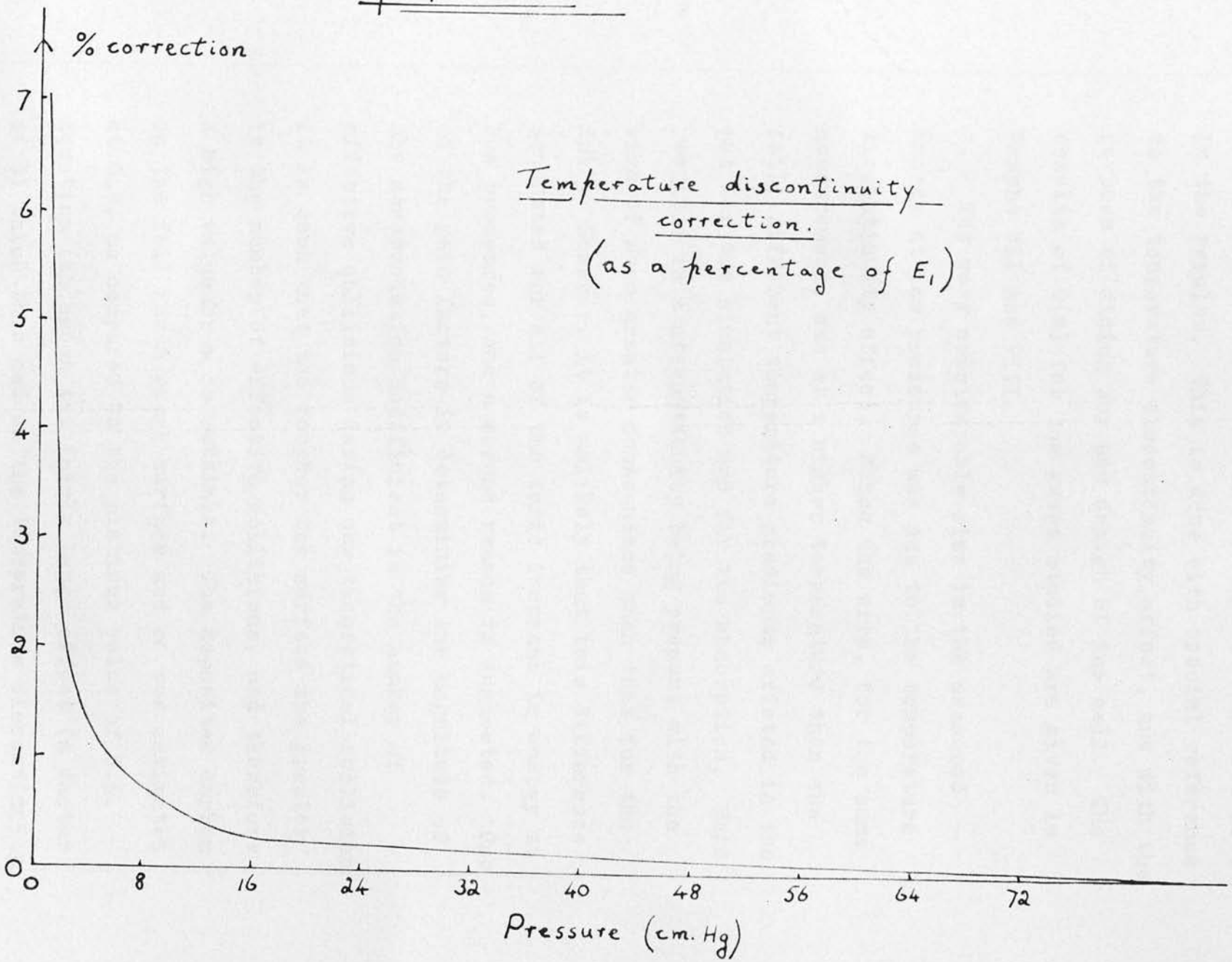

Temperature discontinuity correction.
(as a percentage of E_1)

it is of interest to study briefly the main features in the results. This is done with special reference to the temperature discontinuity effect, and with the purpose of aiding any new design of the cell. The results of Q(m) for the gases studied are given in Graphs VII and VIII.

The very considerable rise in the measured energy at low pressures was due to the temperature discontinuity effect. Since the wire, for the same measurement, was at a higher temperature than the foil, different temperature gradients existed in the gas for the simulation and for the absorption. This resulted in a discontinuity being present with the wire of much greater consequence than that for the foil. However, it is unlikely that this difference accounted for all of the large increase in energy at low pressures, and a second reason is suggested. One of the main factors in determining the magnitude of the accommodation coefficient is the number of effective collisions during one theoretical collision. It is seen that the rougher the surface the greater is the number of effective collisions, and therefore a high value for α is obtained. The deposited carbon on the foil had a rough surface and α was estimated at 0.9, as compared to the platinum value of 0.5. Equation (65 shows the fairly large effect (a factor of 3) which this had on the temperature discontinuity,

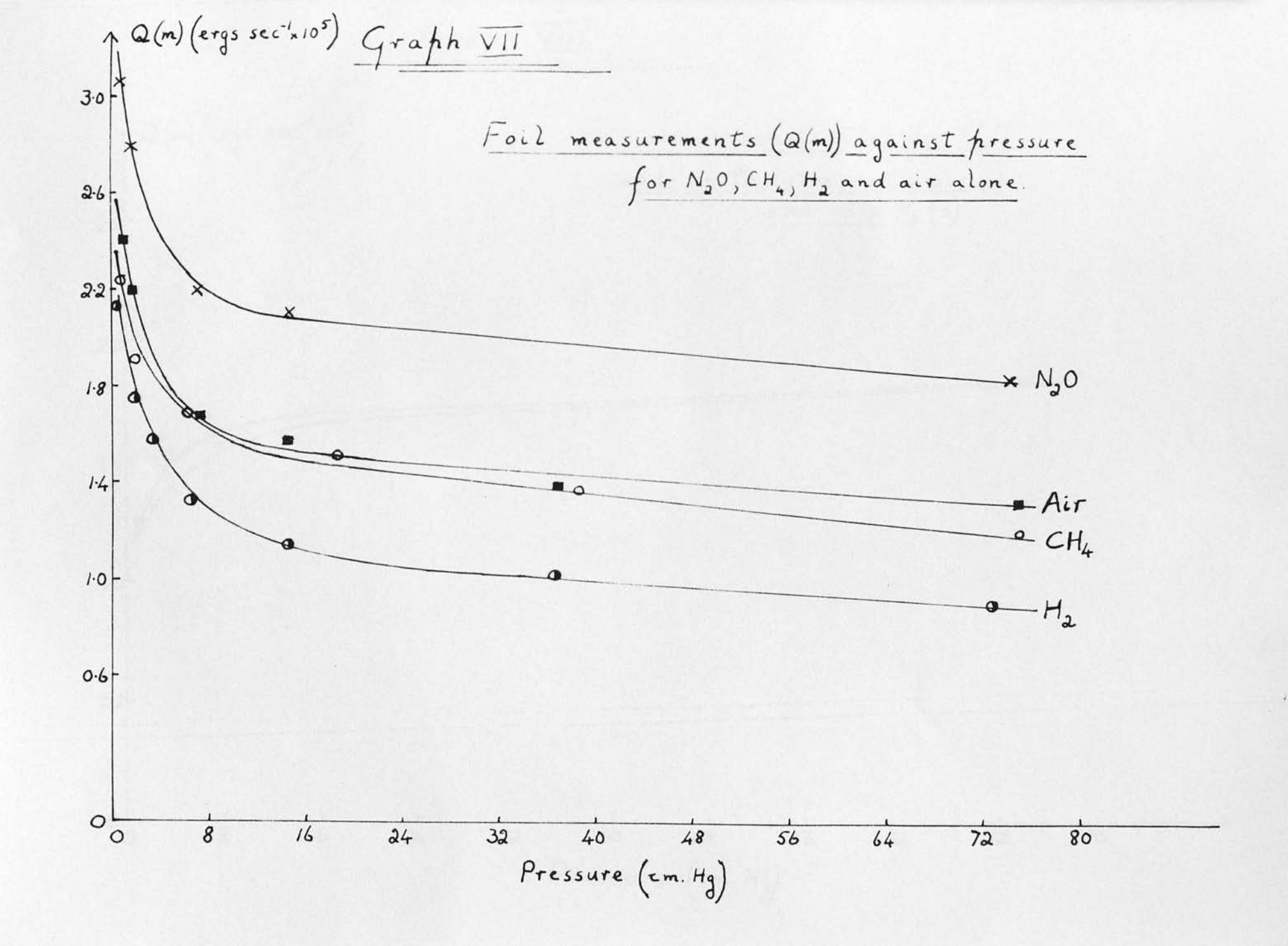
Q(m) (ergs sec⁻¹ x 10⁵)
Graph VII
Foil measurements (Q(m)) against pressure for N₂O, CH₄, H₂ and air alone.
3·0
2·6
2·2
1·8
1·4
1·0
0·6
0
0
8
16
24
32
40
48
56
64
72
80
Pressure (cm. Hg)
N₂O
Air
CH₄
H₂

Graph VIII

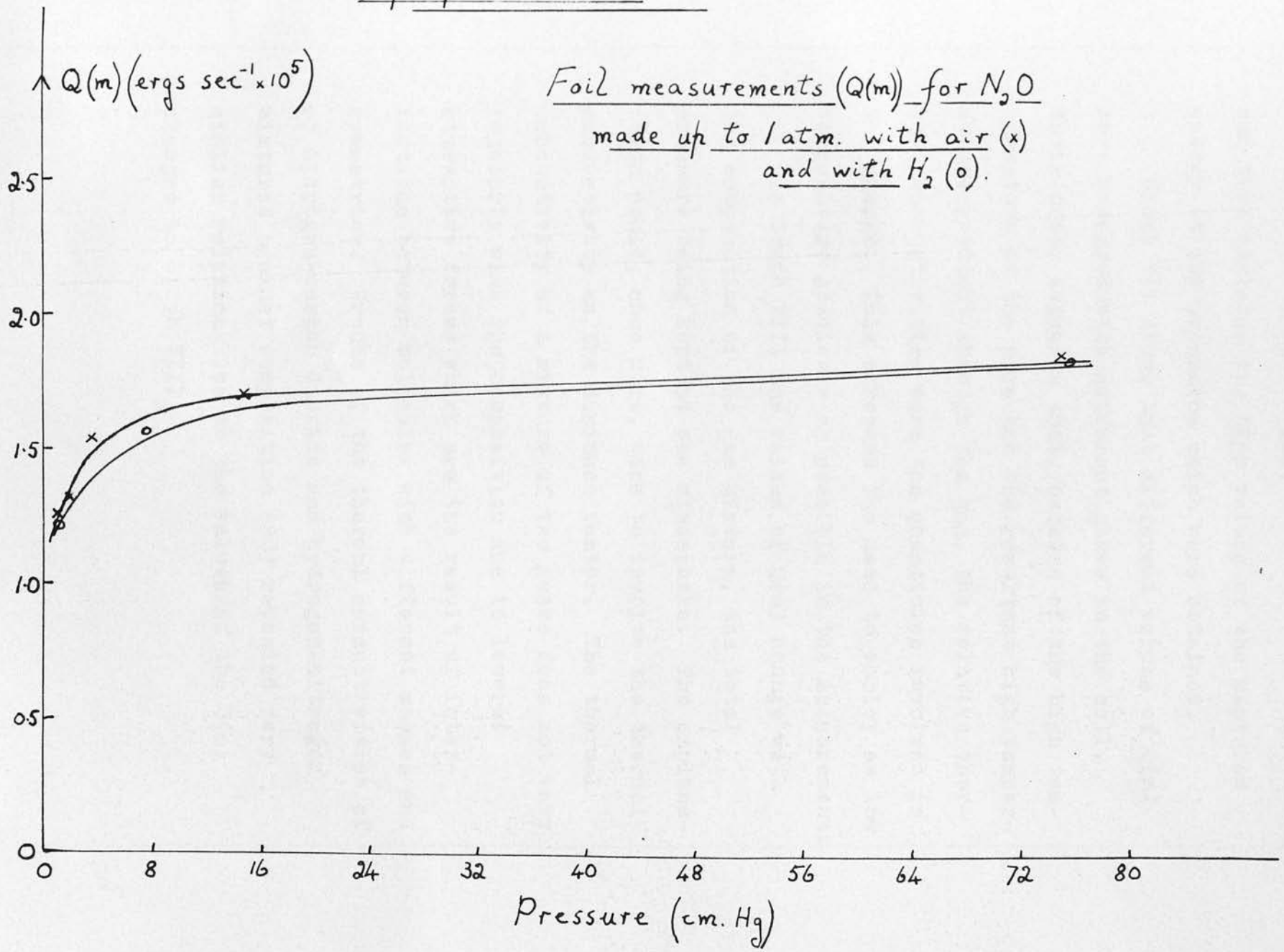
Q(m) (ergs sec^{-1} x 10^5)
Foil measurements (Q(m)) for N_2O made up to 1 atm. with air (x) and with H_2 (o).
2·5
2·0
1·5
1·0
0·5
0
0
8
16
24
32
40
48
56
64
72
80
Pressure (cm. Hg)

and thus explains the high values of the measured energy at low pressures which were obtained.

Graph VII shows that different values of Q(m) were measured with different gases in the cell. Their order suggests that, because of the high tem-:perature of the wire and the resultant high temper-:ature gradient through the gas, the relative ther-:mal conductivities were the quantities involved in the change. This stresses the need to employ as low temperature gradients as possible in the measurements.

In Graph VIII the values of Q(m) change with the composition of the gas mixture, the total pressure being kept at one atmosphere. The explana-:tion would, once more, seem to involve the thermal conductivity as the dominant factor. The thermal conductivity of a mixture of two gases does not vary regularly with the composition due to lowered attractive forces which are the result of inter-:actions between molecules with different masses and symmetries. Graphs of the thermal conductivities of of hydrogen-carbon dioxide and hydrogen-nitrogen mixtures against composition (90) revealed very similar relationships to the values of the Q(m) changes in Graph VIII.

2.2.2.4.2 Temperature of Gas next to Walls

In the preceding discussion it has been assumed that the temperature of the gas next to the walls is the same as the temperature of the outside of the walls, i.e. room temperature.

This can be shown to be valid (88) by using the following equation,

$$T_1 = T_2 + \frac{G_k \ln r_3/r_2}{2\pi \lambda_b l_w}$$

where T_1 and T_2 are the temperatures inside and outside the wall respectively,

G_k is the measured energy,

l_w is the length of the wire,

λ_b is the thermal conductivity of brass,

and r_2 and r_3 are the internal and external radii of the walls.

This assumes cylindrical geometry in the cell which has been the usual approximation.

For a sample case, of high G_k, T_2-T_1 was only 10^{-3}°C, which means that the inside temperature was effectively the same as room temperature, as has been assumed.

2.2.2.5 Effect of Other Absorption Bands on the energy absorbed by the gas.

There are two separate cases to be considered here, viz. the overlapping of the bands in methane and nitrous oxide by atmospheric absorption, and the presence in the region 3 to 5μ of other weak bands of the two gases.

The two bands under study are:

CH_4, the ν_3 band at 3018cm^{-1},
stretching from 2850cm^{-1} to 3200cm^{-1},

and N_2O, the ν_3 band at 2224cm^{-1},
stretching from 2170cm^{-1} to 2260cm^{-1}.

(15)(91)

2.2.2.5.1 Atmospheric overlapping

The strong CO_2 band at 2349cm^{-1} stretches from 2290cm^{-1} to 2385cm^{-1} (15) and therefore does not interfere with either of the above two bands. The combination band centred at 2077cm^{-1} likewise does not interfere, but the fundamental of the $C^{13}O_2$ molecule centred at 2285cm^{-1} does overlap the N_2O band. However, the very small concentration of $C^{13}O_2$ is the atmosphere (c.1.1%) makes this effect completely negligible (less than 0.3%).

The first overtone of the ν_2 band of H_2O vapour is centred at 3151cm^{-1} and stretches from 3020cm^{-1} to 3340cm^{-1} (15). This overlaps the CH_4 band. By calculating the fractional absorption of the overtone

for the region of overlap (estimating a value for the intensity from reference (1)) it was found that the effect was to decrease the average incident energy on the methane band by around 0.5%. This calculation is correct to $\pm$0.3% only, but the effect is practically negligible.

2.2.2.5.2 Other Weak Bands of N_2O and CH_4

The energy absorbed by the gas includes the absorption of weak bands present in the filtered region 3 to 5μ.

For N_2O the $\Pi - \Pi$ transition at 2210cm^{-1} and the combination bands at 2462cm^{-1} and 2798cm^{-1} are all negligible in comparison to the very strong absorption of the ν_3 fundamental. However, the first overtone of the ν_1 band at 2564cm^{-1} is not altogether negligible and can be estimated at 1% of the fundamental ν_3.(1)

For CH_4 it is possible to estimate the effect of the overtone of ν_4 at 2600cm^{-1} and the combination band at 2823cm^{-1} as being 1$\pm$0.5% of the ν_3 fundamental. (29)

These percentage corrections are those applicable for intensity measurements, but the absorption of the weak bands is of more significance as a fraction of the total energy measured at higher reduced pathlengths when the absorption is no longer directly proportional to the intensity of the band.

2.2.2.6 Absorption by the Walls

Due to the fact that the beam of radiation was not perfectly focussed and that therefore it diver-:ged slightly over the length of the cell, wall ab-:sorption took place. This was shown by the results in Table VIII for the energy absorbed by air alone, the absorption by carbon dioxide in the air being negligible in comparison to the values obtained. Having allowed for the effect of end-conduction from the platinum wire, it was noticed that the measured energies increase at low pressures. It was therefore assumed that reflection from the walls on to the foil, supposedly held by the magnet out of the way, was also happening with a resultant temperature dis-:continuity effect at low pressures. From the pre-:vious section it is known that with foil measure-:ments the thermal conductivity of the gas influences the results (Graph VII), and, on the basis of this knowledge, Graph IX was plotted showing the correc-:tion for both methane and nitrous oxide.

Graph IX

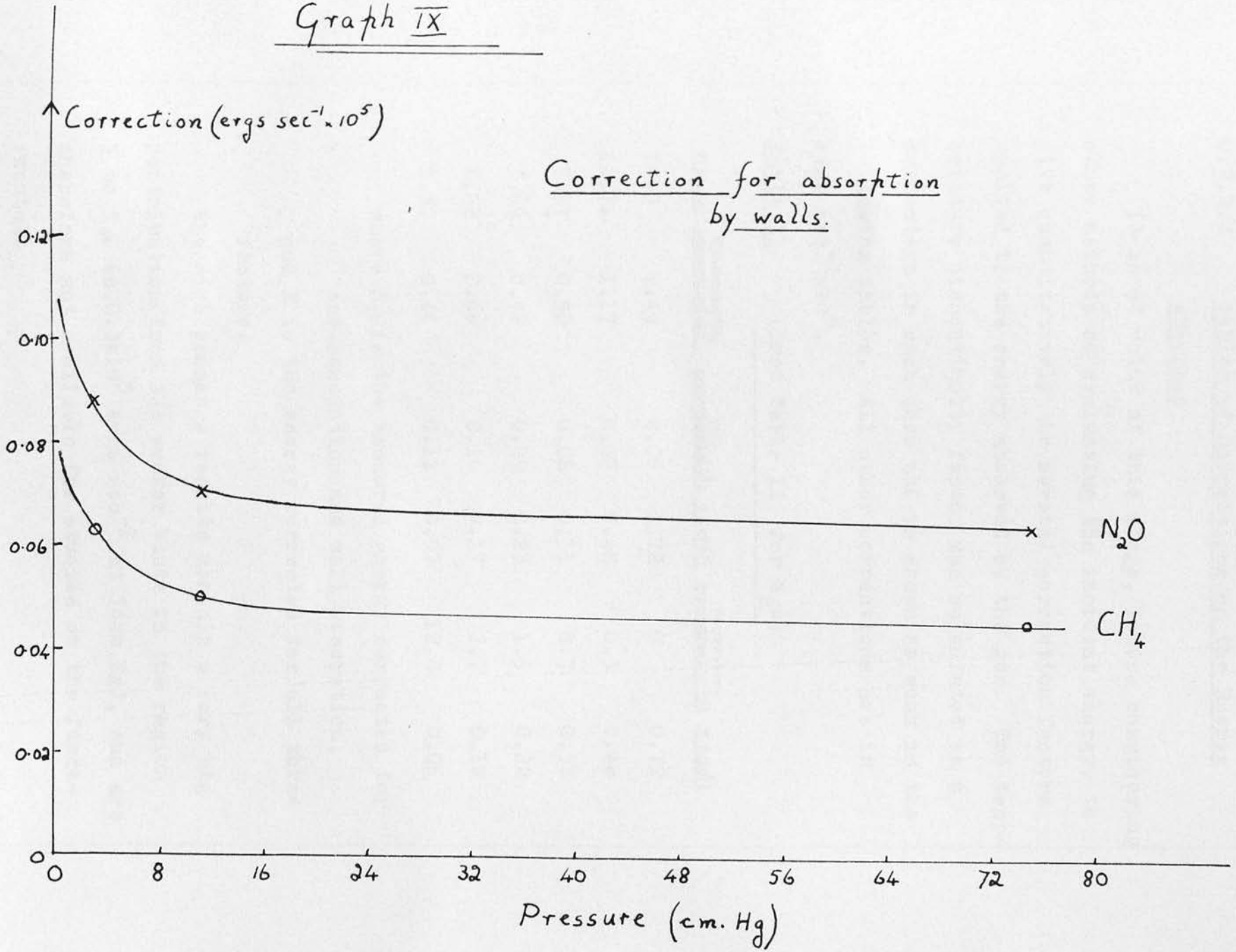
Correction (ergs sec^{-1} × 10^5)
Correction for absorption by walls.
0·12
0·10
0·08
0·06
0·04
0·02
0
0
8
16
24
32
40
48
56
64
72
80
Pressure (cm. Hg)
N_2O
CH_4

2.2.2.7 Tables of Corrections on the Energy Absorbed

It is of value at this stage, before considering other methods of evaluating the incident energy, to give quantitatively the several correction factors applied to the energy absorbed by the gas. The temp-:erature discontinuity factor was calculated as a percentage in each case and is shown as such in the following tables. All other corrections are in ergs $sec^{-1} x10^5$.

Table XI (from Table II for N_2O)

P(cm.Hg)	End-conduction correction($x10^5$)	Wall correction($x10^5$)	E_1($x10^5$)	Temperature discontinuity (%)	E ($x10^5$)
74.0	1.49	0.06	0.72	0	0.72
14.74	1.17	0.07	0.48	0.3	0.48
7.37	0.90	0.08	0.31	0.7	0.31
3.69	0.76	0.09	0.23	1.5	0.22
1.83	0.66	0.10	0.17	2.7	0.16
0.37	0.46	0.11	0.07	12.0	0.06

where E_1 is the measured energy corrected for end-conduction and wall absorption,

and E is the energy corrected for all three factors.

The high pressure results contain a very big contribution from the weaker bands in the region 3 to 5μ (c.$0.3x10^5$ ergs sec^{-1} at 74cm.Hg), and are therefore not available for studies on the funda-:mental.

Table XII (from Table VII) for CH_4

P(cm.Hg)	End-conduction correction($\times 10^{-2}$)	Wall correction($\times 10^5$)	E_1($\times 10^5$)	Temperature discontinuity (%)	E ($\times 10^5$)
74.9	0.77	0.05	0.27	0	0.27
38.5	0.54	0.05	0.16	0.2	0.16
18.6	0.38	0.05	0.09	0.3	0.09
6.8	0.33	0.05	0.07	0.75	0.07
2.0	0.35	0.07	0.06	2.4	0.06
0.95	0.31	0.07	0.047	5.5	0.045

The second series of results on CH_4 was measured using a different incident energy, and is detailed below.

Table XIII (from Table IX) for CH_4

P(cm.Hg)	End-conduction correction($\times 10^{-2}$)	Wall correction($\times 10^5$)	E_1($\times 10^5$)	Temperature discontinuity (%)	E ($\times 10^5$)
32.90	0.30	0.02	0.10	0.2	0.10
10.04	0.18	0.03	0.05	0.5	0.05
3.35	0.15	0.03	0.03	1.5	0.03
0.91	0.16	0.04	0.02	5.8	0.02

2.2.2.8 Calculation of the Incident Energy

From a temperature of the Nernst filament of 1660°K, the ratio Y (see section 2.1.6) was calcul-:ated as 2.39×10^{-14} sec. for methane,

and 2.15×10^{-14} sec. for nitrous oxide.

These values correspond to the results in Tables XI and XII.

Corresponding to the results in Table XIII, the temperature of the Nernst was 1410°K and the ratio Y was calculated as 2.36×10^{-14} sec. for methane.

The energy distributions from which Y was cal-:culated are shown in Graph X for both cases.

As has been stated, no values for Q(m) (see section 2.1.6) were available from measurements using the blackened foil. However, using the thermopile the following figures were obtained (section 2.1.6.1)

The calibration yielded $D = 1.13 \pm 0.10 \times 10^{16}$ quanta sec^{-1} over the area of the aperture.

and $Dh\nu = 0.52 + 0.04 \times 10^{5}$ ergs sec^{-1}

(the main errors coming from $(V_2 - V_1) = 0.82 \pm 0.06$ml. and the quantum efficiency $= 0.60 \pm 0.02$; errors from $N = 0.1071$ and $(1 - \frac{G_2}{G_1}) = 0.274$ were negligible).

Corresponding to this, a potential difference of 17.0 ± 1.0 microvolts was produced in the thermopile.

The potential difference produced by the infra-

Graph X

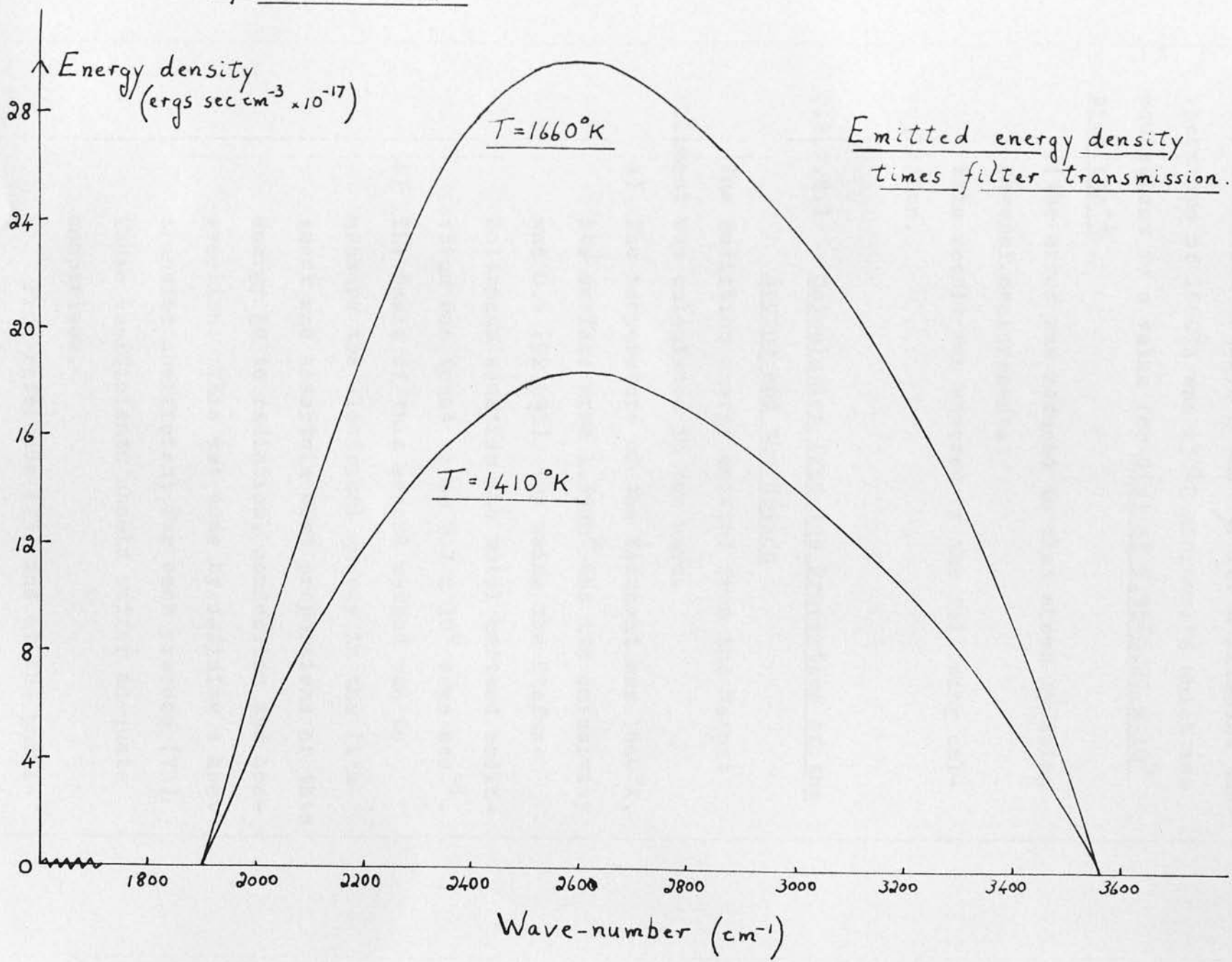
Energy density
(ergs sec cm^{-3} x10^{-17})
28
24
20
16
12
8
4
0
T=1660°K
T=1410°K
Emitted energy density
times filter transmission.
1800
2000
2200
2400
2600
2800
3000
3200
3400
3600
Wave-number (cm^{-1})

:red radiation between 3 and 5μ for a filament tem-:perature of 1660°K was 130±2 microvolts which was equivalent to a value for Q(m) of $3.95 \pm 0.27 \times 10^5$ ergs sec^{-1}

(the error was reduced to that shown by doing several measurements)

This result was checked by the following cal-:culation.

2.2.2.8.1 Calculation from the Properties of the Source and the Optics

The radiation energy emitted from the Nernst filament was calculated in two ways.

a) The temperature of the filament was 1660°K, its surface area 1.39cm^2 and its emissivity was 0.6 (92)(93). By using the Stefan-Boltzmann equation the total emitted radia-:tion was found to be 3.7×10^8 ergs sec^{-1}.

b) The basis of this second method was to measure the electrical energy in the fila-:ment and ascertain what proportions of this energy go to radiation, conduction and con-:vection. This was done by defining a heat transfer coefficient for each process (73). These coefficients should suffer adequate comparison.

From reference (73) and at the parti-:cular temperature used of 1660°K,

$h_c : h_v : h_r = 1.5 : 1.5 : 35$

where h_c, h_v and h_r are the heat transfer coefficients for the processes conduction, convection and radiation respectively.

The measured electrical energy was 3.99×10^8 ergs sec^{-1}, and therefore the energy emitted as radiation was 3.7×10^8 ergs sec^{-1}.

From a) and b),

the emitted radiation energy $= 3.7 \times 10^8$ ergs sec^{-1}

There were many factors in the optical arrangement which reduced the size of this energy value. These were treated separately in detail as follows, except for the effect of atmospheric absorption which was ignored. The result of this calculation was therefore equivalent to Q, and not to Q(m), where $Q = 1.04Q(m)$ (section 2.1.6)

c) The mirror did not give 100% reflection of the radiation. For a front - silvered mirror of the type used the percentage reflected (18) was $96 \pm 1\%$.

d) The source gave out radiation spherically, and the percentage included by the mirror

was calculated from $\frac{d^2}{16r^2} \times 100$

where d is the diameter of the mirror,
and r is the radius of the sphere.

The percentage included was found to be $7 \pm 0.2\%$.

e) Since the filters eliminate all emitted wavelengths except the band 3 to 5μ it was necessary to determine the amount of radiation in this range as a percentage of the total energy emitted. This was readily done using the Stefan-Boltzmann relation-:ships, and the calculated percentage was 11%.

f) From the data supplied by the manufacturers of the filters on their transmission charac-:teristics, it was found that the total per-:centage transmission was 32.5%.

g) Because of the difficulty in focussing the beam of radiation, not all of it entered the cell through the aperture. Of all the fac-:tors involved in this calculation this was the most difficult to estimate, but was judged from the relative areas of aperture and beam to be $50 \pm 10\%$.

h) The transmission of the sodium chloride windows in the region 3 to 5μ should be very close to 100%, but due to a small amount of clouding a value was assumed of 97%.

The effect of the above factors on the emitted radiation energy of 3.7×10^8 ergs sec^{-1} was calcul-:ated, and the resultant value was

$$Q = 4.3 \pm 1.0 \times 10^5 \text{ ergs sec}^{-1}$$

which is equivalent to -

$$Q(m) = 4.14 \pm 1.0 \times 10^5 \text{ ergs sec}^{-1}$$

This result agrees within the limits of error with that obtained using the thermopile, and there-:fore substantiates the use of the thermopile result.

It follows therefore from equation (57 that

$I(o) = 9.8 \pm 0.67 \times 10^{-9}$ ergs for methane,

$I(o) = 8.8 \pm 0.60 \times 10^{-9}$ ergs for nitrous oxide, corresponding to a Nernst tempera-:ture of $1660^{\circ}K$.

Similarly

$I(o) = 5.9 \pm 0.40 \times 10^{-9}$ ergs for methane, corresponding to a Nernst tempera-:ture of $1410^{\circ}K$.

Graph XI

The log of the energy absorbed divided by reduced pathlength against log of reduced pathlength.

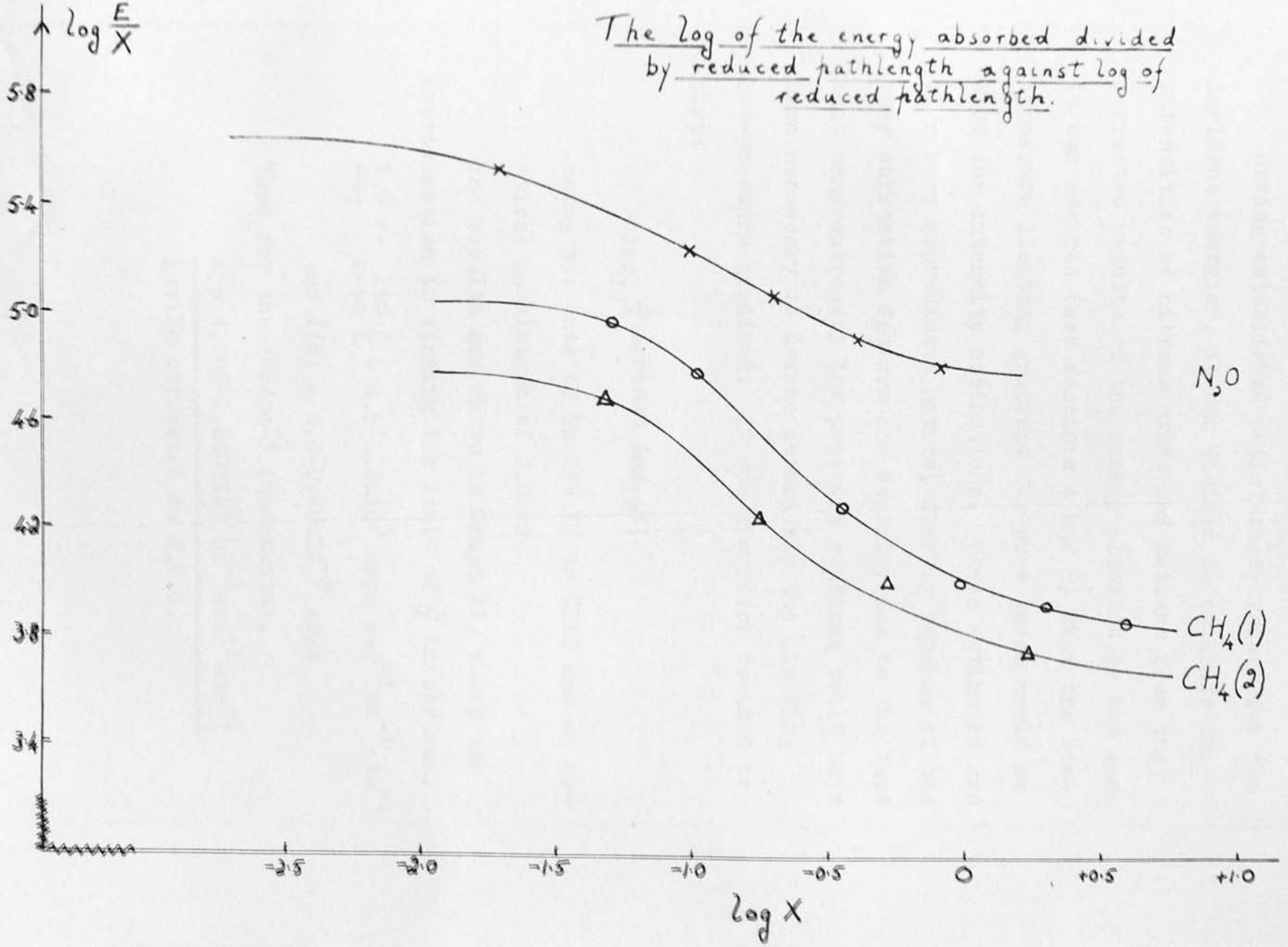

2.2.2.9 Assessment of Results

Having established satisfactory values for the incident energies, it was decided to estimate the intensities of nitrous oxide and methane from the corrected results of the energy absorbed by the gas. It was assumed (see sections 4 and 5) that the low-:pressure limiting gradient for pure gases could be used for intensity estimations. These estimates are of a very approximate nature, firstly because of the many correction factors and secondly due to the fact that many extremely low pressure readings would have been necessary to define accurately the limiting low-pressure gradient. It was therefore decided to plot:

$$\log_{10}\frac{E}{X} \text{ against } \log_{10}X,$$

using the data of Tables XI to XIII and an op-:tical pathlength of 3.80cm.

The results are shown in Graph XI, where the approximation in finding the limit of $\frac{E}{X}$ is obvious.

$\underline{N_2O}$:- $\lim_{x\to o}\frac{E}{X} = 4.5\pm1.0\times10^{5}$ ergs $sec^{-1}cm^{-1}atm^{-1}$

and $I(o) = 8.8\pm0.60\times10^{-9}$ ergs

Thus for the $2224cm^{-1}$ fundamental,

$$A = 4,900\pm1,140\times10^{10}\ cm^{-1}sec^{-1}atm^{-1}$$

having corrected to N.T.P.

CH_4 :-

(1) $\lim_{x \to o} \frac{E}{X} = 1.07 \pm 0.20 \times 10^{5}$ ergs $cm^{-1} sec^{-1} atm^{-1}$

and $I(o) = 9.8 \pm 0.67 \times 10^{-9}$ ergs

and for the $3018 cm^{-1}$ fundamental,

$$\underline{A = 1,020 \pm 205 \times 10^{10} \ cm^{-1} sec^{-1} atm^{-1}}$$

at N.T.P.

(2) $\lim_{x \to o} \frac{E}{X} = 5.62 \pm 1.05 \times 10^{4}$ ergs $sec^{-1} cm^{-1} atm^{-1}$

and $I(o) = 5.9 \pm 0.40 \times 10^{-9}$ ergs

Thus $\underline{A = 900 \pm 180 \times 10^{10} \ cm^{-1} sec^{-1} atm^{-1}}$ at N.T.P.

2.3 Experimental 2)

Because of the many corrections involved in, and the resultant approximate nature of, the previous results (section 2.2), it was decided to construct a new cell incorporating changes in design which would either eliminate or minimise the above factors. This was planned to yield accurate intensity measurements on methane and nitrous oxide.

The part of the cell containing the diaphragm and back-plate unit was left the same, except for a technical advance in attaining a more stable vacuum seal between the rod of the back-plate and the Teflon insulation plug. This was done by using a series of O-rings and is shown in Figure 6.

The absorption part of the cell was completely redesigned, the optical pathlength being shortened by approximately a factor of three (to 1.54 cms.) to enable lower reduced pathlengths to be attained. This pathlength was measured by using a micrometer screw guage on both polished windows before fixing them to the cell, and subtracting this distance from the total, of cell and windows, obtained after fixing. To prevent any slight divergence of the in-:cident beam of radiation causing absorption by the brass walls the sodium chloride window nearest the source was of smaller area than the back window (2.54cm by 2.54cm as against 5.08cm by 5.08cm.)

Vacuum Seal at back of cell

Figure 6

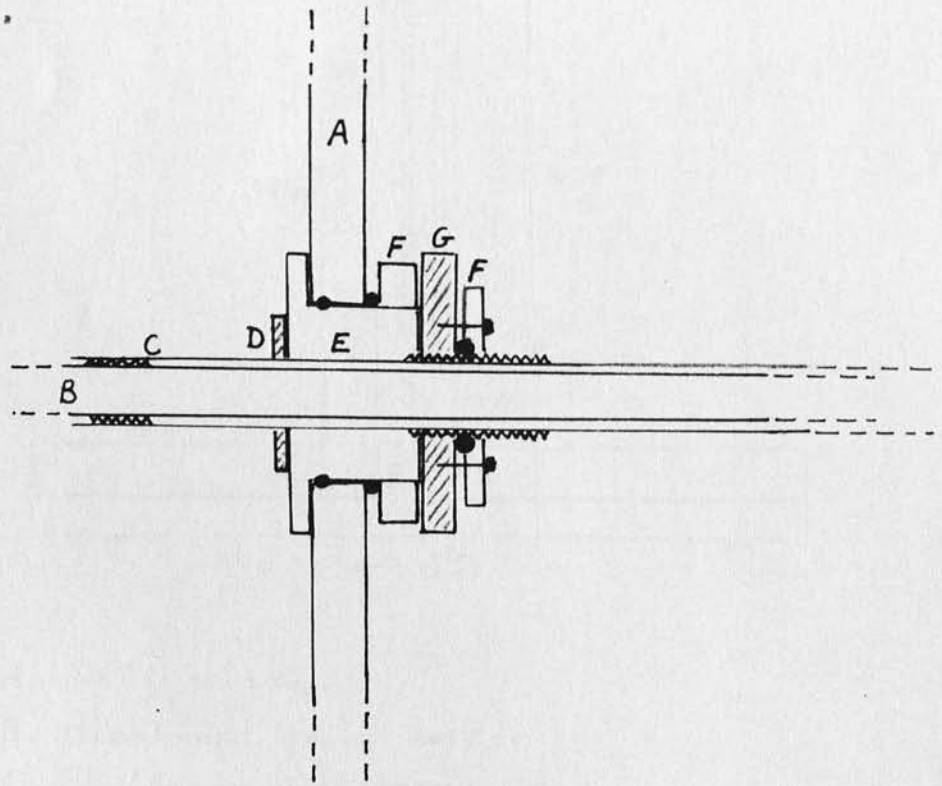

A. Cell wall
B. Steel rod attached to backplate
C. Brass tube
D. Brass flange
E. Teflon plug
F. Two brass plates
G. Nut, tightening on Teflon plug

The black circles represent O-rings.

Final Cell with Major Components

Figure 7

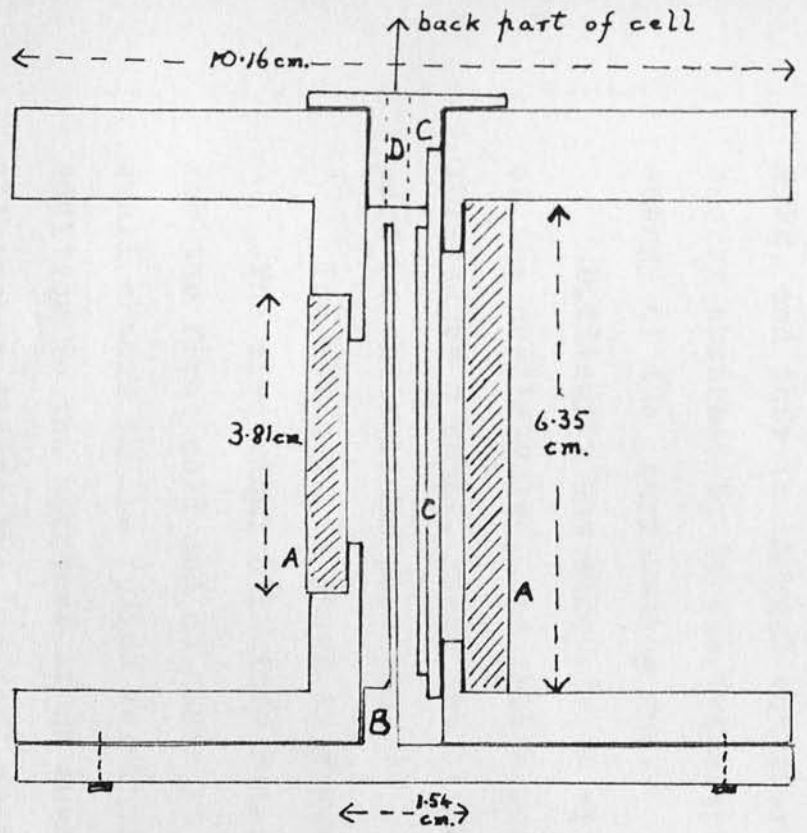

A. NaCl window
B. Blackened foil + holder
C. Platinum wire frame
D. Aperture to diaphragm

Blackened foil and frame

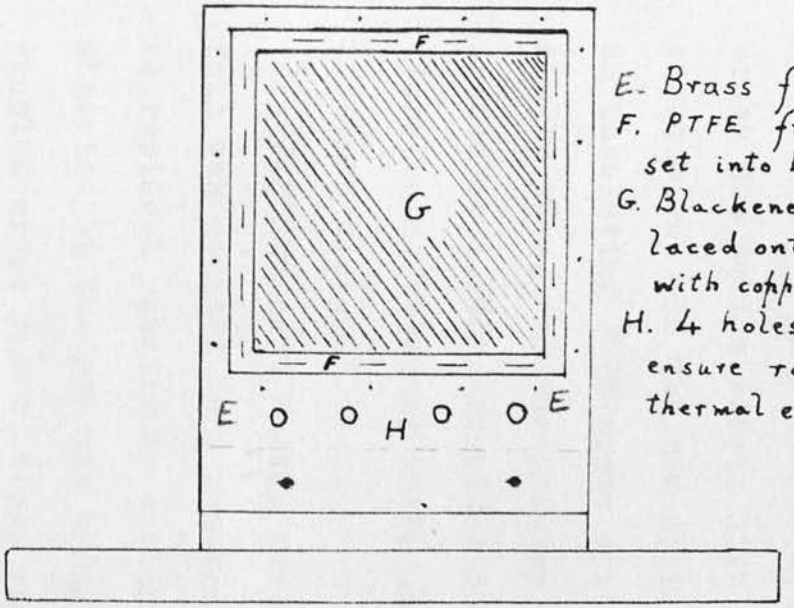

E. Brass frame
F. PTFE frame set into brass
G. Blackened foil laced onto PTFE with copper wire
H. 4 holes to ensure rapid thermal equilibrium

Platinum Wire Frame

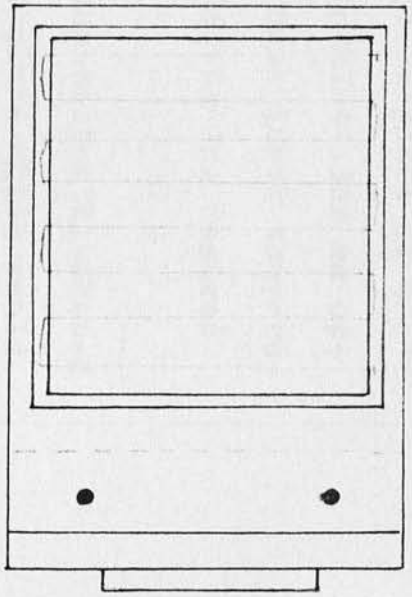

This is similar to above with the grid of wire laced onto PTFE which is set into the brass.

Many of the problems detailed in section 2.2 arose due to the fairly high temperature of the plat-:inum wire. In the new cell a grid of wires held on an insulating PTFE frame was used in place of a single wire, and the greater length, 44.3cm as op-:posed to 1.27cm, resulted in a much lower tempera-:ture being obtained while simulating the desired pressure rise.

For incident energy measurements the blackened foil was mounted on a removeable plate which could be replaced readily by a blank plate when the energy absorbed by the gas was being measured. Thus no problem arose due to stray radiation falling on the foil during gas absorption measurements. The foil was completely encased in a thin, insulating layer of PTFE, and thus in thermal equilibrium all radiant energy absorbed by it was transferred to the heat energy of the surrounding gas.

Difficulty was encountered with the vacuum seal of the needle-valve, and this arrangement was re-:placed by a small, glass tap as near the absorption part of the cell as possible.

The new cell is shown in Figure 7.

The electrical circuitry remained the same as for the first cell and as shown in Figure 5. One small change in the optics was incorporated, viz. the addition to the aperture of an inch long tube which, although reducing the incident energy, ensured much

more adequate collimation of the beam. The effic-:iency of the collimation was checked by measuring the area of the beam on the front and back windows.

Methane and nitrous oxide of the previously stated purity (section 2.1.4) were used. A certain pressure of non-absorbing gas, when added to the varying reduced pathlengths of CH_4 and N_2O used, enables the region of limiting gradient (see equation (30) to be reached at higher values of the reduced pathlength due to broadening of the rotational lines (1). The normal pressure-broadening gases are nitrogen, argon, helium and hydrogen. However, the choice of the broadening gas to be used was deter-:mined by the fact that at low pressures spontaneous emission was found to be a competing process with vibrational-translational energy transfer (section 1.3.2). The gas chosen therefore had to possess many low-lying vibrational modes in order to facili-:tate energy transfer from both the 3018cm^{-1} band of CH_4 and the 2224cm^{-1} band of N_2O. The normal broadening gases do not possess such modes, and would have necessitated total pressures in excess of one atmosphere to ensure that there was no loss due to spontaneous emission. The gas chosen was 'Arcton 13', CF_3Cl, (supplied by I.C.I. Ltd.) which has many vibrational modes below 2000cm^{-1} and which has no fundamental mode in the region of absorption

3 to 5 μ. Unfortunately an infra-red spectrum of the gas showed the presence of a strong overtone par-:tially overlapped by a weaker combination band, in the absorption region. These overlapping bands are simply referred to hereafter as the CF_3Cl overtone. The absorption of this overtone was measured for CF_3Cl alone in order to make the appropriate allowances in the energy absorbed by CH_4 and N_2O when arcton-broadening was used.

The procedure employed in taking measurements was as in section 2.1.5, and the blackened foil method of measuring the incident energy was checked both by direct calculation and by thermopile measurements.

2.4 Results 2)

Before tabulating the results obtained with the second cell, the main correction factors are enume-:rated. For gas absorption, in the pressure ranges considered, convection, radiation from the heated wire and the temperature discontinuity effect were eliminated, whilst with foil measurements it was shown experimentally that neither temperature dis-:continuity nor different thermal conductivities of the gases had any effect on the results.

End-conduction of heat from the wire was still present at around 3% of the total energy, but this correction was calculable with high accuracy (section 2.2.2.1).

It was found, by taking measurements with air and hydrogen, that the cell itself was absorbing radiation and giving rise to a pressure increase. This was caused by small amounts of Araldite, used to secure the sodium chloride windows, overlapping the incident beam from the aperture and filters. The energy absorbed in this way was constant with pressure of gas, and was accurately measurable using the non-absorbing gases, air and hydrogen. The carbon dioxide and water vapour in the air only gave a measurable pressure rise, due to absorption, at high pressures of air.

Although the loss of energy due to radiation from the heated wire was negligible with gas absorp-

:tion measurements, in the case of foil measurements a small percentage loss occurred for both the heated foil and wire since much higher energy values were involved. Using section 2.2.2.2 and an emissivity value for platinum of 0.1, it was calculated that, for the incident energy measured, the loss from foil and wire effectively cancelled one another (the loss was 1% of the values given in Table XVI in both cases to a first approximation).

The effect of atmospheric absorption bands and other bands of CH_4 and N_2O in the region 3 to 5 μ, as detailed in section 2.2.2.5, were taken into account during the final calculations.

For all the results recorded measurements of the current in the Nernst filament were taken. By having previously determined the resistance of the rheostat in the circuit (see Figure 5) and therefore the voltage across the filament, the current measurements were used to allow for any variation in the energy emitted from the source. The correction due to this factor was negligible (less than 0.5%) for results on CH_4, but with N_2O, when a different filament was used, it varied from 0 to 5%.

The actual error resulting from limitations in the accuracy of the millivoltmeter and milliammeter was calculated as 0.7%.

Tables of results, including these correction factors, are now given. Tables XIV to XX, those relating to CH_4 results, have a common incident energy value as detailed in Table XVI. Due to it being found necessary to change the filament, Tables XXI to XXV correspond to a different value of the incident energy.

Table XIV Air alone

Pressure(cm.Hg)	E_1(ergs $sec^{-1} x10^3$)	End-conduction correction (ergs $sec^{-1} x10^3$)	E(ergs $sec^{-1} x10^3$)
1.31	1.537	0.046	1.491
2.12	1.504	0.045	1.459
2.90	1.504	0.045	1.459
4.12	1.523	0.046	1.477
6.37	1.537	0.046	1.491
7.76	1.558	0.046	1.512
9.08	1.584	0.048	1.536
12.79	1.558	0.046	1.512

where E_1 is the energy measured with the wire,

and E is the corrected energy absorbed by the gas.

Table XV H_2 alone

Pressure(cm.Hg)	E_1(ergs $sec^{-1}x10^3$)	End-conduction correction (ergs $sec^{-1}x10^3$)	E (ergs $sec^{-1}x10^3$)
1.02	1.523	0.046	1.477
2.37	1.537	0.046	1.491
5.96	1.504	0.045	1.459
7.19	1.537	0.046	1.491
10.33	1.523	0.046	1.477
13.75	1.523	0.046	1.477

The value obtained for the energy absorbed by the cell itself, as measured in Tables XIV and XV, was used as the cell-constant correction for measurements listed in Tables XVI to XX.

Table XVI Foil measurement of incident energy; air in cell.

Pressure(cm.Hg)	$Q(m)_1$(ergs $sec^{-1}x10^4$)	End-conduction correction (ergs $sec^{-1}x10^4$)	Cell-constant correction (ergs $sec^{-1}x10^4$)	Q(m)(ergs $sec^{-1}x10^4$)
1.32	7.83	0.24	0.15	7.44
3.29	7.59	0.23	0.15	7.21
6.18	8.04	0.24	0.15	7.65
9.32	7.72	0.23	0.15	7.34
12.65	7.90	0.24	0.15	7.51
14.01	7.83	0.24	0.15	7.44
19.78	7.60	0.23	0.15	7.22

where $Q(m)_1$ is the energy measured with the foil, and Q(m) is the incident energy falling on the foil.

Table XVII CH_4 alone

Pressure(cm.Hg)	E_1(ergs $sec^{-1}x10^3$)	End-conduction correction (ergs $sec^{-1}x10^3$)	Cell-constant correction (ergs $sec^{-1}x10^3$)	E (ergs $sec^{-1}x10^3$)
0.62	1.568	0.046	1.48	0.04
0.84	1.604	0.048	1.48	0.08
1.18	1.768	0.054	1.48	0.23
1.99	2.009	0.060	1.48	0.47
3.07	2.371	0.072	1.48	0.82
4.09	2.690	0.081	1.48	1.13
4.56	2.813	0.085	1.48	1.25
5.27	2.864	0.086	1.48	1.30
6.95	3.248	0.096	1.48	1.67
10.34	3.535	0.106	1.48	1.95
14.04	4.144	0.125	1.48	2.54
14.06	4.118	0.125	1.48	2.51
16.30	4.582	0.136	1.48	2.97
18.42	4.576	0.142	1.48	2.95
22.09	5.119	0.157	1.48	3.48
26.21	5.852	0.178	1.48	4.19
33.60	6.504	0.198	1.48	4.83

The percentage error in the values of E at low pressures is very high due to these values being the result of subtracting two much larger quantities. However, their accuracy was greatly helped by doing each reading many times using different sensitivi-:ties of the Proximity Meter. For example, the error in E corresponding to a pressure of 1.18 cmHg

was ±8.3% (this follows from one measurement on E_1 being accurate to ±3%, the many readings taken re-:ducing this error to around ±1%, and the error in the cell-constant being as small as ±0.5% due to the many readings taken, not only at one pressure, but at many pressures), and the error in E corres-:ponding to 0.62cm.Hg was ±44%. At high pressures only one measurement of E_1 was taken, giving an error in E of around 4%.

Table XVIII CF_3Cl alone

Pressure(cm.Hg)	E_1 (ergs sec^{-1} $x10^3$)	End-conduction correction ($ergs\ sec^{-1}\ x10^3$)	Cell-constant correction ($ergs\ sec^{-1}\ x10^3$)	E ($ergs\ sec^{-1}\ x10^3$)
0.84	1.701	0.052	1.48	0.17
1.41	1.785	0.053	1.48	0.25
3.20	2.277	0.069	1.48	0.73
4.82	2.551	0.078	1.48	0.99
6.89	2.795	0.083	1.48	1.23
10.20	3.077	0.093	1.48	1.50
14.61	3.620	0.109	1.48	2.03
18.34	4.134	0.123	1.48	2.53
21.99	4.488	0.132	1.48	2.88
26.05	4.833	0.145	1.48	3.21
30.67	5.734	0.175	1.48	4.08

Table XIX CH_4 - CH_3Cl mixture, constant total pressure

P(T)	P(M)	P(A)	E_1(ergs sec^{-1} $x10^3$)	End-conduction correction (ergs sec^{-1} $x10^3$)	Cell-constant +Arcton correction (ergs sec^{-1} $x10^3$)	E(ergs sec^{-1} $x10^3$)
30.13	4.78	25.35	7.14	0.22	4.64	2.28
30.01	4.05	25.96	6.73	0.20	4.70	1.83
30.02	3.48	26.54	6.40	0.19	4.76	1.45
30.12	3.16	26.96	6.28	0.19	4.80	1.29
29.97	2.78	27.19	6.07	0.18	4.83	1.06
30.07	2.14	27.93	5.92	0.18	4.90	0.84
27.37	1.61	25.76	5.42	0.16	4.68	0.58
30.01	1.23	28.78	5.74	0.18	5.01	0.55

where P(T), P(M) and P(A) are the total pressure, the pressure of methane and the pressure of arcton respectively, in cm.Hg.

Table XX CH_4 - CF_3Cl mixture, at different total pressures

P(T)	P(M)	P(A)	E_1(ergs sec^{-1} $x10^3$)	End-conduction correction (ergs sec^{-1} $x10^3$)	Cell-constant +Arcton correction (ergs sec^{-1} $x10^3$)	E(ergs sec^{-1} $x10^3$)
2.85	0.81	2.04	2.27	0.07	1.90	0.30
4.08	1.16	2.92	2.58	0.08	2.06	0.44
8.03	2.29	5.74	3.40	0.10	2.58	0.72
9.41	2.69	6.72	3.70	0.11	2.69	0.90
15.32	4.37	10.95	4.56	0.14	3.15	1.27
21.11	6.03	15.08	5.34	0.16	3.58	1.60
26.08	7.44	18.64	6.25	0.19	3.97	2.09
31.03	8.84	22.19	7.02	0.22	4.33	2.47

For tablex XIX and XX the percentage error involved in E is discussed fully when calculating a value for the intensity of CH_4.(section 4.1.1)

Table XXI — Air alone, different incident energy from Table XIV

Pressure (cm.Hg)	E_1 (ergs $sec^{-1} \times 10^3$)	End-conduction correction (ergs $sec^{-1} \times 10^3$)	Source correction (ergs $sec^{-1} \times 10^3$)	E (ergs $sec^{-1} \times 10^3$)
1.09	3.14	0.10	+0.02	3.06
2.67	3.14	0.10	-0.02	3.02
3.78	3.11	0.10	+0.07	3.08
5.91	3.12	0.10	+0.08	3.10
7.31	3.12	0.10	+0.08	3.10
14.50	3.19	0.10	+0.08	3.17

where 'source correction' is the correction applied to the results due to the variation in the energy emitted from the Nernst filament.

Table XXII H_2 alone

Pressure (cm.Hg)	E_1(ergs $sec^{-1}x10^3$)	End-conduction correction (ergs $sec^{-1}x10^3$)	Source correction (ergs $sec^{-1}x10^3$)	E(ergs $sec^{-1}x10^3$)
2.02	3.14	0.10	0	3.04
4.97	3.14	0.10	0	3.04
7.59	3.11	0.10	-0.02	2.99
8.70	3.12	0.10	+0.02	3.04
10.37	3.17	0.10	+0.02	3.09

The value obtained for the energy absorbed by the cell itself, as measured in Tables XXI and XXII, was used as the cell-constant correction for measurements listed in Tables XXIII to XXV.

Table XXIII N_2O alone

Pressure (cm.Hg)	E1 (ergs $sec^{-1}x10^3$)	End-conduction (ergs $sec^{-1}x10^3$)	Source correction (ergs $sec^{-1}x10^3$)	Cell-constant (ergs $sec^{-1}x10^3$)	E (ergs $sec^{-1}x10^3$)
0.32	3.45	0.11	-0.07	3.05	0.22
0.49	3.68	0.11	-0.11	3.05	0.41
0.62	4.04	0.12	-0.14	3.05	0.73
0.79	4.35	0.14	-0.08	3.05	1.08
1.16	5.23	0.16	-0.22	3.05	1.80
2.17	6.67	0.20	+0.07	3.05	3.49
2.90	8.19	0.26	-0.24	3.05	4.64
3.48	8.82	0.28	-0.29	3.05	5.20
4.31	8.91	0.28	-0.29	3.05	5.29
7.04	10.60	0.33	0	3.05	7.22
9.71	12.23	0.38	0	3.05	8.80
13.32	13.17	0.40	-0.24	3.05	9.48

As for Table XVII a large number of readings were taken for the low pressure measurements, thus giving greater accuracy. The error in E corresponding to 0.32cm.Hg was calculated as $\pm$17%, and corresponding to 1.16cm.Hg the error was $\pm$3%.

Table XXIV CF_3Cl alone

Pressure (cm.Hg)	E_1 (ergs $sec^{-1}x10^3$)	End-conduction (ergs $sec^{-1}x10^3$)	Source correction (ergs $sec^{-1}x10^3$)	Cell-constant (ergs $sec^{-1}x10^3$)	E (ergs $sec^{-1}x10^3$)
24.70	10.15	0.31	0	3.05	6.79
29.37	10.37	0.32	+0.10	3.05	7.10
34.42	12.52	0.39	-0.21	3.05	8.87
36.01	11.92	0.37	-0.08	3.05	8.42
39.77	12.92	0.40	-0.21	3.05	9.26
45.03	13.30	0.41	+0.46	3.05	10.30

These measurements were taken for two reasons:

a) to extend arcton measurements to higher pressures than was done in Table XVIII.

b) the ratio of the two cell-constants, ob-:tained for the two sources, was used to calculate the incident energy in the second case, and the ratio of arcton ab-:sorption at a specified pressure was a useful check on this result.

Table XXV N_2O - CF_3Cl mixture, constant total pressure.

P(T) (cm.Hg)	P(N) (cm.Hg)	P(A) (cm.Hg)	E_1 (ergs $sec^{-1}x10^3$)	End-conduction correction (ergs $sec^{-1}x10^3$)	Source correction (ergs $sec^{-1}x10^3$)	Cell-constant +Areton correction (ergs $sec^{-1}x10^3$)	E (ergs $sec^{-1}x10^3$)
38.13	4.01	34.12	21.93	0.64	+0.41	11.49	10.21
38.17	3.01	35.16	19.78	0.59	+0.62	11.70	8.11
37.91	2.04	35.87	17.77	0.53	+0.97	11.83	6.38
38.23	1.82	36.41	17.71	0.53	+0.99	11.97	6.20
38.11	1.40	36.71	17.20	0.51	+0.25	12.01	4.93
37.97	1.07	36.90	16.04	0.48	+0.29	12.06	3.79
38.13	0.89	37.24	15.45	0.45	+0.21	12.10	3.11

where P(N) is the partial pressure of N_2O in cm.Hg.

The results expressed in Tables XIV to XXV are shown in Graphs XII to XIX.

Graph XII

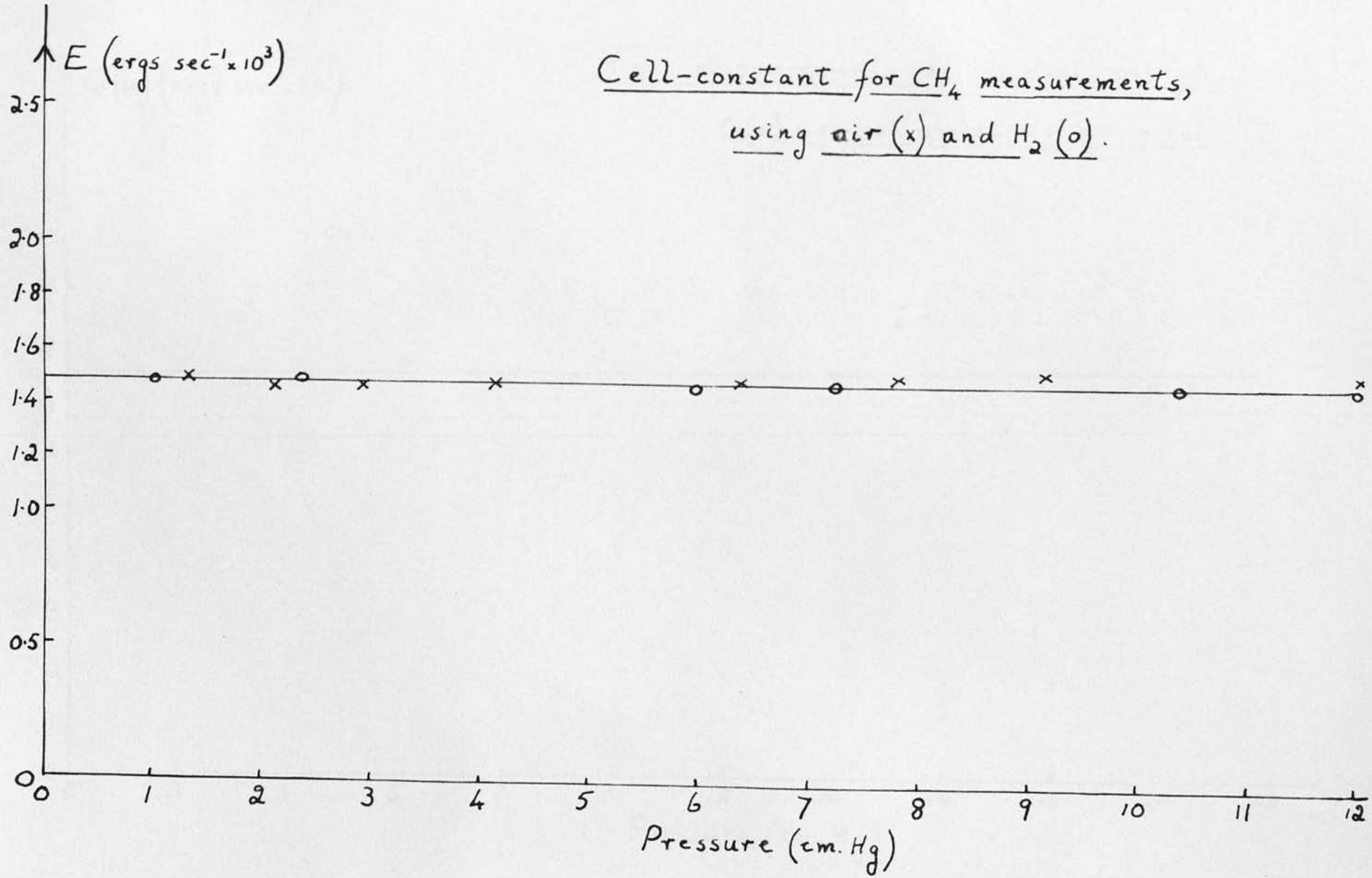
E (ergs sec⁻¹ x 10³)
Cell-constant for CH4 measurements, using air (x) and H2 (o).
2·5
2·0
1·8
1·6
1·4
1·2
1·0
0·5
0
0
1
2
3
4
5
6
7
8
9
10
11
12
Pressure (cm. Hg)

Graph XIII

Foil measurements of incident energy, Q(m) against pressure of air in cell.

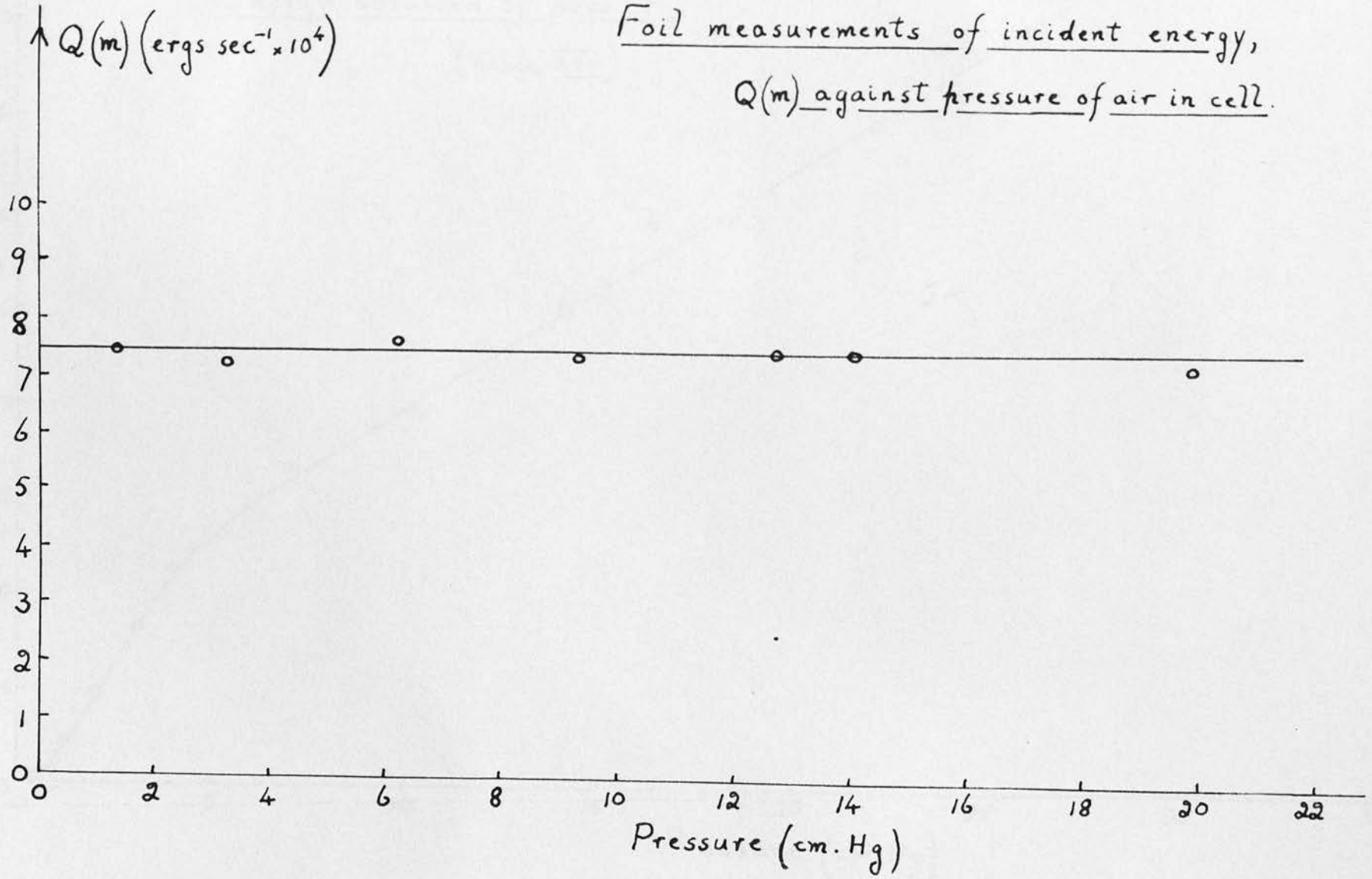

Graph XIV

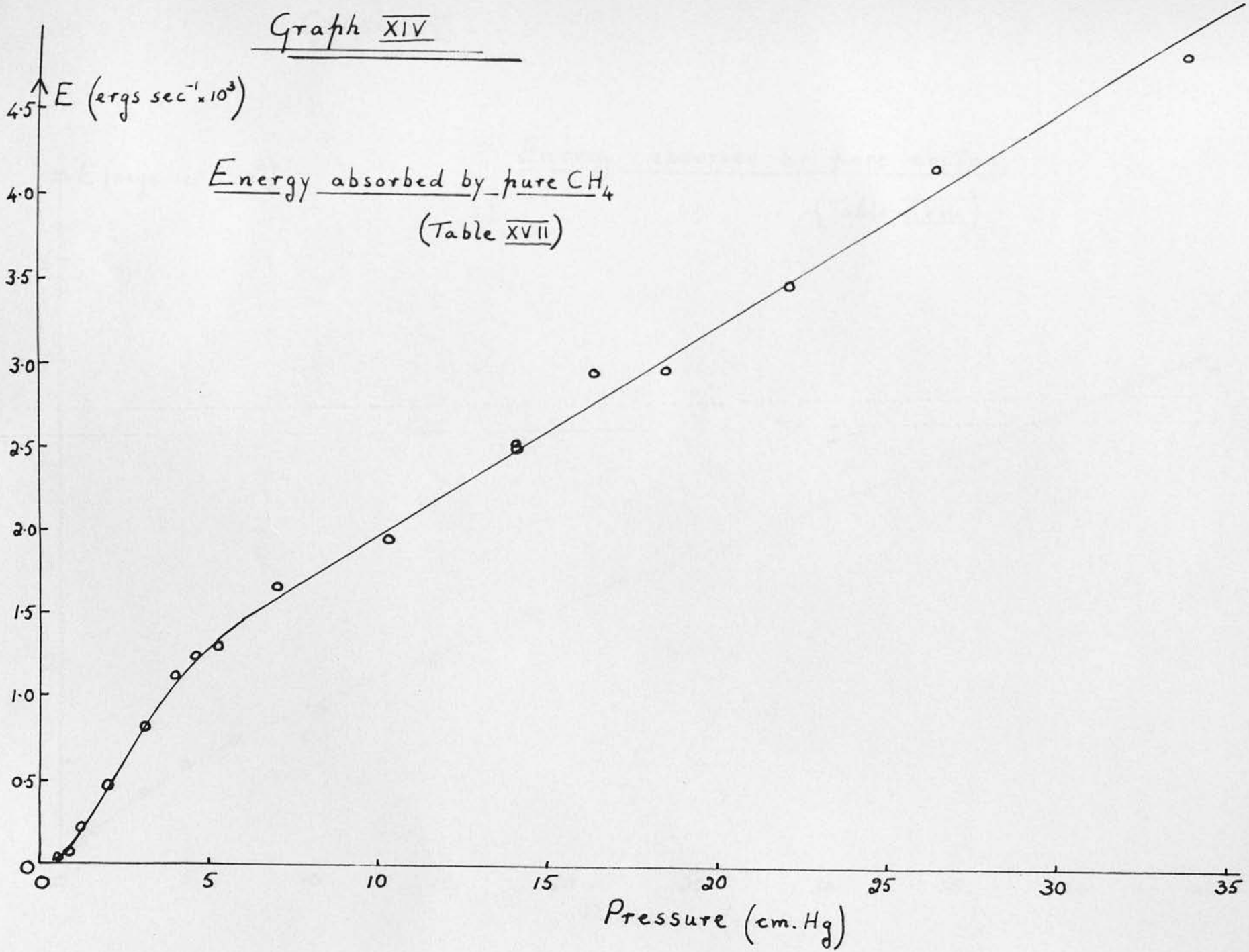
E (ergs sec⁻¹ × 10³)
Energy absorbed by pure CH₄
(Table XVII)
4·5
4·0
3·5
3·0
2·5
2·0
1·5
1·0
0·5
0
0
5
10
15
20
25
30
35
Pressure (cm. Hg)

Graph XV

Energy absorbed by pure arcton.
(Table XVIII)

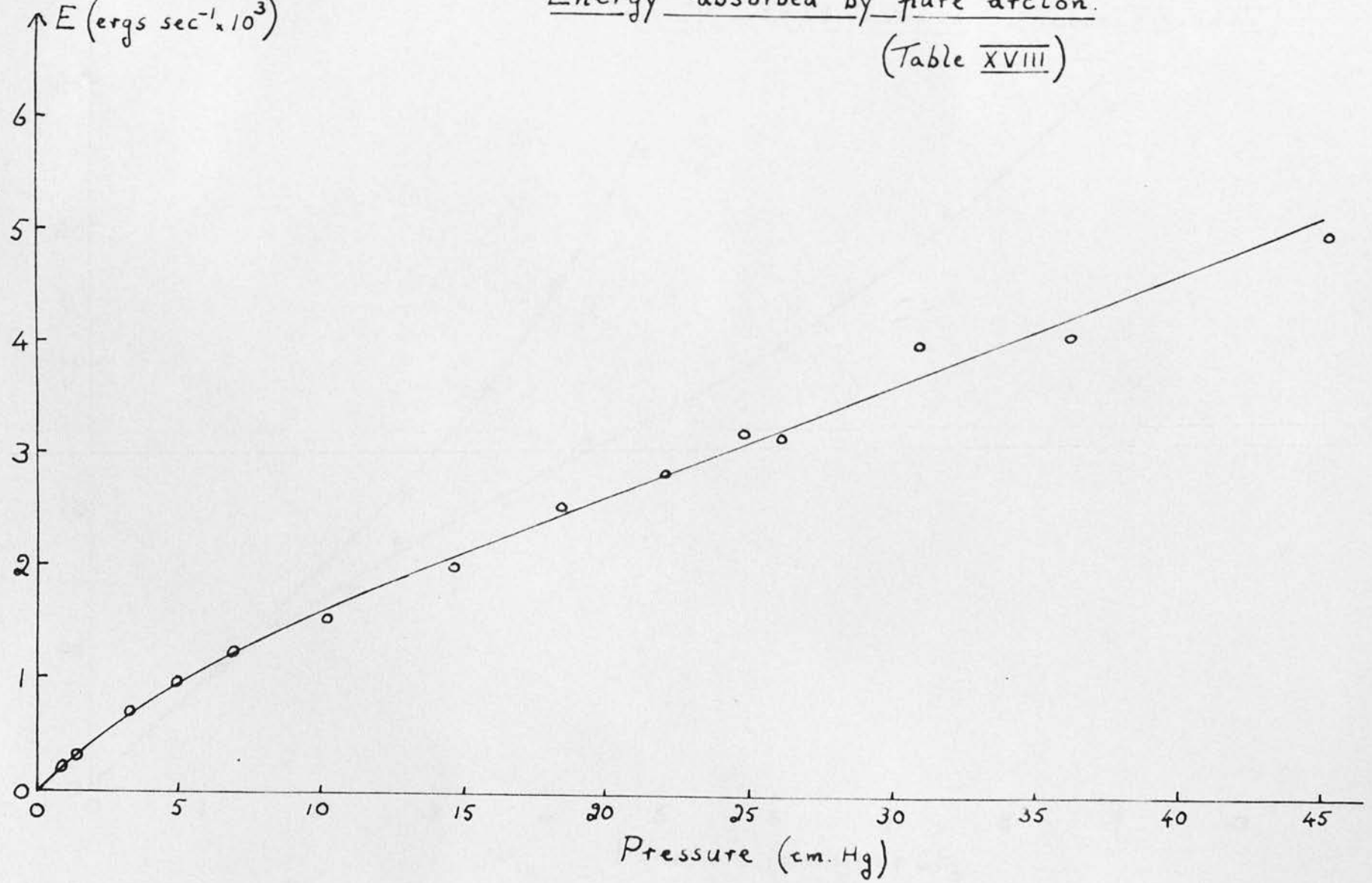

Graph XVI

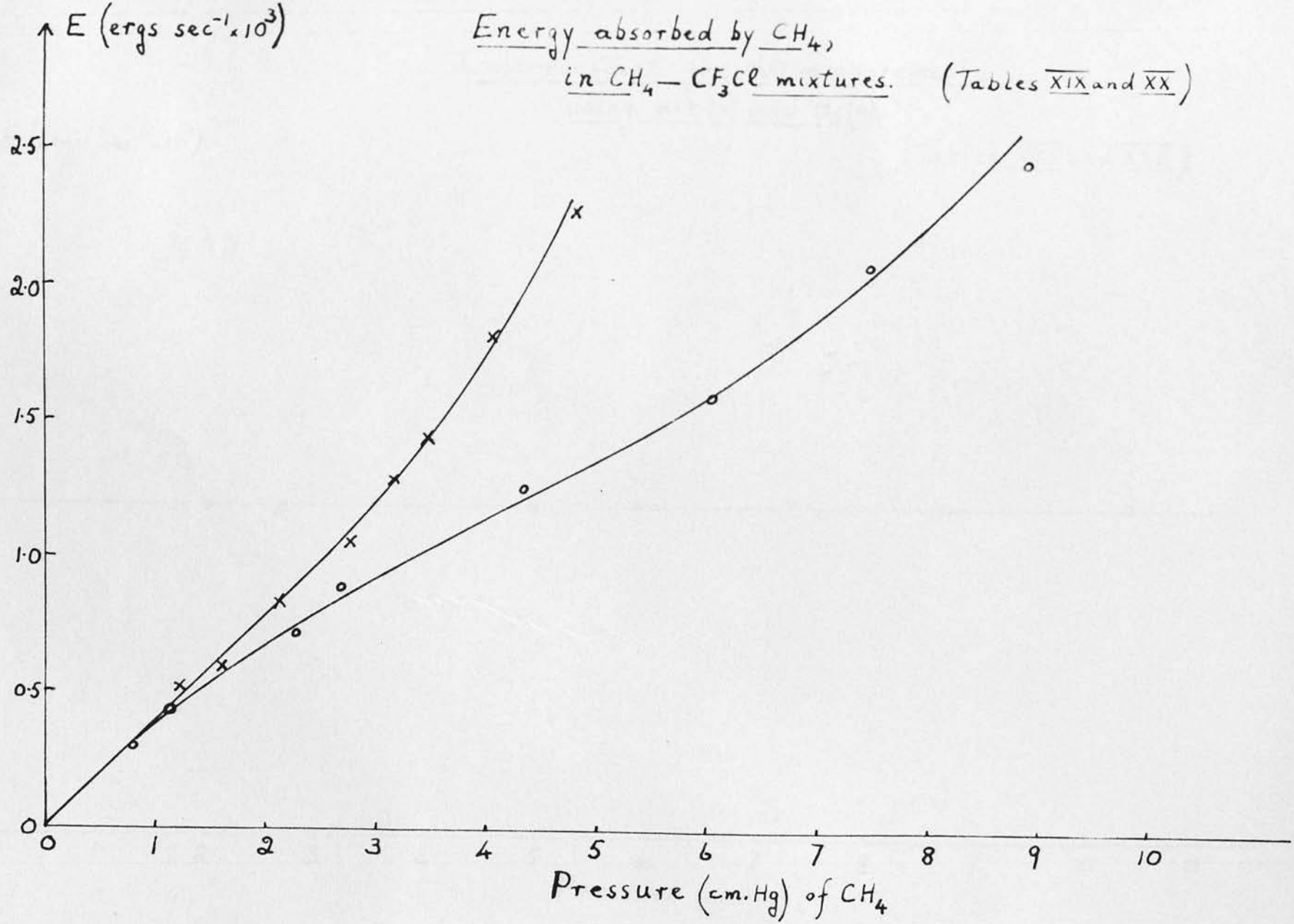
E (ergs sec⁻¹ × 10³)
Energy absorbed by CH4, in CH4 — CF3Cl mixtures. (Tables XIX and XX)
2·5
2·0
1·5
1·0
0·5
0
0
1
2
3
4
5
6
7
8
9
10
Pressure (cm. Hg) of CH4

Graph XVII

Cell-constant for N_2O measurements, using air (x) and H_2 (o).

(Tables XXI and XXII)

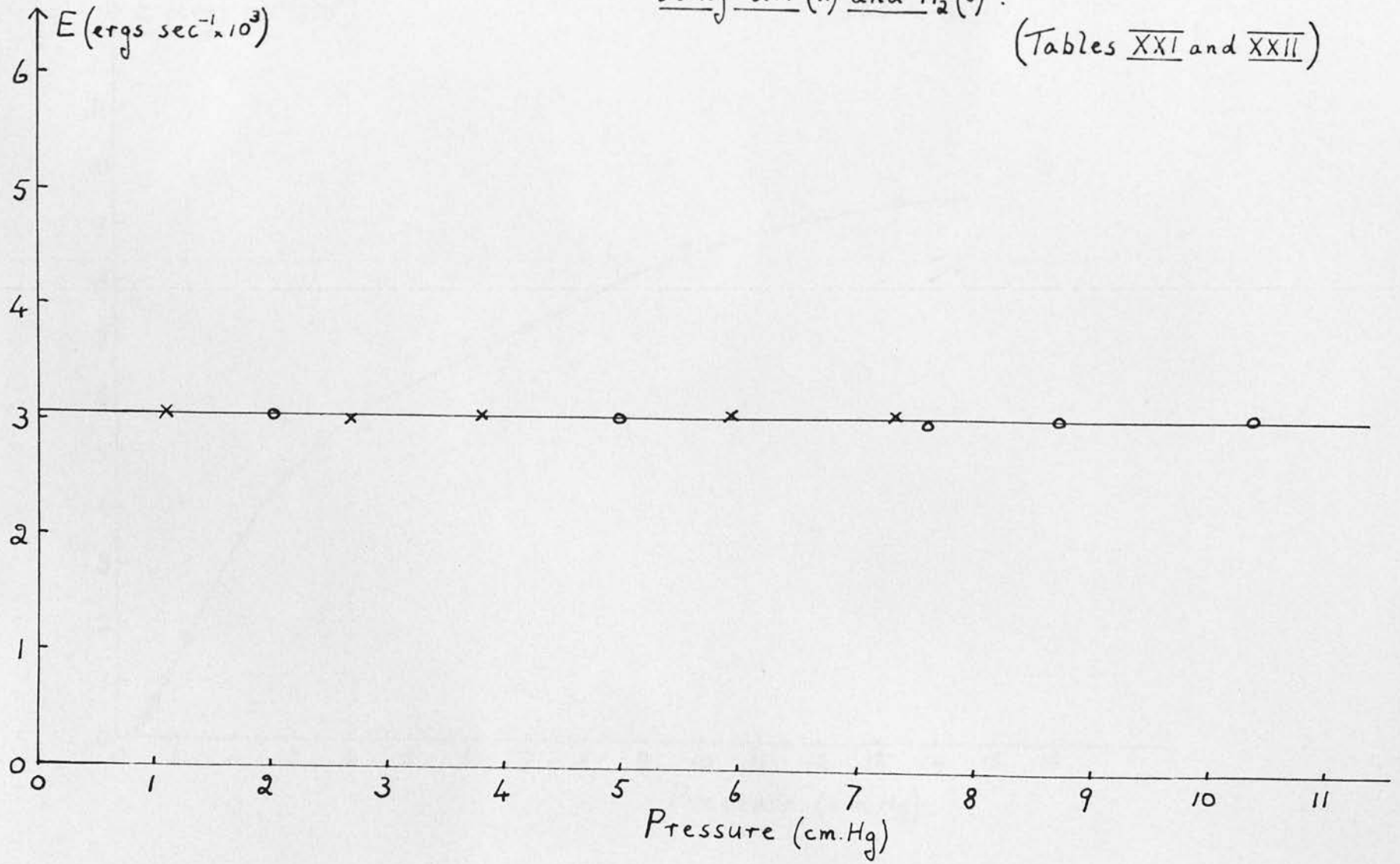

Graph XVIII

Energy absorbed by pure N_2O,
(Table XXIII)

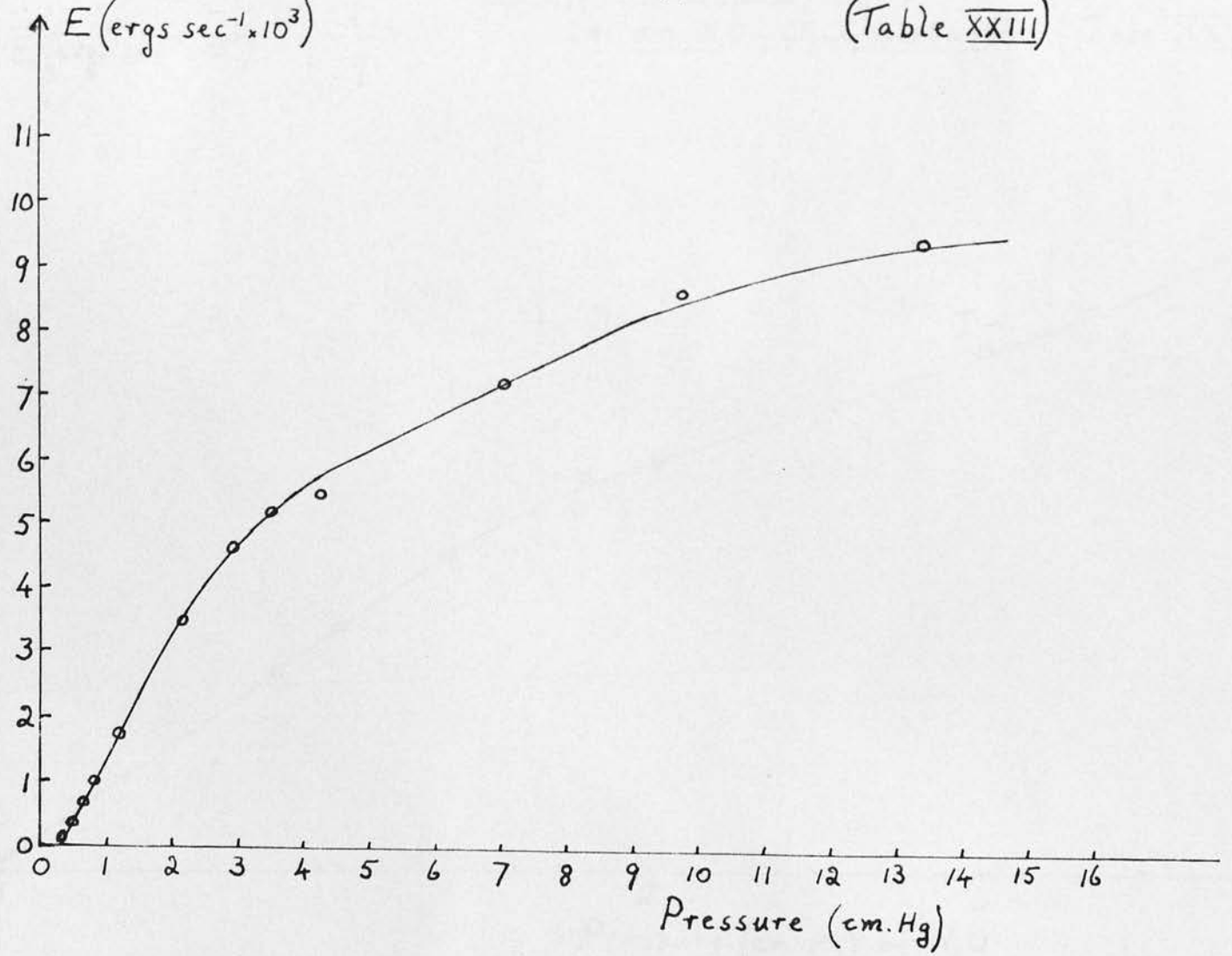

Graph XIX

Energy absorbed by N_2O, in an N_2O—CF_3Cl mixture. (Table XXV)

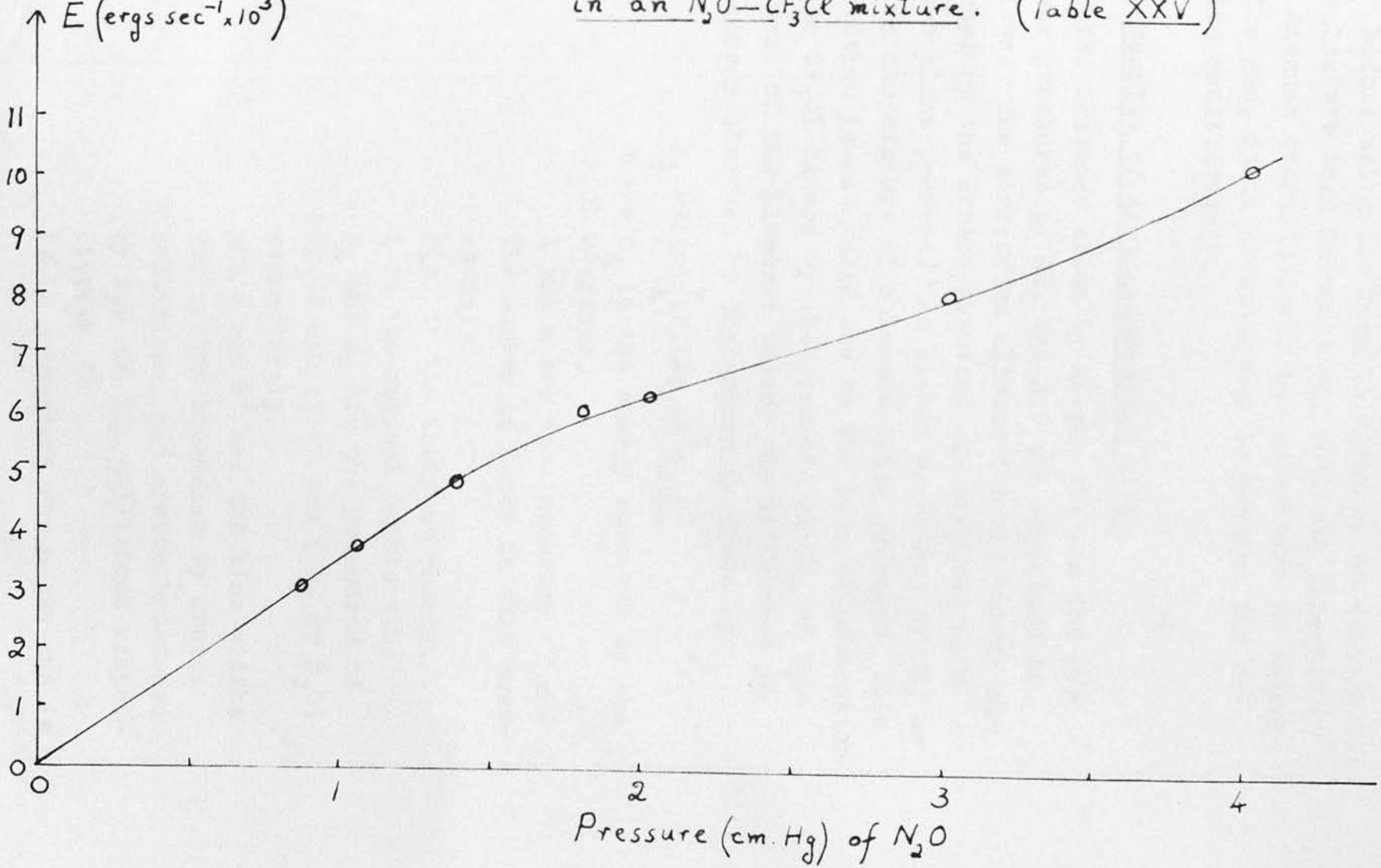

3. General Features of Results 2)

Before using the results detailed in section 2.4 to calculate band intensities, estimate line-widths and discuss quantitatively the relaxation of energy in the gas, it is advantageous to examine the results qualitatively.

3.1 Results of Arcton-broadened lines

The features shown by Graphs XVI and XIX for higher pressures of CH_4 and N_2O are explained as follows. The correction allowed for the energy absorbed by the arcton overtone was measured with arcton alone present. At higher pressures of CH_4 or N_2O in the mixture of constant total pressure, this correction is not valid due to the induced adsorption in the CF_3Cl caused by the presence of CH_4 or N_2O. In terms of the Elsasser theory the difference in the energy absorbed by the arcton is shown by

$$E_A = 2I(o)\left[An\,l(\delta p_A + \delta^1 p_o)\right]^{\frac{1}{2}}$$

where E_A is the energy absorbed by the CF_3Cl overtone,

A and n are the intensity of and the number of lines in this overtone,

I(o) is the incident energy,

l is the optical pathlength,

p_A and p_o are the pressures of CF_3Cl and other gas (CH_4 or N_2O) respectively,

and δ and δ^1 are the line-widths for arcton broadened by arcton collisions, and arcton broadened by N_2O and CH_4 collisions respectively

(δ is a constant for a gas and is

equivalent to b_c at one atmosphere)

When δp_A is much greater than $\delta^1 p_o$ the correction, measured with CF_3Cl alone, is valid. This is so at low partial pressures of CH_4 and N_2O up to around 3cm.Hg, partly due to the fact that δ is greater than δ^1 but largely due to the big difference between p_A and p_o. That δ is greater than δ^1 follows from the highly polar properties of CF_3Cl, and also from the result on the optical collision diameter of the self-:broadened CF_3Cl overtone (given in section 4.2.3).

Thus it follows that although line-widths of CH_4 and N_2O, broadened by CF_3Cl, cannot be estimated from Graphs XVI and XIX, the limiting gradient at low pressures is a valid measure for calculations on the intensities.

The results in Table XX and Graph XVI for dif-:ferent total pressures of the mixture CH_4 -CF_3Cl are markedly affected by induced absorption in the CF_3Cl, but at low pressures approach the same limiting grad-:ient as the results in Table XIX (made up to a con-:stant pressure). It is suggested that the CF_3Cl correction, as measured with pure CF_3Cl, is the full correction at these low pressures because the absorp-:tion of the CF_3Cl in the mixture was in a region not greatly affected by changes in the line-shape.

The low pressure data in Graphs XVI and XIX thus give a measure of the band intensities, except for the small correction necessary for other bands in the region 3 to 5μ (section 2.2.2.5)

3.2 Results on Pure Gases

The results of measurements on CH_4 and N_2O alone, when corrected for the effect of the other bands in the absorption region, are available at higher pres-:sures for estimates of the average line-widths over the bands. The correction for the other bands was

more difficult to calculate for a pure gas than for pressure-broadened lines, but by assuming the form of the change in energy absorbed with pressure to be the same as for the fundamental bands it was estimated that the low-pressure linear region for these other bands extended to approximately 6cm.Hg for CH_4 and 3cm.Hg for N_2O. Since the correction is very small (c.1 to 2% in the energy measured), only a negligible error is introduced in the gradient by assuming the linear region to extend to 10cm.Hg for CH_4 and 6cm.Hg for N_2O, at which pressures estimates of the line-widths can readily be made.

The Elsasser relationship between the energy absorbed and the reduced pathlength was found to be valid for higher pressures, a linear plot being obtained with both gases. For N_2O this high pressure linear relationship was shown to a pressure of around 8 or 9cm.Hg above which the absorbed energy levelled off, again as approximately predicted by Elsasser. However, the above high-pressure linear plot did not extrapolate to zero at zero pressure but curved over as shown in Graphs XV, XIV and XVIII. The theory predicts a linear relationship at all pressures, except for the small effect of the Doppler line-shape at low pressures, according to the equation

$$E = I(o)m\ 2\pi bf(x)$$

(section 1.3.1.2)

where x is a constant for a pure gas when collision broadening is dominant.

It is therefore obvious that for the bands considered the Elsasser theory does not apply at low pressures. It is suggested that the very strong absorption near the line-centres, which is dominant at low pressures, gives rise to different absorption relationships but that at higher pressures the change in energy absorbed with pressure comes from the wing absorption obeying the Elsasser relationship. This

low-pressure feature was also shown by the CF_3Cl overtone, and is discussed more fully later.

An estimate of the average line-width for CH_4 was made more approximate by the presence of the Q branch. Because with the ν_3 band of CH_4 $B^{1}-B^{11} = 0.019\ cm^{-1}$ (94), partial splitting of the Q branch occurs at fairly high pressures (c.5 to 10cm.Hg) (see section 1.3.1.7), and therefore the Kaplan and Eggers approach (section 1.3.1.7.3) was not applicable. Since this splitting was present and a linear relationship between energy absorbed and pressure was found at higher pressures, the approxi-:mation of regarding the Q branch lines as being the same as the P and R lines was made (section 1.3.1.7.1)

At very low pressures of both CH_4 and N_2O loss in the measured absorbed energy occurred due to spon-:taneous emission. This is shown by Graphs XIV and XVIII where the measured energy does not extrapolate to zero, and made more obvious by plotting $\log_{10}\frac{E}{P}$ against $\log_{10}P$ (where P is the pressure in cm.Hg) as in Graphs XX and XXI. In order to examine the energy transfer process quantitatively it was necessary to know the actual energy absorbed at these low pressures. Because of the previously mentioned deviations from the simple theory this was done empirically using both

the form of the relationship before the fall-off due to spontaneous emission occurred and the general features of the CF_3Cl curve which was not affected by loss in energy transfer. This is described in detail in section 4.3.1.

3.3 Other graphs

Graph XII shows the cell-constant for the CH_4 measurements (Tables XIV and XV)

Graph XVII shows the cell-constant for the N_2O measurements (Tables XXI and XXII)

Graph XIII shows the incident energy (foil) measurements (Table XVI)

4. Calculations

4.1 Intensities of CH_4, N_2O and CF_3Cl

4.1.1 3,018cm^{-1} band of CH_4

From a temperature of the Nernst filament of 1420°K, the ratio Y (see section 2.1.6) was calculated as 2.36×10^{-14} secs. for CH_4. The error was negligible here due to the fact that even a 100°K error in the temperature resulted in less than a 1% change in Y.

Q(m) was calculated from the properties of the source and the optics (section 2.2.2.8.1) to be $8.1 \pm 2.2 \times 10^4$ ergs sec^{-1}.

Using the calibrated thermopile in a way analogous to section 2.2.2.8, Q(m) was measured as $7.4 \pm 0.5 \times 10^4$ ergs sec^{-1}.

The blackened foil measurements gave a value for Q(m) of 7.5×10^4 ergs sec^{-1} from Table XVI and Graph XIII. The average error of each reading taken at different pressures was 4% and, since eight different measurements were recorded, the overall error in the measurement was 1.5%. In section 2.4 it was stated that radiation losses from the heated foil and wire were the same, and this calculation was accurate to an overall effect on Q(m) of 0.5%. Thus from the foil measurements,

$$\underline{Q(m) = 7.5 \pm 0.15 \times 10^{4} \text{ ergs sec}^{-1}}$$

This is in excellent agreement with the thermo-:pile result.

It therefore follows from section 2.1.6 that

$$I(o) = 1.04\ Q(m)Y$$

$$\underline{= 1.84 \pm 0.04 \times 10^{-9} \text{ ergs}}$$

for the 3,018cm^{-1} band of CH_4.

From Graph XVI the limiting gradient of the absorbed energy was readily calculable as 3.04×10^{4} ergs sec^{-1} atm^{-1}. The average error in each point giving this limiting gradient (from Table XIX) was $\pm$10% (this follows from subtracting two larger values, each of accuracy around $\pm$1%). The number of measurements applicable in Table XIX, and the limiting gradient ob-:tained from Table XX, reduce this error to $\pm$4%.

From section 2.2.2.5, in order to allow for other bands present in the region 3 to 5μ, and also to correct for the small atmospheric overlapping of the 3,018cm^{-1} band, a percentage of 0.5% was sub-:tracted from this limiting gradient.

Therefore the limiting gradient was:

$$\underline{3.03 \pm 0.12 \times 10^{4} \text{ ergs sec}^{-1} \text{atm}^{-1}}$$

The intensity of the 3,018cm^{-1} band of CH_4,

$A = \lim_{x \to o} \frac{E}{XI(o)}$, where X = pl with l=1.54cm.,

therefore is equal to $1,069 \pm 48 \times 10^{10} cm^{-1} sec^{-1} atm^{-1}$ at $294^{o}K$.

<u>At N.T.P. $A = 993 \pm 44 \times 10^{10} cm^{-1} sec^{-1} atm^{-1}$</u>

4.1.2 <u>$2,224 cm^{-1}$ band of N_2O</u>

A different Nernst filament was used as source at a temperature of $1510^{o}K$. Y was calculated as <u>2.12×10^{-14} secs. for N_2O at $2,224 cm^{-1}$</u>

Q(m) was calculated from the value used for methane and the ratio of the cell-constants corres-:ponding to the two different sources (this ratio was checked by doing similar measurements on CF_3Cl), and its value was:

<u>$Q(m) = 1.55 \pm 0.03 \times 10^{5}$ ergs sec^{-1}</u>

It therefore follows that

$I(o) = 3.41 \pm 0.07 \times 10^{-9}$ ergs for the $2,224 cm^{-1}$ band of N_2O.

From Graph XIX and assessing the error in a similar way to section 4.1.1 the limiting gradient was $2.71 \pm 0.11 \times 10^{5}$ ergs $sec^{-1} atm^{-1}$. From this was sub-:tracted 1% to allow for other bands in the region

3 to 5μ (section 2.2.2.5) giving

$$\underline{2.68 \pm 0.11 \times 10^{5} \text{ ergs sec}^{-1}\text{atm}^{-1}}$$

Thus, for the 2,224cm^{-1} band of N_2O, with l = 1.54cm.,

$$A = 5{,}102 \pm 230 \times 10^{10} \text{cm}^{-1}\text{sec}^{-1}\text{atm}^{-1} \text{ at } 294^{\circ}\text{K}$$

and $\underline{\text{at N.T.P., } A = 4{,}740 \pm 210 \times 10^{10} \text{cm}^{-1}\text{sec}^{-1}\text{atm}^{-1}}$

4.1.3 $\underline{2{,}400 \text{ cm}^{-1} \text{ band of } CF_3Cl}$

As stated in section 2.3 this band consisted of a strongly absorbing overtone overlapped by a weaker combination band. It was impossible to separate these bands and difficult to assess their relative intensi-:ties, and this section is only of interest in esti-:mating an intensity for the whole band. Only an estimate is possible since the limiting gradient was determined from measurements on the pure gas, and the incident energy had to be corrected for the atmos-:pheric absorption of CO_2 between 2290cm^{-1} and 2385cm^{-1} which overlaps the CF_3Cl band.

From Table XVIII and Graphs XV and XXII, the limiting gradient was

$$\underline{2.14 \times 10^{4} \text{ ergs sec}^{-1}\text{atm}^{-1}}$$

$$Q(m) = 7.5 \times 10^{4} \text{ ergs sec}^{-1}$$

and $$Y = 2.59 \times 10^{-14} \text{ sec.}$$

By calculating the fractional absorption of the CO_2 in the region of overlap of the two bands, it was found that I(o) was reduced by 20%.

$$\underline{I(o) = 1.60 \times 10^{-9} \text{ ergs}}$$

Thus for the 2,400cm^{-1} band of CF_3Cl,

$$A = 830 \times 10^{10} cm^{-1} sec^{-1} atm^{-1} \text{ at } 294^{o}K.$$

Estimating the error as $\pm$20%, and correcting to N.T.P.,

$$\underline{A = 770 \pm 154 cm^{-1} sec^{-1} atm^{-1}}$$

The interest of this result lies in the fact that this overtone is extremely intense, its intensity being of the same order of magnitude as the fundamentals in most molecules.

4.2 Estimates of Line-Widths

4.2.1 Self-broadening of the 3,018cm^{-1} band of CH_4

Using the approximation discussed in section 3.2, the gradient of the energy absorbed against pressure relationship, shown in Graph XIV, was found for the higher pressure region of CH_4. The correc-:tion for other bands present in the absorption region was calculated as 1½% at 7cm.Hg pressure and 2% at 10cm.Hg. Applying this small correction the resultant gradient was

$$9.36\times10^{3} \text{ ergs sec}^{-1}\text{atm}^{-1}$$

Equation (27 for a pure gas gives

$$E = 2I(o)(Am\delta l)^{\frac{1}{2}}p$$

where δ is the variation of the collision line-width for the 3,018cm^{-1} band per atmosphere pressure for CH_4-CH_4 collisions.

$I(o) = 1.84\times10^{-9}$ ergs,

$A = 1,069\times10^{10}$ cm^{-1}sec^{-1}atm^{-1} at 294^{o}K,

$l = 1.54$cm.,

$m = 70$, this coming from reference (29) and including the number of lines in the Q branch,

$\frac{dE}{dp} = 9.36 \times 10^{3}$ ergs $sec^{-1} atm^{-1}$

and thus $\underline{\delta_{CH_4-CH_4} = 0.18 \pm 0.05 \text{ cm}^{-1} \text{atm}^{-1}}$

at 294°K , an estimated error of ±30% having been allowed for the approximation.

The optical collision diameter, σ, is directly related (1) to δ by

$$\sigma^2 = 2.8\, \delta\, T^{\frac{1}{2}} \left(\frac{M_1 M_2}{M_1 + M_2}\right)^{\frac{1}{2}}$$

where T is the temperature in °K, and M_1 and M_2 are the molecular weights of the colliding species.

Thus, $\underline{\sigma_{CH_4-CH_4} = 4.9 \pm 1.0 \text{ A}^{\circ}}$ for the 3,018 cm^{-1} fundamental at 294°K.

4.2.2 Self-broadening of 2,224cm^{-1} band of N_2O

In a similar way to section 4.2.1, except that no difficulties due to the presence of a Q branch arose, the following values were obtained.

I(o) = $3.41 \pm 0.07 \times 10^{-9}$ ergs,

A = $5,102 \pm 230 \times 10^{10}$ $cm^{-1} sec^{-1} atm^{-1}$ at 294°K,

l = 1.54cm.,

m = 100 , from reference (91) ,

$\frac{dE}{dp}$ $= 3.8 \pm 0.1 \times 10^4$ ergs $sec^{-1} atm^{-1}$ (Graph XVIII)

and thus $\delta_{N_2O-N_2O} = 0.13 \pm 0.01$ $cm^{-1} atm^{-1}$ at 294^oK

giving $\sigma_{N_2O-N_2O} = 5.33 \pm 0.28$ A^o for the 2,224cm^{-1} fundamental at 294^oK.

4.2.3 Self-broadening of the 2,400cm^{-1} band of CF_3Cl

The following values were obtained.

$I(o) = 1.60 \times 10^{-9}$ ergs,

$l = 1.54$cm.,

$\frac{dE}{dp} = 7.70 \pm 0.23 \times 10^3$ ergs $sec^{-1} atm^{-1}$ (Graph XV)

$A = 830 \pm 170 cm^{-1} sec^{-1} atm^{-1}$ at 294^oK

The above values for A and $\frac{dE}{dp}$ include the absorption of the combination band. The allowance for this band, as has been indicated, was difficult but, in order to isolate the overtone, it was estimated from the spectrum that the overtone was 3 to 5 times as strong as the combination band. The values of A and $\frac{dE}{dp}$ were therefore reduced by 25%.

The number of lines in the overtone was calculated from the bandwidth of 120cm^{-1} and a spacing

between lines of $2cm^{-1}$. The spacing was estimated from data on similar symmetrical top molecules (15).

i.e. m = 60.

For the CF_3Cl overtone at $2,400cm^{-1}$,

$\delta_{CF_3Cl-CF_3Cl} = 0.20 \pm 0.06 cm^{-1} atm^{-1}$ at $294^{\circ}K$, the error being estimated at $\pm 30\%$.

and $\sigma_{CF_3Cl-CF_3Cl} = 9.6 \pm 1.9$ A$^{\circ}$

4.3 Probability of Vibrational-Translational Energy Transfer

From section 1.3.2 and equation (56 it is seen that, at low pressures of the pure gas, spontaneous emission can result in the energy measured by the present method being lower than the energy absorbed by the gas.

From equation (56,

$$\frac{E}{V.h\nu_{01}} = \Delta N_e \left[Zp_{10} + (1-g)A_{10} \right]$$

where E is the energy absorbed in cell.

If E(m) is the energy actually measured, then

$$\frac{E(m)}{V.h\nu_{01}} = \Delta N_e Zp_{10} \qquad (68$$

It therefore follows that

$$\Delta N_e = \frac{(E-E(m))}{Vh\nu_{01}(1-g)A_{10}} \qquad (69$$

and substituting in equation (68 yields

$$p_{10} = \frac{E(m)}{E-E(m)} \quad \frac{(1-g)A_{10}}{Z} \qquad (70$$

Thus the relaxation time for the degradation of energy in a particular vibrational mode to trans-:lational energy is given by (see section 1.3.2.1)

$$\tau = \left(\frac{E-E(m)}{E(m)}\right) \frac{p}{(1-g)A_{10}\left[1-\exp\left(-\frac{h\nu_{01}}{kT}\right)\right]} \quad \text{at 1 atmosphere,} \qquad (71$$

where p is the pressure in atmospheres.

From Graphs XIV and XVIII the fall-off in the measured energy is seen to occur for both CH_4 and N_2O. In order to estimate a value for τ it was therefore necessary to find the quantities (E-E(m)) and g, the other factors in equation (71 being readily available.

4.3.1 Calculation (E-E(m))

As indicated in section 3.2 the value of E at low pressures was not calculable from simple theory. The relationship between the absorbed energy and the pressure was known experimentally down to fairly low pressures (to the pressure at which the fall-off due to spontaneous emission occurred) and an extension of this relationship to zero pressure was required.

Having allowed for the presence of other bands in the absorption region, $\log_{10}\frac{E}{P}$ against $\log_{10}P$ was plotted for each gas as shown in Graphs XX, XXI and XXII. For CF_3Cl the full absorption of the overlap-:ping overtone and combination bands was plotted. With the CF_3Cl plot no complications arose due to loss of spontaneously emitted radiation or increased absorption because of Doppler contributions to the line-shape. This latter point is substantiated from equation (44 where

$\frac{E(\text{total})}{E(\text{collision})} = 1 + \frac{3}{16} a^{-2} x^{-1}$ to a first approximation,

with $a = \frac{b_c}{b_D} (\ln 2)^{\frac{1}{2}}$ and $x = \frac{SX}{2\pi b_c}$ (section 1.3.1.5)

For CF_3Cl, x=5.14 and $a=1.40 \times 10^{2} p$ where p is the pressure in atmospheres, and the Doppler contribu-:tion is thus calculated as 1% at 1cm.Hg pressure. The low-pressure relationships in these Graphs in-:dicate that the line-shape is of decreasing impor-:tance the lower the pressure, and thus even this small, theoretical contribution is not applicable, i.e. although the theoretical Doppler contribution increases at low pressures, the effect of the line-:shape on the energy absorbed is so small that no Doppler contribution is observed.

The experimental CF_3Cl plot in Graph XXII was fitted accurately by an exponential relationship.

For CH_4 and N_2O an exponential plot was fitted to the experimental results, before the fall-off due to re-emission occurred, and continued to low pres-:sures as shown in Graphs XX and XXI. With N_2O no allowance was made for the Doppler contributions for similar reasons to above with CF_3Cl, but with CH_4 where x=6.43 and a=40.3p below 2cm.Hg pressure the contributions were calculated as follows. Having determined the theoretical, fractional effect of the Doppler line-broadening for CH_4 using the

Graph XX

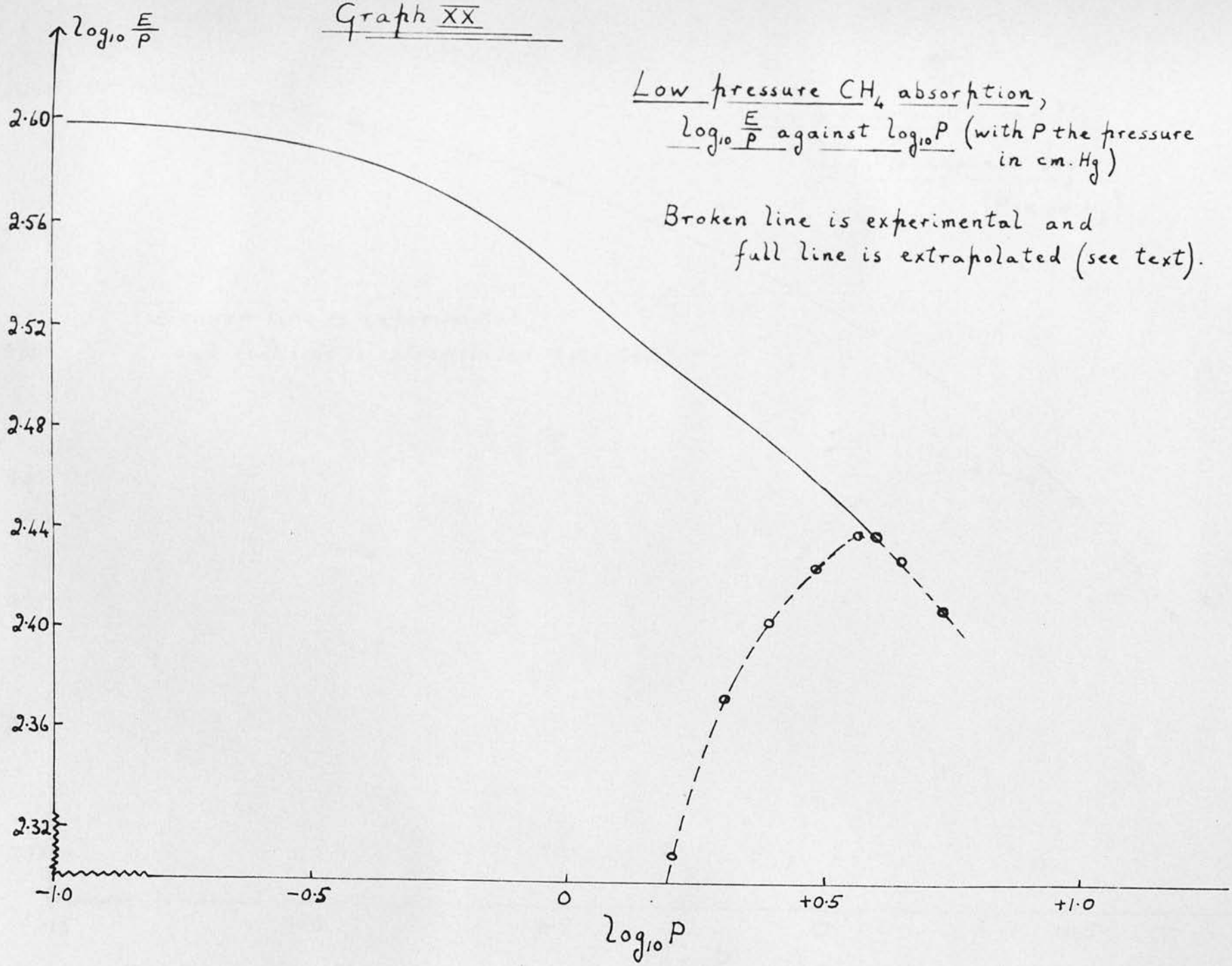

Low pressure CH_4 absorption,
$\log_{10}\frac{E}{P}$ against $\log_{10}P$ (with P the pressure in cm. Hg)

Broken line is experimental and full line is extrapolated (see text).

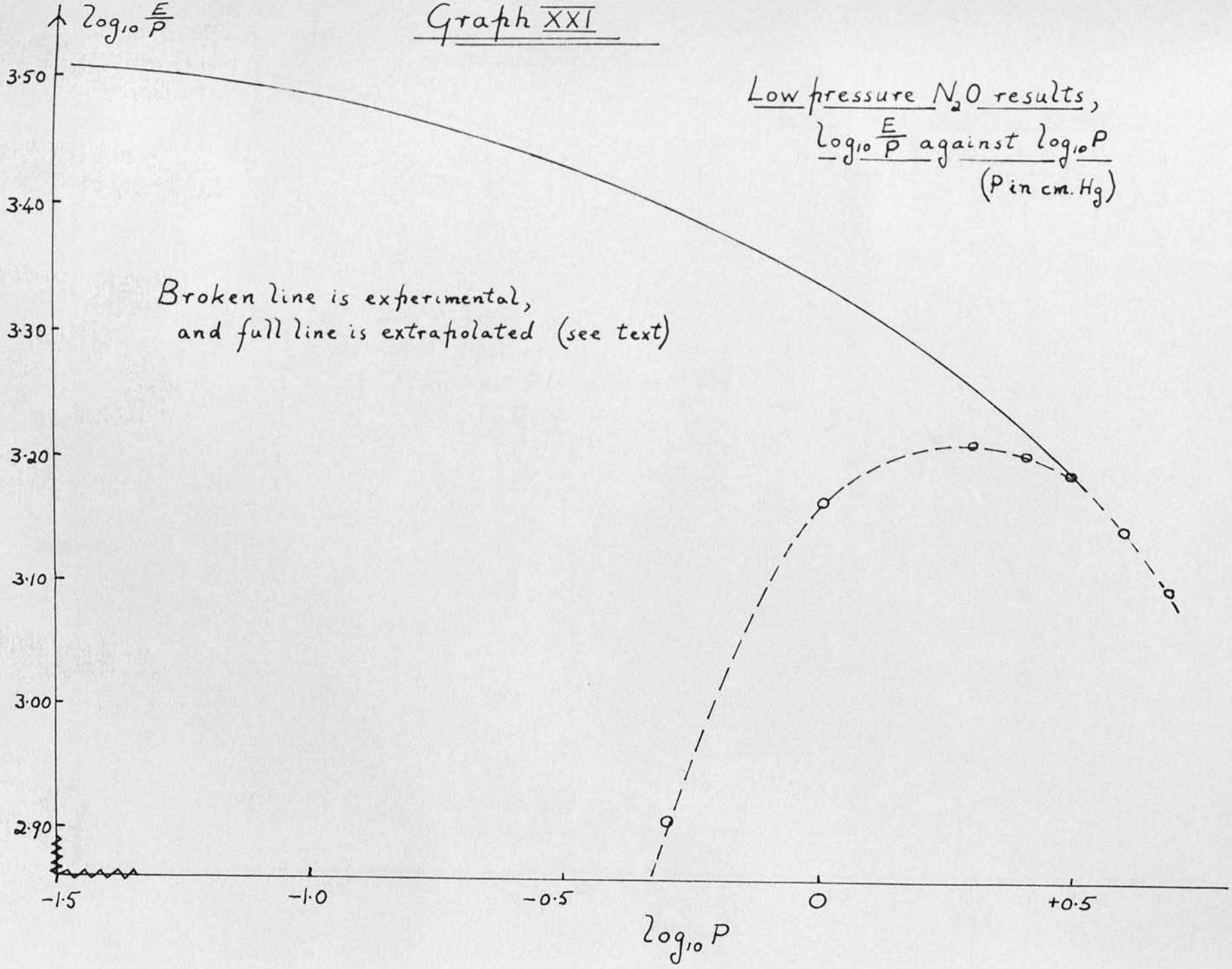
Graph XXI
$\log_{10}\frac{E}{P}$
Low pressure N_2O results,
$\log_{10}\frac{E}{P}$ against $\log_{10}P$
(P in cm. Hg)
Broken line is experimental,
and full line is extrapolated (see text)
3·50
3·40
3·30
3·20
3·10
3·00
2·90
−1·5
−1·0
−0·5
0
+0·5
$\log_{10}P$

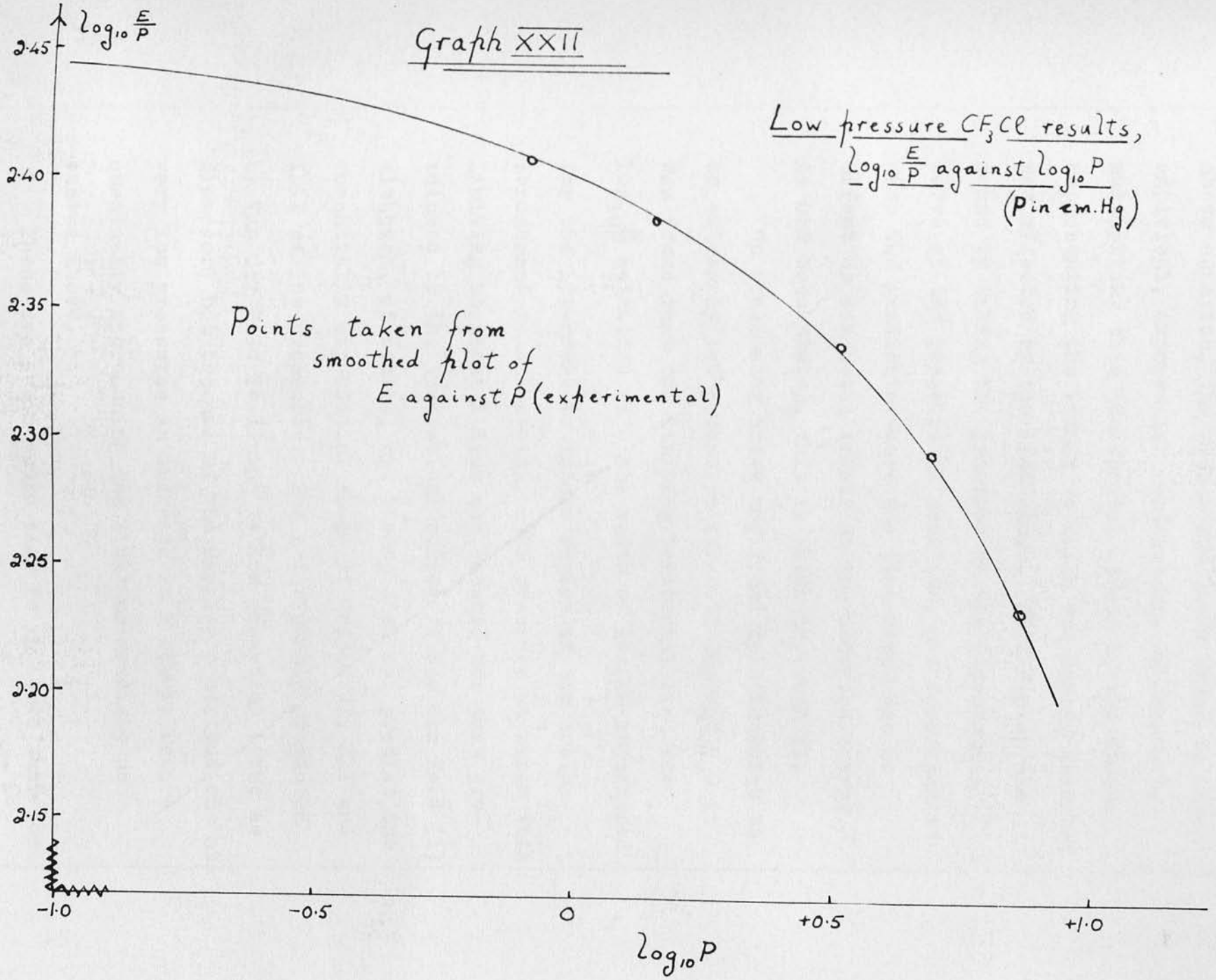
Graph XXII
Low pressure CF_3Cl results,
$\log_{10}\frac{E}{P}$ against $\log_{10}P$
(P in cm. Hg)
Points taken from smoothed plot of E against P (experimental)
$\log_{10}\frac{E}{P}$
2·45
2·40
2·35
2·30
2·25
2·20
2·15
−1·0
−0·5
0
+0·5
+1·0
$\log_{10}P$

above equation, the percentage to be added to the empirical, exponential relationship was found by multiplying this theoretical effect by the factor representing the extent to which the energy absorbed was affected by the line-shape. This factor was found by taking the gradient of the exponential curve at the pressure in question, and comparing it with the gradients where the line-shape has no effect or has total effect on the absorbed energy. As has been stated, this is shown in Graph XX.

On continuing these empirical relationships to to extremely low pressures for both CH_4 and N_2O it was found that the limiting horizontal line for $\log_{10}\frac{E}{P}$ coincided with the value of $\log_{10}\frac{E}{P}$ determined for the low-pressure linear region of the arcton-:broadened relationships. The pressure at which this limiting horizontal line was reached was that pre-:dicted by the theoretical curves of Van der Held (1) although, of course, his theory does not predict the essentially exponential shape of Graphs XX, XXI and XXII at low pressures. The relationship predicted by Van der Held is linear to low pressures (same as Elsasser) but because of the Doppler contributions at very low pressures an increase in E occurs before eventually approaching the limiting gradient as stated above.

These two facts would seem to indicate that the

suggestion of an intense central portion of the line absorbing dominantly at low pressures is correct. This gives rise to a different relationship with pressure which approaches theory both at very low and fairly high pressures.

Having established the relationship between E and P at low pressures, Graphs XXIII and XXIV were constructed. Because of the very small values of the measured energies, and a certain approximation in E due to the Doppler effect, below 1cm.Hg pressure, all values used for calculations were taken in the range 1cm.Hg to 2.5cm.Hg where the desired quantity (E-E(m)) could be determined with most accuracy.

4.3.2 Calculation of the Factor g

g is a fraction which varies from 0, when none of the spontaneously emitted radiation is re-absorbed, to 1, when all this re-emitted energy is absorbed. The distribution of the re-emitted energy with fre-:quency, over the band under study, is exactly the same as for the absorption spectrum.

For a constant I(o) over the band it has been suggested that the strong absorption near the line-:centres is dominant at low pressures, but as the pressure increases the wing contributions become responsible for the change in absorbed energy with

Graph XXIII

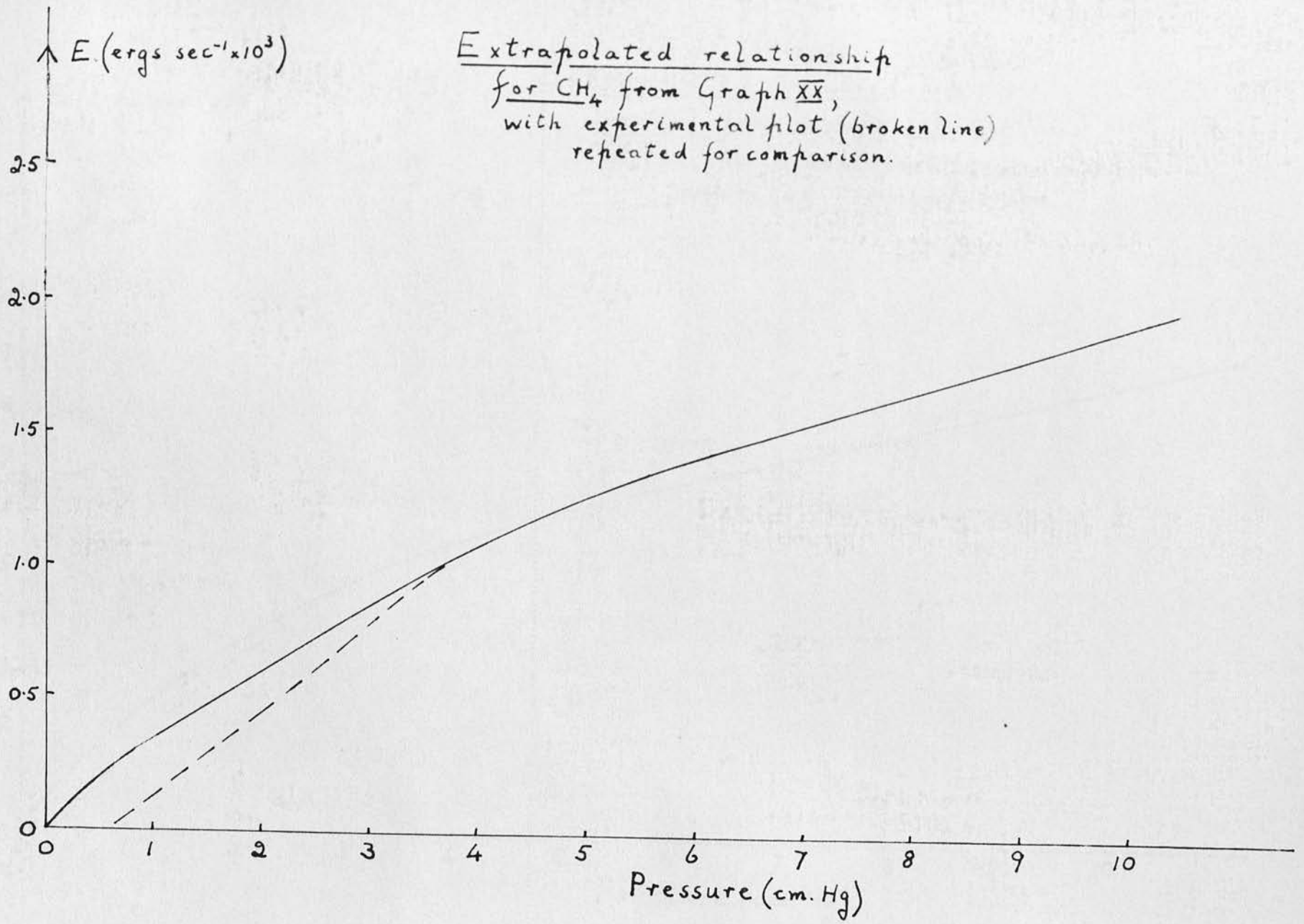
E (ergs sec⁻¹ x 10³)
Extrapolated relationship for CH4 from Graph XX, with experimental plot (broken line) repeated for comparison.
2·5
2·0
1·5
1·0
0·5
0
0
1
2
3
4
5
6
7
8
9
10
Pressure (cm. Hg)

Graph XXIV

Extrapolated relationship for N_2O from Graph XXI, with experimental plot (broken line) repeated for comparison.

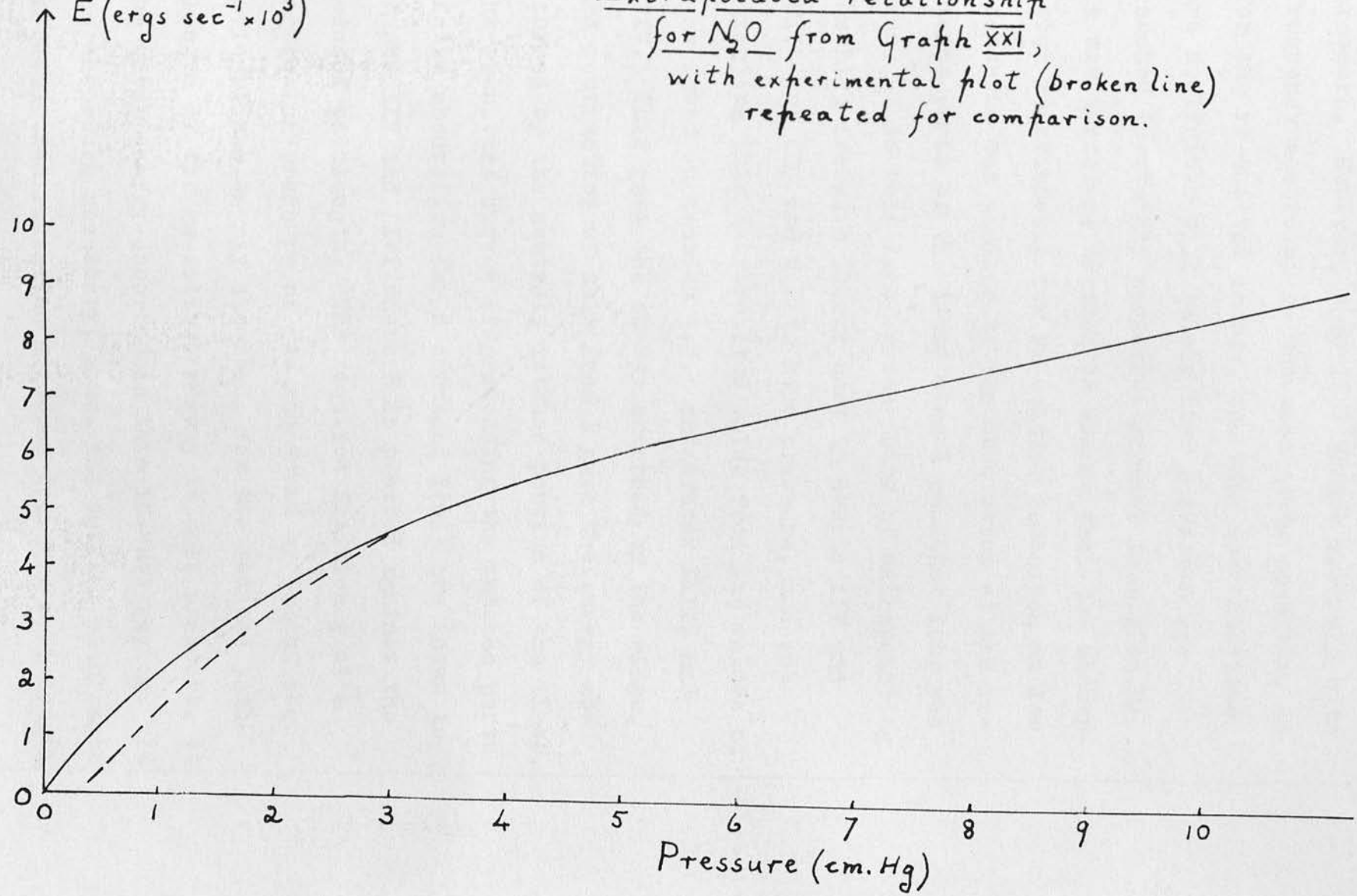

pressure. However, when I(o) varies markedly with frequency according to the absorption spectrum, as for the re-emitted energy, the wing contributions are negligible till fairly high pressures are reached (certainly pressures greater than 10cm.Hg). It was therefore decided to assume that the absorp-:tion relationship for re-emitted radiation at low pressures was similar to the absorption of the in-:tense parts of the lines when a constant I(o) was used. This relationship was found by extrapolating the high-pressure linear part in Graphs XIV and XVIII for CH_4 and N_2O to zero pressure, and sub-:tracting this extrapolated value from the values of E as found in section 4.3.1 and Graphs XXIII and XXIV. This gave the energy absorbed by the wings, and subtraction of this from E gave the energy ab-:sorbed by the central, intense portion of the lines. The resultant curves (representing the intense parts of the absorption for a constant I(o)) are shown in Graphs XXV and XXVI where E is plotted against the reduced pathlength. The required fraction g at a particular pressure of gas was found by taking the ratio of the energy absorbed, for the reduced path-:length of the re-emitted energy at this pressure, to the total energy absorbed in this intense region. It was therefore necessary, since the optical pathlength of re-emitted radiation differed from the cell length,

Graph XXV

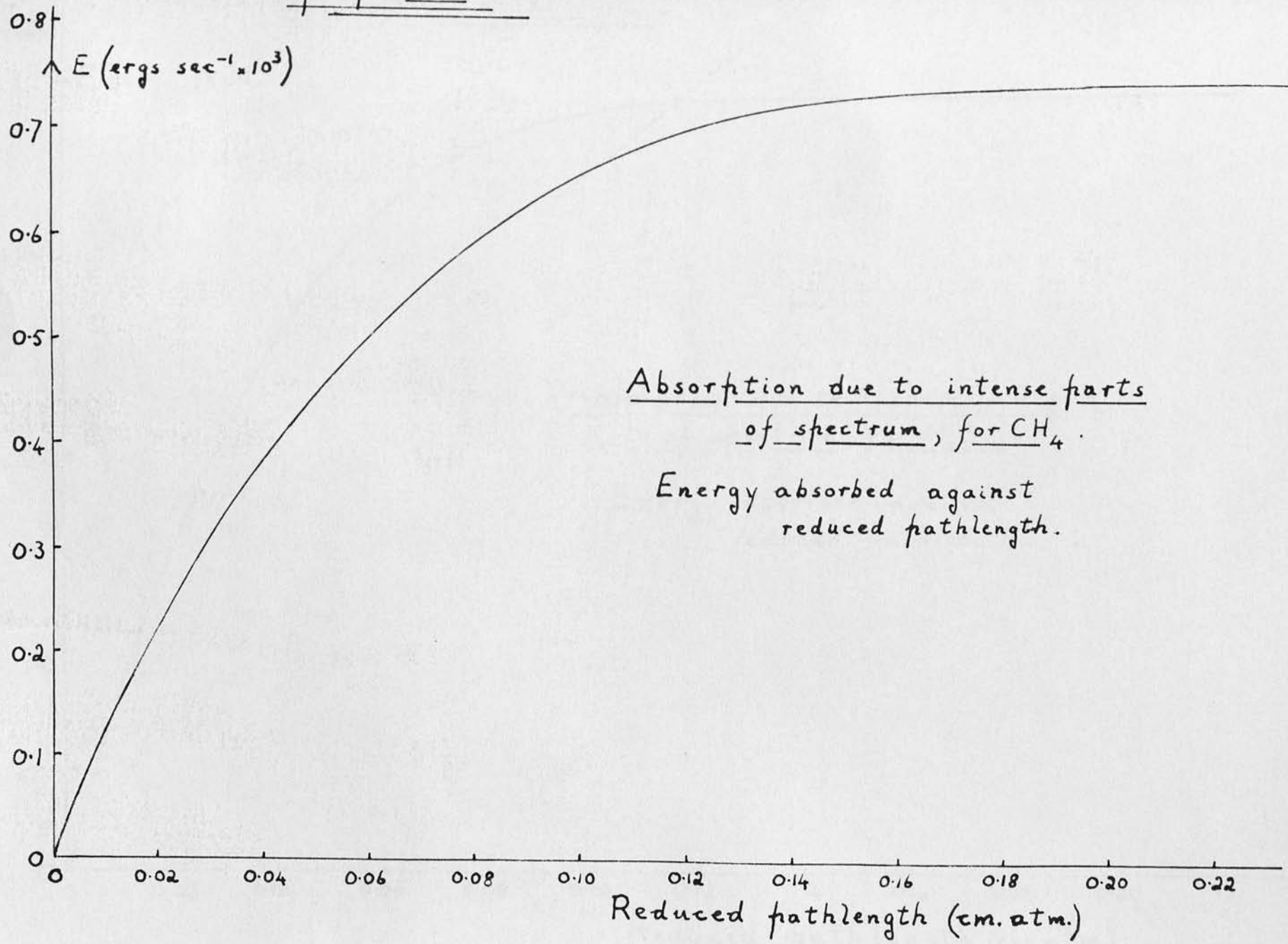

Absorption due to intense parts of spectrum, for CH_4.

Energy absorbed against reduced pathlength.

Graph XXVI

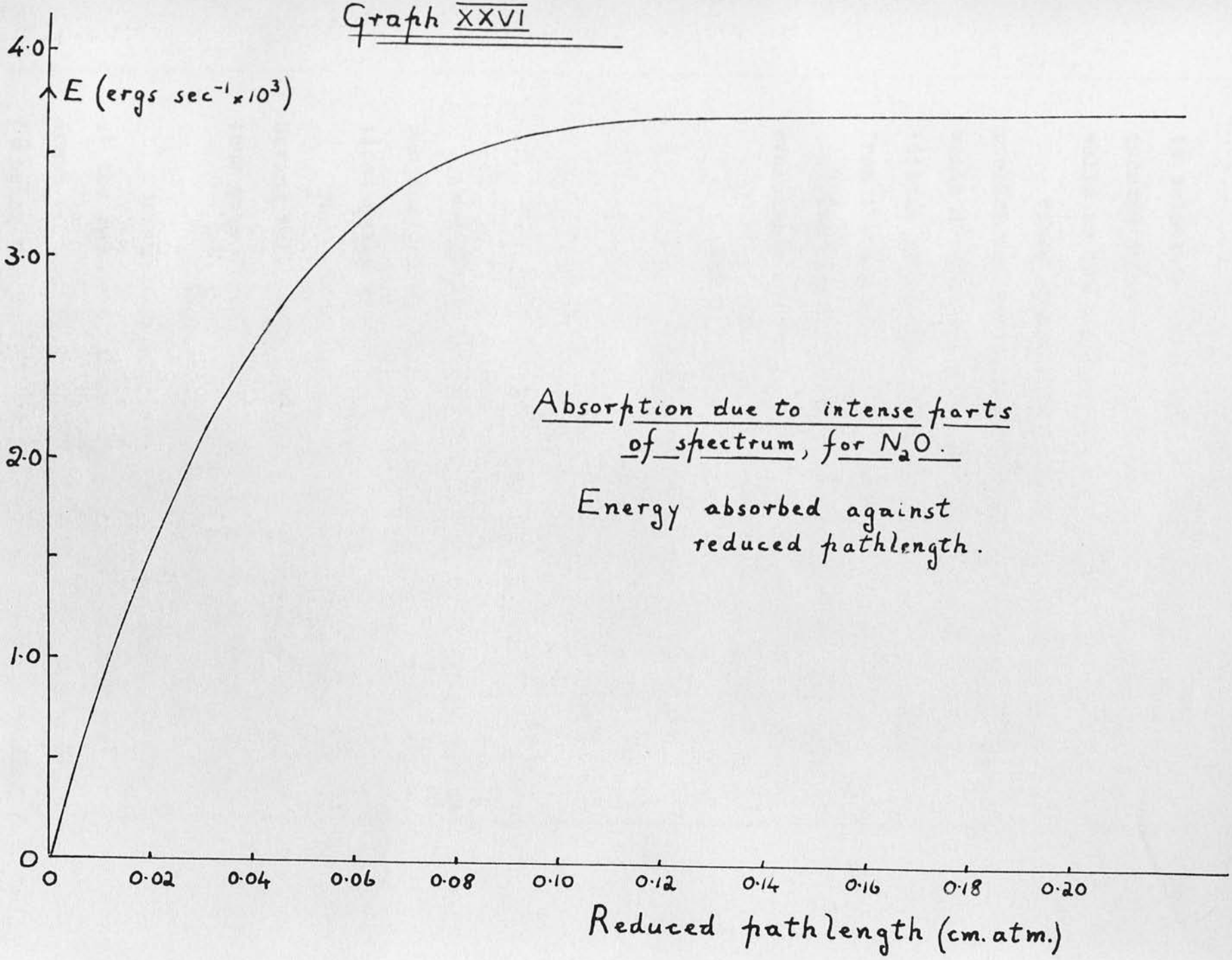

Absorption due to intense parts of spectrum, for N_2O.

Energy absorbed against reduced pathlength.

to calculate the average distance a re-emitted quantum travels through the gas before reaching the walls in the absence of absorption.

Since spontaneous emission is isotropic the problem was to calculate the mean distance of the walls of the cell from the centre, under the con-:dition of uniform distribution of the radiation from the centre.

The exact treatment of this problem i.e. the evaluation of the integral

$$\frac{1}{4\pi}\iint 1 \, ds$$

where l is the distance from the centre to the walls, and the integration is over a unit sphere, centre at the centre of the cell,

was found to yield intractable integrals, and it was decided to find the average value of l by numer-:ical analysis.

The dimensions of the cell were measured and, having taken into account the presence of the plati-:num wire frame, were found to be on average

1.30cm., 4.73cm and 5.49cm.

Considering one wall and a unit sphere, centre at the centre of the cell, lines of latitude were drawn on the sphere at equal, colatitive angles θ (θ being the angle from the line of length d joining

the centre of the sphere to the centre of the wall). θ was taken at 10^{o} intervals and the lines of lati-:tude projected on to the wall. The projections were circles or parts of circles, with radius, r, equal to d tan θ. For all points on the circle $l = d \sec \theta$.

Considering one quarter of the wall, as shown in Figure 8, the angle α subtended at the centre of the projected circle by the arc on the wall was 90^{o} for low values of θ but less than 90^{o} for higher values of θ. However,

$$\sin \alpha = \frac{c}{r}$$

where c is a dimension of the quarter wall as shown,

and thus, from $r=\tan \theta$, α was found for each value of θ taken.

The circles falling outside the quarter wall were eliminated, having determined them in each case from the condition that d tan θ (or r) must be less than the value of the diagonal of the quarter wall for the circle of angle θ to count.

l was averaged over the circles of latitude in the following way. The length of arc for the circle of angle θ was αr where $\alpha = \frac{\pi}{2}$ for the quadrants and the radian measure of α for the smaller arcs. Thus the length of arc on the sphere was $\frac{\alpha r}{l}$.

Typical Quarter-wall of cell

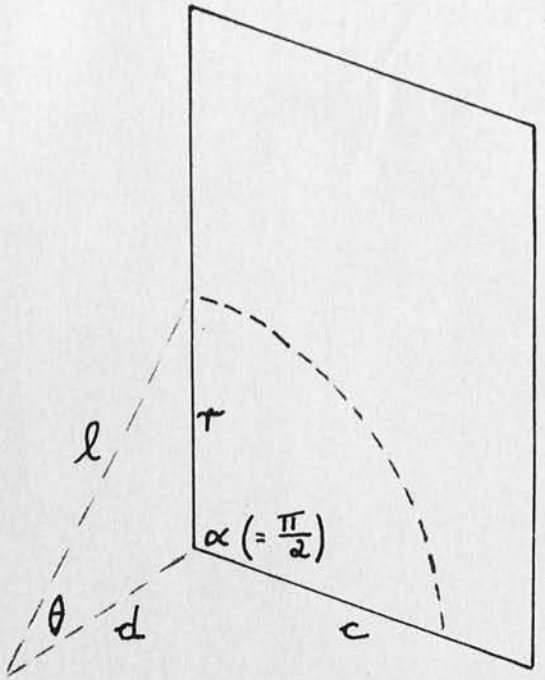

Figure 8

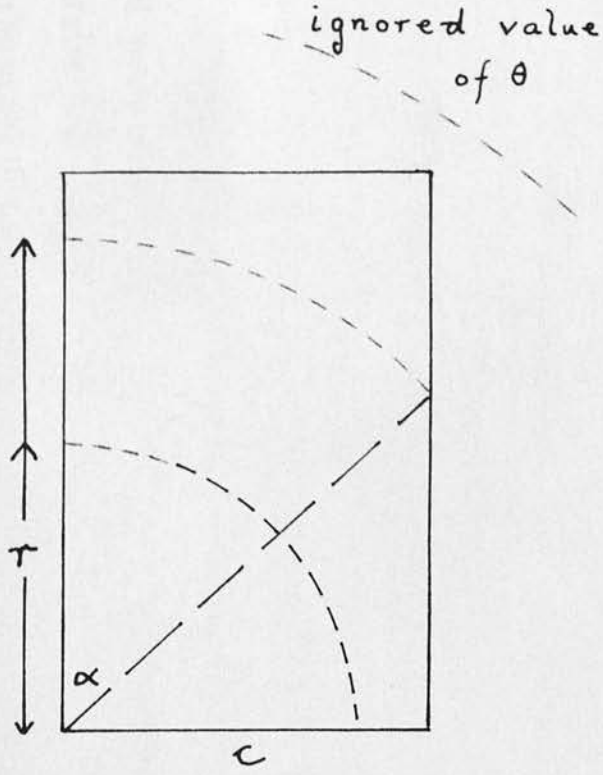

Different values of θ.

The average of l for the quarter wall was therefore -

$$\frac{\Sigma \frac{\alpha r}{l} l}{\Sigma \frac{\alpha r}{l}}$$

which equals $\frac{\Sigma \alpha \, d \tan\theta}{\Sigma \alpha \sin\theta}$

since $r = d \tan\theta$ and $l = d \sec\theta$

The appropriate range of θ and values of α and d were found for each wall, and the average distance from the centre to the walls, under uniform distri-:bution from the centre, was calculated.

The results were as follows.

a) For the wall measuring <u>1.30cm by 4.73cm</u>

$\theta(^\circ)$	α	$\alpha \tan\theta$	$\alpha \sin\theta$
10	1.5708	0.2769	0.2727
20	0.7084	0.2579	0.2423
30	0.4227	0.2441	0.2114
40	0.2862	0.2402	0.1840
50	0.2002	0.2386	0.1534
60	0.1373	0.2378	0.1189

In this case d = 2.745cm.,

and thus,

$$\Sigma \alpha \, d \tan\theta = 4.1051,$$

and $\Sigma \alpha \sin\theta = 1.1827.$

b) For the wall measuring 4.73cm by 5.49cm

$\theta(^\circ)$	α	$\alpha \tan\theta$	$\alpha \sin\theta$
10	1.5708	0.2769	0.2727
20	1.5708	0.5718	0.5372
30	1.5708	0.9070	0.7854
40	1.5708	1.3181	1.0097
50	1.5708	1.8721	1.2032
60	1.5708	2.7208	1.3603
70	1.5708	4.3158	1.4761

With d = 0.65cm., $\Sigma \alpha$ d $\tan\theta$ = 7.7886

$\Sigma \alpha \sin\theta$ = 6.6446

c) For the wall measuring 1.30cm by 5.49cm

$\theta(^\circ)$	α	$\alpha \tan\theta$	$\alpha \sin\theta$
10	1.5708	0.2769	0.2727
20	0.8555	0.3114	0.2926
30	0.4960	0.2864	0.2480
40	0.3337	0.2800	0.2145
50	0.2333	0.2780	0.1787
60	0.1594	0.2761	0.1380
70	0.1001	0.2750	0.0941

With d = 2.365cm., $\Sigma \alpha$d $\tan\theta$ = 4.6917, and

$\Sigma \alpha \sin\theta$ = 1.4386

$$\bar{l} = \frac{\Sigma \alpha \, d \tan\theta}{\Sigma \alpha \sin\theta}$$ and therefore

$\bar{l}$ = 1.79cm.

The error in $\bar{l}$, although difficult to estimate, should be small.

Having determined the optical pathlength for spontaneous emission, the reduced pathlength at any pressure was p l, and the value of g was obtained from Graphs XXV and XXVI.

4.3.3 A Check on the above Calculations

Since several assumptions, as to the form of the relationship between absorbed energy and pressure, were made in sections 4.3.1 and 4.3.2 a check on their approximate correctness was carried out as follows.

From equation (68,

$$E(m) = V.h\nu_{01}\Delta N_e Z p_{10}$$

For two different measurements at two pressures 1 and 2,

$$\frac{E(m)_1}{E(m)_2} = \frac{\Delta N_{e1}\ p_1}{\Delta N_{e2}\ p_2} \qquad (72$$

where p_1 and p_2 are the pressures in atmospheres.

From equation (69,

$$\Delta N_e = \frac{(E-E(m))}{V.h\nu_{01}(1-g)A_{10}}$$

and therefore

$$\frac{\Delta N_{e1}}{\Delta N_{e2}} = \frac{(E-E(m))_1}{(E-E(m))_2} \frac{(1-g_2)}{(1-g_1)}$$

giving from equation (72,

$$\frac{E(m)_1}{E(m)_2} = \frac{p_1}{p_2} \frac{(E-E(m))_1}{(E-E(m))_2} \frac{(1-g_2)}{(1-g_1)} \qquad (73$$

Thus if the right-hand side of equation (73 gives a ratio in agreement with the measured left-:hand side ratio, the results are at least shown to be self-consistent and are very probably correct.

The following values were obtained from the smoothed plots in the appropriate Graphs -

	N_2O		CH_4	
Compared pressures	1cm.Hg and 1.5cm.Hg	1cm.Hg and 2cm.Hg	1.5cm.Hg and 2cm.Hg	2cm.Hg and 2.5cm.Hg
$\frac{E(m)_1}{E(m)_2}$	0.61	0.46	0.65	0.73
$\frac{p_1}{p_2}$	0.67	0.50	0.75	0.80
$\frac{(E-E(m))_1}{(E-E(m))_2}$	1.51	2.17	1.13	1.29
$\frac{(1-g_2)}{(1-g_1)}$	0.61	0.43	0.80	0.79
Left-hand side	0.62	0.47	0.68	0.81

The results for N_2O were consistent to within a few percent, and for CH_4 were consistent to within 5% in the range 1.5 to 2cm.Hg pressure when the combined effects of Doppler broadening and a very small value for (E-E(m)) (producing a large percentage deviation) were at a minimum.

4.3.4 Estimates of Relaxation Times

4.3.4.1 3,018cm^{-1} band of CH_4

Although the relationship between E and p was found empirically, the possibility of a slightly different plot at low pressures due to the presence of the Q branch existed. It followed that, even though the results were consistent in the range 1.5 to 2cm.Hg, a large error was present in (E-E(m)).

With P=1.5cm.Hg,

$E(m)=0.29\pm0.01\times10^3$ ergs sec^{-1}. (the error follows from Table XVII),

$E-E(m)=0.19\pm0.05\times10^3$ ergs sec^{-1} (estimated from the uncertainty due to the Q branch)

$g=0.47\pm0.03$ (estimated from the procedure for finding g)

$A_{10}=91\pm4$ sec^{-1} at 294^{o}K, calculated from the intensity measurement.

Using equation (71,

τ was determined as $265 \pm 145\ \mu$sec. at 294^{o}K.

With P=2cm.Hg, $\tau = 225 \pm 150\ \mu$sec.

(with a bigger error in E-E(m))

4.3.4.2 2,224cm^{-1} band of N_2O

This band does not have a Q branch and an esti-:mate of greater accuracy was possible. The following results were obtained.

With P = 1cm.Hg,

$E(m) = 1.50 \pm 0.03 \times 10^{3}$ ergs sec^{-1}

$E-E(m) = 0.65 \pm 0.16 \times 10^{3}$ ergs sec^{-1} (allowing a 6% error in the value of E)

$g = 0.44 \pm 0.03$

$A_{10} = 236 \pm 11$ sec^{-1}

Using equation (71, $\tau = 43 \pm 11\ \mu$sec. at 294^{o}K

Similarly with P=1.5cm.Hg, $\tau = 43 \pm 13\ \mu$sec.

and with P=2.0cm.Hg, $\tau = 42 \pm 21\ \mu$sec.

The similarity in these results reflects the self-consistency demonstrated in section 4.3.3

4.3.4.3 2,400cm^{-1} overtone band of CF_3Cl

No fall-off in the measured energy was observed above a pressure of 1cm.Hg, and although quantitat-:ively difficult to discuss because of the overlap-:ping combination band, it was established that

$\tau < 50\,\mu$sec. for the overtone band at 294°K, using equation (71. The significance of this is dis-:cussed in section 5.

4.4 Summary of Results

The above results are summarised and two quan-:tities, σ(kinetic) which is the kinetic collision diameter (calculated from the measured viscosities), and β which is the relaxation time of the lowest vib-:rational mode in the molecule, are given for comparison.

	CH_4 3,018cm^{-1} band	N_2O 2,224cm^{-1} band	CF_3Cl 2,400cm^{-1} overtone
A(at N.T.P.) $cm^{-1}sec^{-1}atm^{-1}$	$993 \pm 44 \times 10^{10}$	$4,740 \pm 210 \times 10^{10}$	$580 \pm 170 \times 10^{10}$
A_{10} (at 294°K) sec^{-1}	91 ± 4	236 ± 11	33 ± 10
B_{10} (at 294°K) $cm^3 ergs^{-1} sec^{-2}$	$2.0 \pm 0.09 \times 10^{16}$	$1.30 \pm 0.06 \times 10^{17}$	$1.58 \pm 0.53 \times 10^{16}$
δ(at 294°K) $cm^{-1}atm^{-1}$	0.18 ± 0.05	0.13 ± 0.01	0.20 ± 0.06
σ(optical) A^o	4.9 ± 1.0	5.33 ± 0.28	9.6 ± 1.9
τ(at 294°K) μsec.	245 ± 145	43 ± 11	50
σ(kinetic) A^o	3.88	3.88	4.9
β(at 294°K) μsec.	1.5	0.9	0.1

5. Discussion

5.1 Intensity Measurements

The results obtained for the intensities of both CH_4 and N_2O are very similar to those of other workers using different techniques. For N_2O the results, listed in Table I, of pressure-broadened measurements on the 2,224cm^{-1} band vary considerably, but with references (47) and (48) great care was taken to ensure the correct conditions of measure-:ment. Their results of $4,950 \times 10^{10}$ and $4,850 \times 10^{10}$ $cm^{-1} sec^{-1} atm^{-1}$ are within the experimental error of the value obtained in the present study.

With CH_4 the following values of the intensity of the 3,018cm^{-1} band have been determined:-

971×10^{10} $cm^{-1} sec^{-1} atm^{-1}$ (51),

$1,075 \times 10^{10}$ $cm^{-1} sec^{-1} atm^{-1}$ (43),

and 978×10^{10} $cm^{-1} sec^{-1} atm^{-1}$ (96),

where the methods used were infra-red dispersion studies, inert gas pressure-broadening and self-:broadening respectively. Although in the literature the highest value is taken as being the most accur-:ate (97), the present result of 993×10^{10} $cm^{-1} sec^{-1} atm^{-1}$ substantiates the lower values.

This work was not expected to yield results in violent disagreement with the previous values since calculations of the atomic polarizations of the

molecules from the intensities agreed, to a first approximation, with those estimated from dielectric constant measurements (98)(99)(100). However, the results of this method indicate the validity of pressure-broadening measurements, when sufficient care is taken, to within 5%. Since the only other method not using a spectrometer, viz. infra-red dispersion studies, is subject to many theoretical difficulties of interpretation, this was a very use-:ful check.

With regard to the actual method, it was hoped that this would be simpler and quicker experimentally than the complexities of high-pressure work, as well as being theoretically more direct. It is therefore useful to summarise the advantages and the dis-:advantages:

a) Advantages

1) No difficulties due to finite spectro-:meter slit-width or lack of sensitivity in the wings of the band (section 1.4) were present.

2) The operation of the apparatus at pressures of below one atmosphere meant that difficulties due to incomplete mixing of a small pressure of absorbing gas and a high pressure of inert gas, and the pressure-induced adsorption of the

absorbing gas on the walls of the cell were eliminated. (section 1.4.1)

3) Constructional problems in both cell and gas-line design were reduced by using low pressures.

4) With pressure-broadening measurements, as has been stated, great care must be taken to ensure optimum conditions, e.g. to ensure that the absorption coefficient is constant over the spectrometer slit-:width in use. Because of the theoretical simplicity and certainty of the low pressure linear region only one set of measurements is necessary with the present method. Therefore, when allied to the fact that a simple energy measurement and not a graphical integration is involved, the method is very much quicker and simpler.

5) The line-shape of certain bands demands, with pressure-broadening experiments, the use of a very high pressure of inert gas (greater than 30atm). At these high pressures (section 1.4.1) pressure-induced absorption takes place. In the present method no such difficulty arises.

6) Bands of low intensity (e.g. overtones) can easily be measured. This follows from

the fact that the pressure of gas at which the low-pressure linear region is reached is proportional to a and inversely pro-:portional to $k(o)_D$, where

$$a = \frac{b_c}{b_D} (\ln 2)^{\frac{1}{2}},$$

and $k(o)_D$, the absorption coefficient at the line centre for Doppler broadening,

$$= \frac{S}{b_D} \left(\frac{\ln 2}{\pi}\right)^{\frac{1}{2}}$$ where S is the line intensity.

To a first approximation (ignoring possible changes in the number of lines in a band), therefore, the extent of the linear region for bands is inversely proportional to the intensity. Whereas for a fundamen-:tal of high intensity pressures of as low as 1cm.Hg have to be used, pressures of an atmosphere could be used with low intensity bands thus enabling sufficient sensitivity in the energy measurements to be attained.

b) Disadvantages

In listing the disadvantages in the method, suggested remedies for many of them are dis-:cussed.

1) In finding the absorbed energy two larger quantities were subtracted, i.e. the cell-constant and/or the absorption of the

CF_3Cl. This gave rise to the biggest error in the final results.

The absorption by the cell itself could obviously be eliminated in any new design, since it was simply due to too wide a beam being allowed through the aperture and filters. The absorption by the broadening gas, i.e. the CF_3Cl, could be eliminated in two ways; either by using a totally non-absorbing gas and experiment-:ally determining the required pressure before loss of energy to spontaneous emission occurred, or by filtering the in-:cident energy to a smaller band. The latter method could only be employed when the absorption bands of the gas under study and of the broadening gas did not overlap. By eliminating the need to subtract two quantities to obtain the absorbed energy it is estimated that the error in the intens-:ity measurements would be reduced from 5 to under 2%.

2) The effect of atmospheric absorption be-:tween the source and the cell is an in-:herent difficulty in this method, although of little importance in the bands of CH_4 and N_2O considered above. There are two

problems, one of overlap of an atmospheric band with the band of the gas in the absorp-:tion cell, and one of the effect on the incident energy measured over a region in-:cluding an atmospheric band. With the latter, when no direct overlapping occurs, the problem can be completely overcome by the use of a monochromator, isolating the absorption band in question and eliminat-:ing any atmospheric absorption. The method used above of calculating the effect is, however, perfectly adequate being accurate to within 1% of the total incident energy measured (it is dependent, of course, on a knowledge of the intensi-:ties of the atmospheric bands). With direct overlapping of a strong atmospheric band the problem can only be overcome by enclosing both source and cell in a con-:tainer which is filled with a non-infra-:red active gas. The experimental diffi-:culties here would be considerable. For direct overlapping of a weak atmospheric band, e.g. the water vapour overtone over-:lapping the 3,018cm^{-1} band of CH_4, cal-:culation of the fractional absorptivity of the weak band, although approximate, should in almost all cases suffice because of the

very small correction necessitated (0.5% in the quoted example). Although not applicable in this example (15) the individual lines in each band could coincide and the weak atmospheric band would need to be treated as a strong one.

3) A small error was introduced in the results obtained for CH_4 and N_2O by the presence of other absorption bands in the filtered region. Because of the high absorption of the bands studied, the error here was very low. This difficulty would be readily eliminated by the use of a monochromator as above.

4) In the design of the final cell many factors (section 2.2.2) were taken into account. For this method to yield accurate results each of these factors must be fully considered and allowances made when necessary.

5) The apparatus has a limiting sensitivity but energies much lower than measured above could be determined. Since two larger quantities were being subtracted to yield the energy absorbed no problems of sensitivity arose. However, with incident energies of 10^{-8} to 10^{-9} ergs per frequency

unit (as above) the lowest energy required to define the low-pressure linear region of absorption is approximately 0.2 to 0.8×10^{3} ergs sec^{-1}, and this, even in the absence of extraneous absorptions increasing the measured signal, is well within the scope of the apparatus. With optimum setting a factor of 10 to 20 lower than this could be attained.

6) When compared with methods using a spectrometer, the above suffers from the need to carry out separate measurements on absorbed and incident energies. However, the development of the technique using the blackened foil offers a very accurate determination of the incident energy.

Although spectrometer measurements using pressure-broadening have the advantage of being a fully developed technique, and although the present method essentially substantiates the results ob-:tained from them, it would seem fair to conclude that the direct measurement of the absorbed energy offers great accuracy and considerable ease and rapidity of measurement. It is interesting to speculate on further developments in this field as follows. Having established the intensity of a parti-:cular band and by using a stable source of radiation,

it should be possible to do very rapid comparative measurements. If the incident beam were chopped at a certain frequency and the diaphragm used as a microphone, selective amplification of the amplitude of the resultant wave would give high accuracy in the measurement of the energy absorbed. Having as-:certained with a few measurements that the linear region of absorption was attained in each case, a direct comparison of the amplitudes corresponding to two absorption bands could be carried out. This would give the ratio of the energies absorbed, whilst a measurement of the temperature of the source and a knowledge of the filter characteristics would yield the ratio of the incident energies. Since the in-:tensity of one of the bands is assumed known, and the linear region relationships are applicable, then the intensity of the unknown band would follow directly.

5.2 Line-Widths, and the effect of Line-Shapes on the Absorbed Energy

Reviews on line-shapes have been written by Breene (101) from a theoretical viewpoint and by Ch'en and Takeo (102) on the experimental results. The number of results related to vibration-rotation bands is, however, very small.

The variation of line-width over a band branch can be quite considerable (16)(31)(32) but, because of the difficulties encountered in making measure-:ments on individual lines, the average line-width in a band is a very useful value to obtain. It is also of practical value since it is the average line-width which is used in emissivity calculations (1).

The results obtained in this work for pure CH_4, N_2O and CF_3Cl were based on Elsasser's theory al-:though this theory was not fully descriptive of the relationship between the absorbed energy and the pressure. It was decided (section 4) that the change in the energy absorbed with pressure at higher pressures, when the relationship was linear, was due to the physical changes suggested by Elsasser for a pure gas. By employing the full analysis detailed in section 1.3.1.4, Penner(1) found for CO that the Elsasser approximation yielded a result for the line-:width which was approximately 50% too low. This may also be true of the results in this work, but a full analysis would be necessary to show it; and since the values obtained are fairly high (compared, for example, to the $0.06cm^{-1}atm^{-1}$ for CO) it would seem that Penner's conclusions are not general.

For the $589cm^{-1}$ band of N_2O values of $0.20cm^{-1}$ atm^{-1} (103) and $0.21cm^{-1}atm^{-1}$ (58) for the average line-width have been obtained, although in the second

reference only a branch maximum was studied. For the 1,285cm^{-1} band Thorndike (58) obtained 0.13cm^{-1}atm^{-1}. A value of 0.3cm^{-1}atm^{-1} was obtained for 2,224cm^{-1} band (56) but this was based on a wrong assumption. It is seen that the present value of 0.13cm^{-1}atm^{-1} for the 2,224cm^{-1} band is in agreement with the results obtained with N_2O.

With CH_4 the result of 0.18cm^{-1}atm^{-1} is approxi-:mate because of the presence of the Q branch, and no other value for the 3,018cm^{-1} band is available with which to compare it. However, using purely com-:parative measurements (57) it was found that the optical collision diameter for CH_4-CH_4 collisions was approximately the same as for CH_4-CO collisions (this was for the 1306cm^{-1} band). Assuming that this means the approximate equality of the collision diameters for CH_4 and CO, a value is obtained of 4.5 to 5.0A^{o} (for the 1306cm^{-1} band), which is in very good agree-:ment with the present result of 4.9A^{o} for the 3,018cm^{-1} band. Comparative measurements on a single line in the 3,018cm^{-1} band ($J = 4 \longrightarrow 5$) with a single line in the HCl fundamental ($J = 2 \longrightarrow 3$) have been made (104), but no estimates of the average line-:width can be made from this.

A high result for the line-width of 0.20cm^{-1}atm^{-1} was obtained with the CF_3Cl overtone at 2,400cm^{-1}, but a high optical collision diameter is to be ex-:pected for this molecule because of its strong polar

properties.

Considering the kinetic collision diameters (section 4.4) and the relative polarities of CH_4, N_2O and CF_3Cl the results on the optical collision diameters of these three molecules are obviously in the correct order.

As has been indicated in section 4, simple theory for a pure gas predicts a linear relationship between the absorbed energy and the pressure, ex-:tending from the region in which the 'error function law' (section 1.3.1.2) is applicable to very low pressures when the effect of Doppler broadening changes the amount of energy absorbed. In the ab-:sence of the Doppler effect this linear region should pass through zero. The present work showed that, for the three bands studied, an initial low-pressure absorption took place not obeying simple theory al-:though a linear region was obtained at higher pressures. This linear region, when extrapolated, did not pass through zero.

It is unlikely that this low-pressure high ab-:sorption was due purely to the Doppler effect since it can be shown (1) for a pure Doppler line that the energy absorbed approaches $2.5\ (\frac{2\pi kT}{mc^2})^{\frac{1}{2}} I(o)\omega_o$,

with ω_o the wave-number of the line-centre, as the

reduced pathlength becomes very large. Extending this to a band, it was found that the total energy absorbed by the Doppler line-shape was approximately a factor of 10 less than the value of the energy obtained by extrapolating to zero pressure the linear region of absorption for the three bands considered. Having dismissed the Doppler effect as a possible explanation, it was suggested that the high absorption coefficients near the line-centre gave rise to an absorption relationship at low pressures which was similar in some respects to that obtaining for an absorbing gas made up to constant pressure with an inert gas.

There is considerable difficulty in predicting the form of this relationship theoretically, although the empirical extrapolation used in section 4 should be approximately correct.

Many gases have been found not to obey simple theory, e.g. HCl and HBr (1) ; and N_2O made up with N_2 was found to give results yielding an $X^{\frac{1}{3}}$ relationship, rather than an $X^{\frac{1}{2}}$ one, at higher pressures (48). However, results on pure gases which have been assumed to obey simple theory can be shown to have the same low-pressure features as found in this work. Thorndike (58), working on the 589cm^{-1} band of N_2O, although not extending his results to low enough pressures to leave the linear region, found that his

plot did not extrapolate to zero (he suggested that this was due to the Doppler effect, but did not state how this was possible). On examining Penner's results on CO (both fundamental and overtone) and NO (1), although these were not extended below the linear region, it was found that an extrapolation of the straight line plot did not, once more, go through zero (nor could the extrapolated value be explained by the Doppler effect); however, the smaller the value of the cell-length used the more closely did the extrapolation come to zero. These facts would seem to indicate a general process for low pressures of pure gases not associated with the Doppler effect. It is therefore of value to draw up a table showing the extrapolated value of the fractional absorptivity, $A_R(o)$, in each case compared with properties which might affect this value.

l is the optical pathlength,

A is the intensity of absorption,

δ is the line-width at latm. pressure,

d is the distance between lines in the absorption band.

	$A_R(0)$	l(cm.)	$A(cm^{-1}sec^{-1}atm^{-1})$	$\delta(cm^{-1}atm^{-1})$	$d(cm^{-1})$
$CH_4(3,018cm^{-1})$	0.04	1.54	$993x10^{10}$	0.18	9.0
$N_2O(2,224cm^{-1})$	0.3	1.54	$4,740x10^{10}$	0.13	0.86
$N_2O(589cm^{-1})$	0.06	30.0	$900x10^{10}$	0.20	0.86
$CF_3Cl(2,400cm^{-1})$	0.04	1.54	$580x10^{10}$	0.20	-
$CO(2,143cm^{-1})$	0.02	10.1	$710x10^{10}$	0.06	4.0
$NO(1,876cm^{-1})$	0.01	6.22	$190x10^{10}$	0.04	-

These figures indicate that probably the main factor influencing $A_R(o)$ is the intensity of absorp-:tion, and it suffices to conclude that the relation-:ship between the absorbed energy and the pressure for low pressures of pure gases does not follow simple theory, but is dependent in a more complicated way on the properties of the band absorption.

5.3 Relaxation of Vibrational Energy

The study of the probability of vibrational-:translational energy transfer has received consider-:able attention in recent years (33). Many methods have been used to determine the time taken for the transfer of translational energy to vibrational energy, and vice versa; the main techniques being the measurement of the velocity and the absorption of sound in gases, shock wave and impact tube studies (33). These procedures essentially only give infor-:mation on the lowest-lying vibrational mode in the molecule (there are a few exceptions), since the transfer takes place from translational energy to vibrational energy and naturally the most available mode of vibration is firstly excited.

In the present work the excited vibrational modes were not the most low-lying in the molecule and the question of interest was whether the energy was lost to translation by collision in one step, or whether the collisions with other molecules produced a step-

:wise mechanism down the available vibrational modes in the molecule.

The theory of energy transfer (33) yields the following expression for the reciprocal relaxation time,

$$f = \left(\frac{4\pi}{3^{\frac{1}{2}}}\right) N B r_o^{\,2}\, v^* \exp\left(-3y^* + \frac{h\nu}{2kT}\right)$$

where $f = \frac{1}{\tau}$ with τ the relaxation time,

N is the molecule density,

r_o is the distance of closest approach of the molecules,

$B = \frac{32\,\pi^4 m^2 \nu}{h\alpha^2 M}$, with m the reduced mass of the system,

ν the frequency of vibration,

h Planck's constant,

α a constant in the pot-:ential energy function,

and M the reduced mass of the oscillator,

$v^* = (\frac{4\pi^2 kT\nu}{\alpha m})^{\frac{1}{3}}$ with k Boltzmann's constant, and T the absolute tempera-:ture,

$$y^* = (\frac{2\pi^4 m\nu^2}{\alpha^2 kT})^{\frac{1}{3}}$$

It was found, using values from reference (33), that the ratio of f for the 1,306cm^{-1} band of CH_4 (the lowest-lying mode of vibration) to f for the 3,018cm^{-1} band (studied in this work) assuming the mechanism was by one step, was approximately 10^{-6}. Since the established value of the relaxation time for the 1,306cm^{-1} band is 1.5×10^{-6} sec., this means that if the energy was lost from the 3,018cm^{-1} band to translation in one step the resulting relaxation time would be of the order of 1 sec. Similar results were determined for the 2,224cm^{-1} band of N_2O. The step-wise process with its much smaller energy jumps theoretically yielded values from 10^{-4} to 10^{-6} sec., dependent on the route taken by the energy loss.

The results obtained for the 3,018cm^{-1} mode of CH_4 and the 2,224cm^{-1} mode of N_2O were 245 and 43μsec.

respectively, both of which show conclusively that the step-wise process is the operative method for vibrational-translational energy transfer from higher modes of vibration.

Many indications that the above is true have been obtained in other work and some of these are now mentioned. Although ultrasonic measurements normally only give information on the lowest mode of vibra-:tion, in those molecules with two, well-separated, low-lying modes it has been observed (105) that the velocity dispersion curves show two distinct parts. This has been interpreted as revealing relaxation of the energy in two modes, and a good example (105) of this is CH_2Cl_2 with bands at 283cm^{-1} and 704cm^{-1} yielding results of 0.2×10^{-8} and 9.5×10^{-8} sec. res-:pectively. These results would indicate a step-wise mechanism.

One method has been devised to study these higher modes. This makes use of the optic-acoustic effect; if there is a time-lag between the absorption of a vibrational quantum and its degradation to

thermal energy in an absorption cell, then a result-:ant phase difference should exist between the modu-:lation of the incident radiation and the emitted sound wave. Details of this method can be found in reference (33). The results which have been obtained are of dubious significance because of other phase-:lags present in the measurements (106)(107)(108), but definitely indicate a step-wise process for loss of vibrational energy.

The only result recorded for either of the two bands in CH_4 and N_2O studied in this work is by a technique which examines the change in vibrational temperature with time (109). In a rapidly flowing gas stream heated at one part of the apparatus the vibrational temperature at a small distance from the heat source has not attained equilibrium with the translational temperature. By measuring the vibra-:tional temperature using an infra-red spectrometer and the translational temperature with suitably placed thermocouples, the difference between the two can be found. The change of vibrational temperature

with time can be determined from a knowledge of the rate of flow of the gas and a measure of the vibra-:tional temperature at several distances from the heat source. The relaxation time follows from

$$\frac{dT_v}{dt} = \frac{1}{\tau}(T_v - T_t)$$

where t is the time,

and T_v and T_t are the vibrational and translational temperatures respectively.

The result quoted for the 2,224cm^{-1} mode of N_2O was approximately 100μsec at one atmosphere of gas. However, the results varied from 100μsec at 392^{o}K to 260μsec at 340^{o}K to 160μsec at 319^{o}K (the temperature range studied being from 46^{o}C to 119^{o}C) which would appear to be an incorrect temperature dependence. The value obtained is therefore of dubious significance.

It is seen from the above that, as yet, no definite results exist for the relaxation time of higher modes of vibration, and that therefore no meaningful comparisons with the present results can be made.

Assuming the validity of the present results it is interesting to speculate on the possible routes taken by the collisional deactivation of the vibra-:tional energy.

CH_4 has four fundamental modes of vibration, at 3,018cm^{-1}, 2,914cm^{-1}, 1,526cm^{-1} and 1,306cm^{-1}. It has been shown (110) that the rapid transfer of energy for the lowest mode (τ = 1.5μsec) is due to the action of the rotating molecule. The transfer of translational energy to rotational to vibrational is more rapid than the normal translational - vibrational transfer. However, energy in the 3,018 cm^{-1} mode is almost certain to undergo an extremely fast deactivation to the very close 2,914cm^{-1} mode; this mode is a stretch of the four hydrogen atoms and cannot be affected by the rotation of the mole-:cule in the same manner as the other modes which have a twisting vibration. It is therefore likely that the second deactivation (from the 2,914cm^{-1} mode to the 1,526cm^{-1} mode) is much slower than the

others due to this factor. The result of 245μsec. substantiates this mechanism since if each step took place in a similar manner then the relaxation time for the 3,018cm^{-1} mode would be much shorter (the longest jump of 1,388cm^{-1} being not much greater than 1,306cm^{-1}, and only lengthening the relaxation time from simple theory by a factor of two or three). The suggested route of collisional de-activation is therefore

3,018cm^{-1} $\longrightarrow$ 2,914cm^{-1}, very rapid,

2,914cm^{-1} $\longrightarrow$ 1,526cm^{-1}, slow, time determining step,

1,526cm^{-1} $\longrightarrow$ 1,306cm^{-1}, very rapid,

and 1,306cm^{-1} $\longrightarrow$ ground level, rapid.

N_2O has three fundamental modes of vibration at 2,224cm^{-1}, 1,285cm^{-1} and 589cm^{-1}. Although many possible routes exist for the deactivation of the vibrational energy in the highest fundamental mode (e.g. via overtones of the 589cm^{-1} mode) the most likely is the straightforward

$2{,}224cm^{-1} \longrightarrow 1{,}285cm^{-1}$, rate determining step,

$1{,}285cm^{-1} \longrightarrow 589cm^{-1}$, comparatively rapid,

$589cm^{-1} \longrightarrow$ ground level, rapid.

Herzfeld (111) calculated for the $2{,}349cm^{-1}$ mode of CO_2 that the most likely route was the straightforward one above (CO_2 being very similar to N_2O), although this is in opposition to the theoretical findings of Laidler (112) who suggested that energy transfer is very unlikely between sym-:metric and antisymmetric stretching.

The proposed rate determining step for the N_2O degradation involves a jump of $939cm^{-1}$, which from theory would be approximately a factor of 30 to 40 times longer than the $589cm^{-1}$ jump which is estab-:lished at $1\mu sec$. The result obtained for the $2{,}224cm^{-1}$ mode of $43\mu sec$. is therefore in very good agreement with the straightforward vibrational-:translational, stepwise mechanism.

The remaining result from this work is the rapid deactivation of the CF_3Cl overtone at $2{,}400cm^{-1}$ (τ being certainly less than $50\mu sec$). Below the corresponding fundamental at $1{,}210cm^{-1}$ there are many vibrational modes and it can be assumed that energy transfer from the $1{,}210cm^{-1}$ mode to the ground state is very rapid. The value obtained (33) for the

lowest-lying mode is 0.1 μsec. The result therefore shows that collisional deactivation of an overtone to its fundamental is a rapid process, and cannot be explained by one step (in this case of approximately 1,200cm^{-1}) which takes place with the normal vibrational-translational mechanism. Two explana-:tions are possible:

a) that a step-wise mechanism can exist between the overtones of the various fundamentals. This would give a series of small jumps similar to the degradation of energy from the highest fundamental, and would be a rapid process.

b) that a completely different mechanism is res-:ponsible for the transfer, i.e. an initial vibrational-vibrational transfer involving the change from one molecule containing two quanta of energy to two molecules containing one vibrational quantum each (this being different from the normal process of degradation to trans-:lational), followed by degradation to the ground level. If this mechanism is correct then it would seem to be dependent on the exactly similar symmetries of the colliding species, and should not exist when the colliding molecules are different. This could readily be tested by studying the relaxation process of an overtone in collision with a foreign gas.

The findings in this work that degradation of vibrational energy from an overtone is very rapid are in agreement with studies on high overtones (113) (33) using fluorescence techniques, flash spectroscopy and direct spectroscopic investigations.

REFERENCES

1. Penner, "Quantitative Molecular Spectroscopy and Gas Emissivities," Pergamon Press, London, 1959.
2. Mills, Annual Reports of the Chem. Soc., 55, 55 (1959).
3. Hanson, Nielsen, Schaffer and Wagonner, J. Chem. Phys., 27, 40 (1957).
4. Herman and Wallis, J. Chem. Phys., 23, 637 (1955).
5. Wilson, J. Chem. Phys., 27, 986 (1957).
6. Gallup, J. Chem. Phys., 27, 1338 (1957).
7. Hornig and McKean, J. Phys. Chem., 59, 1133 (1955).
8. McKean and Schatz, J. Chem. Phys., 24, 316 (1956).
9. Mills, Mol. Phys., 1, 107 (1958).
10. Burnelle and Coulson, Trans. Faraday Soc., 53., 403 (1957).
11. Ellison and Shull, J. Chem. Phys., 23, 1950 (1955).
12. Higuchi, J. Chem. Phys., 24, 535 (1956).
13. Wilmshurst, J. Phys. Chem., 62, 631 (1958).
14. Wilmshurst, J. Chem. Phys., 28, 733 (1958).
15. Herzberg, "Molecular Spectra and Molecular Structure, "Van Nostrand Co., New York, 1956.
16. Benedict, Herman, Moore and Silverman, Canad. J. Phys., 34, 830, 850 (1956).
17. Foley, Phys. Rev., 69, 616 (1946).
18. Smith, Jones and Chasmar, "Detection and Measurement of Infra-red Radiation," Oxford University Press, London, 1957.

19. Elsasser, Phys. Rev., 54, 126 (1938).

20. Matossi, Mayer and Rauscher, Phys. Rev., 76, 760 (1949)

21. Ladenburg and Reiche, Ann. Physik., 42, 181 (1913)

22. Kaplan and Eggers, J. Chem. Phys., 25, 876 (1956).

23. Matheson, Phys. Rev., 40, 813 (1932).

24. Penner and Tsien, J. Chem. Phys., 20, 827 (1952).

25. Weber and Penner, J. Chem. Phys., 21, 1503 (1953).

26. Penner and Weber, J. Chem. Phys., 19, 1361 (1951).

27. van der Held, Z.Physik, 70, 508 (1931).

28. Plass and Fivel, Astrophys. J., 117, 225 (1953).

29. Plyler, Tidwell and Blaine, J. of Research of the Nat. Bureau of Standards, 64A, 201 (1960).

30. Penner and Areoste, J. Chem. Phys., 23, 2244 1955.

31. Lindholm, Z.Physik, 113, 596 (1939).

32. Bourgin, Phys. Rev., 29, 794 (1927).

33. Cottrell and McCoubrey, "Molecular Energy Transfer in Gases," Butterworth Press, London, 1961.

34. Wilson and Wells, J. Chem. Phys., 14, 578 (1946).

35. Ramsay, J. Amer. Chem. Soc., 74, 72 (1952).

36. Russell and Thompson, Spectrochim. Acta, 9, 133 (1957).

37. Kuipers, J. Mol. Spectroscopy, 2, 75 (1958).

38. Penner and Weber, J. Chem. Phys., 19, 807 (1951).

39. Golike, Mills, Person and Crawford, J. Chem. Phys., 25, 1266 (1956).

40. Dickson, Mills and Crawford, J. Chem. Phys., 27, 445 (1957).

41. Nyquist, Mills, Person and Crawford, J. Chem. Phys., 26, 552 (1957).

42. Weber and Penner, J. Chem. Phys., 19, 974 (1951).

43. Welsh, Pashler and Dunn, J. Chem. Phys., 19, 340 (1951).

44. Welsh, Pashler and Dunn, J. Chem. Phys., 20, 1646 (1952).

45. Crawford, Welsh, Macdonald and Locke, Phys. Rev., 80, 469 (1950).

46. Thorndike, Wells and Wilson, J. Chem. Phys., 15, 157 (1947).

47. Eggers and Crawford, J. Chem. Phys., 19, 1554 (1951).

48. Callomon, McKean and Thompson, Proc. Roy. Soc., 208A, 332 (1951).

49. Watari and Kinumaki, Science Reports of the Research Institutes, Tohoku University, Series A, Vol. 13, No. 1, 48 (1961).

50. Rollefson and Rollefson, Phys. Rev., 48, 779 (1935).

51. Rollefson and Havens, Phys. Rev., 57, 710 (1940).

52. Kelly, Rollefson and Schurin, J. Chem. Phys., 19, 1595 (1951).

53. Gerlovin, Optics and Spectroscopy, Vol IX, No. 5, 349 (1960).

54. Veingerov and Slobadskaya, Izvest. Akad. Nauk. SSSR, Ser. Fiz. 11, 420 (1947).

55. Herzberg and Spinks, Proc. Roy. Soc., 147A, 434 (1934).

56. Cross and Daniels, J. Chem. Phys., 2, 6 (1934).

57. Coggeshall and Saier, J. Chem. Phys., 15, 65 (1947).

58. Thorndike, J. Chem. Phys., 16, 211 (1948).

59. Penner, J. Chem. Phys., 19, 272 (1951).

60. Conn and Avery, "Infra-Red Methods," Academic Press, London, 1960.

61. Luft, Z. tech. Physik, 5, 97 (1943).

62. Cottrell and Read, unpublished, University of Edinburgh.

63. Delany, Thesis, University of London, 1959.

64. Mori, Reports of Scientific Research Institutes, Tokyio, 385 (1955).

65. Matheson, Thesis, University of Edinburgh, 1962.

66. Leighton and Forbes, J. Amer. Chem. Soc., 52, 3146 (1930).

67. Gregory and Archer, Proc. Roy. Soc., 110A, 91 (1926).

68. Taylor and Johnson, J. Chem. Phys., 14, 219 (1946).

69. Kannuluik and Martin, Proc. Roy. Soc., 141A, 144 (1933).

70. Kannuluik and Martin, Proc. Roy. Soc., 144A, 496 (1934).

71. Kannuluik and Law, Proc. Roy. Soc. of Victoria, 58, 142 (1947).

72. Fishenden and Saunders, "Heat Transfer", Clarendon Press, Oxford, 1950.

73. Bosworth, "Heat Transfer Phenomena", Assoc. General Publications Ltd., Sydney, 1952.

74. Kraussold, Forsch. Gebiete Ingen., 5, 186 (1934).

75. Beckmann, Forsch, Gebiete Ingen., 2, 165 (1931).

76. Smoluchowski, Ann. Physik., 64, 101 (1898).

77. Knudsen, Ann. Physik., 34, 593 (1911).

78. Jaffe, Ann. D. Physik., 6, 195 (1930).

79. Jaffe, Phys. Rev., 61, 643 (1942).

80. Kennard, "Kinetic Theory of Gases", McGraw-Hill, New York, 1938.

81. Ubbelohde, J. Chem. Phys., 3, 219 (1935).

82. Schafer et al, Ann. D. Physik, 42, 176 (1942).

83. Waelbroeck and Zuckerbrot, J. Chem. Phys., 28, 524 (1958).

84. Wright and Gray, Trans. Faraday Soc., 57, 657 (1961).

85. Archer, Phil. Mag., 7, 19, 901 (1935).

86. Archer, Proc. Roy. Soc., 165A, 474 (1938).

87. Dickens, Proc. Roy. Soc., 143A, 517 (1934).

88. Gregory, Proc. Roy. Soc., 149A, 35 (1935).

89. Gregory, Phil. Mag., 7, 22, 257 (1936).

90. Ibbs and Hirst, Proc. Roy. Soc., 123A, 134 (1928).

91. Thompson and Williams, Proc. Roy. Soc., 208A, 326 (1951).

92. Sutherland, "Infra-red and Raman Spectra," Methuen & Co. Ltd., London, 1935.

93. Wiegand, Z. f. Physik., 30, 40 (1924).

94. Childs, Proc. Roy. Soc., 153A, 555 (1936).

95. Brand and Speakman, "Molecular Structure," Arnold Ltd., London, 1960.

96. Armstrong and Welsh, Spectrochim. Acta, 16, 840 (1960).

97. Mills, Mol. Phys., 1, 107 (1958).

98. Whiffen, Trans. Faraday Soc., 54, 327 (1958).

99. Illinger and Smyth, J. Chem. Soc., 32, 787 (1960).

100. Rao, Trans. Faraday Soc., 59, 43 (1962).

101. Breene, "The Shift and Shape of Spectral Lines," Geophysical Research Papers, No. 41, Air Research and Development Command, 1955.

102. Ch'en and Takeo, Rev. Mod. Phys., 29, 20 (1957).

103. Adel, Phys. Rev., 71, 806 (1947).

104. Benesch and Elder, Phys. Rev., 91, 308 (1953).

105. Lambert and Salter, Proc. Roy. Soc., 243A, 78 (1957).

106. Slobodskaya, Izvest. Akad. Nauk. SSSR, 12, 656 (1948).

107. Delany, Thesis, University of London, 1959.

108. Jacox and Bauer, J. Phys. Chem., 61, 833 (1957).

109. Gauthier and Marcoux, Canad. J. of Physics, 39, 1130 (1961).

110. Cottrell and Matheson, Trans. Faraday Soc., 58, 2336 (1962).

111. Herzfeld, "Inelastic Collisions of atoms and simple molecules," Disc. of the Faraday Soc., 33, 22 (1962).

112. Gil and Laidler, Proc. Roy. Soc., 251A, 66 (1959).

113. McGrath and Norrish, Proc. Roy. Soc., 242A, 265 (1957).

ACKNOWLEDGEMENTS

I should like to thank Professor T.L. Cottrell for his help and advice throughout this work, Mr. Sheddan and the technical staff of the laboratories for their kind assistance and the Department of Scientific and Industrial Research for the award of a Research Studentship.

ABSTRACT

Absolute intensities of infra-red absorption have been determined for the ν_3 bands of CH_4 and N_2O from direct measurements on the infra-red energy absorbed. The energy was measured as a pressure rise in a constant-volume absorption cell having allowed a steady-state, with heat loss to the walls, to be attained. The pressure rise was simulated by introducing a known amount of heat energy from an electrically heated wire. The energy incident on the gas was measured by using within the cell a thin, blackened foil which absorbed all the radiation and in thermal equilibrium transferred this energy to heat energy of the gas. The resultant pressure rise was simulated by the heated wire as for the gas absorption. The value obtained for the incident energy was checked by measurements with a calibrated thermopile.

The results of 993×10^{10} and $4{,}740 \times 10^{10}$ $cm^{-1}sec^{-1}$ at N.T.P. for the ν_3 bands of CH_4 and N_2O respectively confirmed that the normal method of determination, using pressure-broadened, spectrometer measurements, yields accurate results when sufficient care is taken to ensure optimum conditions of measurement.

Although the simple Elsasser theory was not fully descriptive of results on the energy absorbed for pure gases, it was used to estimate average linewidths of 0.18 and 0.13 $cm^{-1}atm^{-1}$ for the bands in CH_4

and N_2O respectively.

The technique used did not measure all the absorbed energy at very low total pressures. This was due to the fact that with decreasing pressure spontaneous emission became a competing process with the vibrational-translational energy transfer involved in the determination. The magnitude of this loss was used to estimate relaxation times of 245 and 43 μ sec. for the ν_3 bands of CH_4 and N_2O respectively.